

**THE ROLE OF HUMAN MESENCHYMAL STEM
CELLS IN REPAIR OF BONE**

A DISSERTATION

SUBMITTED ON FRIDAY, JULY 31, 2009

TO THE DEPARTMENT OF BIOMEDICAL SCIENCES

IN PARTIAL FULFILLMENT OF THE REQUIREMENTS

OF THE GRADUATE SCHOOL

OF TULANE UNIVERSITY

FOR THE DEGREE

OF

DOCTOR OF PHILOSOPHY

BY

William Gunn

APPROVED

Darwin Prockop, M.D., Ph.D.

Carl Gregory, Ph.D.

Don Phinney, Ph.D.

Matt Burow, Ph.D.

Erik Flemington, Ph.D.



William Gunn
This work is licensed by under a
[Creative Commons Attribution-Share Alike 3.0](https://creativecommons.org/licenses/by-sa/3.0/)
Unported License

ACKNOWLEDGEMENTS

I would like to gratefully thank the following people:

Dr. Darwin Prockop for his continual guidance and support throughout my time in his lab. His wonderful attitude and enthusiasm for science has been inspiring.

My committee members for their time, guidance, and confidence that I am qualified for my doctorate.

Carl Gregory, and Scott Olson, without whose mentorship this work would not have been possible.

Linda Ledet for her assistance and caring.

The past and present members of the Center for Gene Therapy, of which there are too many to list. Their advice, training, and help has been invaluable.

My parents, Lawrence and Mary Gunn, for being proud of me and supporting me throughout my education.

My wife Elaina, who has so kindly pretended to understand and be interested in my work for so long.

And my larger New Orleans family of friends who have always been on hand to help.

TABLE OF CONTENTS

ACKNOWLEDGEMENTS	II
TABLE OF CONTENTS	III
OVERVIEW	1
<i>Human Multipotent Stromal Cells</i>	1
<i>MSCs Applications</i>	3
<i>MSCs and Wnt Signaling</i>	7
<i>MSCs and Multiple Myeloma</i>	10
<i>Myeloma Treatment</i>	14
<i>Animal models of multiple myeloma</i>	15
II. DKK1 IN MSC DIFFERENTIATION	17
INTRODUCTION.....	17
MATERIALS AND METHODS.....	19
<i>Dkk1 cell -binding assay</i>	19
<i>Radioligand binding assay</i>	20
<i>Spectrophotometry</i>	21
<i>Tissue culture</i>	21
<i>Mineralization Protocol</i>	21
<i>Detection and quantification of mineralization</i>	22
<i>Arsenazo III calcium assay</i>	23
RESULTS	24
CONCLUSION	35
III. MSCS AND MULTIPLE MYELOMA	40
INTRODUCTION.....	40
MATERIALS AND METHODS.....	43

<i>Cell Culture</i>	43
<i>Production of Dkk1</i>	44
<i>Mineralization Assay</i>	45
<i>Preparation of conditioned medium and growth curves</i>	47
<i>Western Blotting</i>	48
<i>Reverse transcription-polymerase chain reaction assay</i>	49
<i>ELISA</i>	49
<i>Microscopy</i>	50
RESULTS	51
CONCLUSION	61
IV. MULTIPLE MYELOMA AS A MODEL BONE DISORDER IN THE MOUSE.	65
INTRODUCTION.....	65
MATERIALS AND METHODS.....	67
<i>Animal Handling</i>	67
<i>Histology</i>	69
<i>Pathology</i>	69
<i>Histomorphometry</i>	70
<i>Drug administration</i>	74
<i>ELISAs</i>	74
STATISTICS.....	74
RESULTS	75
CONCLUSION	107
V. FINAL DISCUSSION AND FUTURE PERSPECTIVES	112
REFERENCES	116

OVERVIEW

Human Multipotent Stromal Cells

Human multipotent stromal cells were first characterized by Alexander Friedenstein as fibroblastic colony-forming cells from the non-hematopoietic, culture vessel-adherent fraction of bone marrow^{1,2,3}. Bone marrow transplants had provided circumstantial evidence for the presence of precursor cells of the various components of bone marrow stroma: osteoblasts, adipocytes, chondrocytes, among others, while *in vitro* culture and differentiation of these colony-forming units provided more direct evidence of their existence. *In vivo* culture of the cells as implanted diffusion chambers or as ectopic transplants³, showed formation of bony structures including bone marrow and established the CFU-F cells as a multipotent progenitor population capable of reconstituting bone marrow in an ablated recipient. These findings, along with their easy expansion in culture, initially suggested MSCs may have clinical applications in the areas of bone marrow transplant support and tissue repair. Since then, various groups have since studied the *in vitro* differentiation capacity of MSCs and the cells have also been extensively used as non-viral vectors for gene therapy.

Early evidence of the role of MSCs in bone formation and homeostasis was provided by experiments where single colony-derived MSC cultures were implanted in host animals, resulting in an ectopic

ossicle containing bone cells, stroma, and adipocytes of donor origin and hematopoietic cells of recipient origin³. Interestingly, not all of the implants form the complete ossicle. Some form only bone, some only form fatty deposits, and some only form fibrous tissue, incapable of supporting hematopoiesis. Less often, cartilaginous tissue is found. Because this heterogeneity implies that the original CFU-F population is composed of cells of different capacity or a range of developmental stages, considerable work has been done to find the *a priori* indicators of multipotentiality. One of the first markers for multipotency, STRO-1, was derived by injecting mice with CD34⁺ bone marrow cells, in the hopes of finding a monoclonal that would isolate the CFU-F population of bone marrow^{5,6}. While STRO-1 did isolate the CFU-F population, it also stained some B lymphocytes and nucleated red cells. Further work to get the required purity led to the development of a panel of markers, including CD29, CD34, CD44, CD106, and CD166. Unfortunately, due to variation in isolation, culture, and assay techniques, inconsistent results were obtained using the various panels and a means of isolating only multipotent cells has yet to be found⁷. Because the gene expression and surface marker profile of even single-cell derived colonies changes over time in culture, full understanding of the cell state necessary and sufficient for multipotentiality, the “stemness” state, awaits techniques which can take a more comprehensive look at the gene expression and chromatin repression profiles of MSCs in culture.

MSCs Applications

Despite the difficulties in defining exactly which population of cells or culture condition is best for clinical applications, progress has nonetheless been made on a number of fronts. On an infrastructural level, standardized isolation techniques have been developed to ensure that even if different isolates don't contain exactly the same cells, they will nonetheless show similar activity when handled the same way. Culture conditions have been developed which minimize the risk of transplant rejection, and differentiation protocols have been refined to more accurately measure the expression of the desired phenotype. Improvements have also been seen in stable genetic modification of MSCs and in engineering of implantable scaffolds on which MSCs can be seeded. On an applied level, clinical trials are now being carried out for many disorders, with autoimmune disorders such as graft versus host disease and transplant rejection being most prominent, followed by tissue repair applications involving the heart, vasculature, bone, and other organs. An exact count of the number of pre-clinical studies is difficult to obtain, but it can be assumed that for every application proceeding to the clinical stage, there are many more which haven't advanced to that stage yet. Table II-1 - MSC Clinical Trials as reported by <http://clinicaltrials.gov>. Table II-1 shows the distribution of MSC clinical trials by disease, as reported by <http://clinicaltrials.gov> using a search

for the term “mesenchymal stem cell”. This term, although not the recommended term⁷, was used as it is the term under which the majority of the trials are listed.

	Phase I	Phase II	Phase III	Total
autoimmune	8	10	3	21
Cardiac	7	14	0	21
Bone	5	5	1	11
Cancer	3	4	1	8
Other	8	11	0	19

Table II-1 - MSC Clinical Trials as reported by <http://clinicaltrials.gov>.

Of note is that all of these trials are cell therapy trials. Unlike with hematopoietic stem cells, there aren't well-known means of mobilizing endogenous MSCs, so existing approaches have focused on autologous or allogeneic administration of the cells themselves.

There are at least three mechanisms by which the therapeutic benefits of MSCs are realized: Direct or paracrine interactions with cells of the injured tissue, differentiation of MSCs into tissue-specific progenitors to augment the existing cells, and fusion of MSCs with the injured tissue. Cell-cell interactions are thought to be the main

therapeutic mechanism operating in autoimmune applications⁸. These approaches take advantage of the activity of MSCs on regulatory T cells (T_{reg}). The presence of MSCs has been shown to inhibit the mixed lymphocyte reaction in culture and, *in vivo*, MSCs reduce the clinical grade of GVHD^{9,10,11,12,13,14}. The interaction of MSCs with T_{reg} cells wherein T_{reg} cells are activated by cell-cell contact with MSCs supports the theory that MSCs act directly on T_{reg} cells, which then suppress the activity of the other components of the immune system, alleviating the inflammatory symptoms¹⁵. This mechanism is also thought to be the principal mechanism whereby MSCs decrease the signs of transplant rejection^{8,9,12,15,16,17,18,19,20,21,22}.

In contrast to the cell-cell contact important for the MSC effect on autoimmune disorders, tissue repair depends on differentiation of MSCs and paracrine signaling between MSCs and endogenous progenitor cells in the target tissue^{7,24}. Differentiation of MSCs to replace injured or aging tissue is the most straightforward approach. This has been shown to be an important part of the therapeutic effects seen in bone and cartilage repair^{25,26}. For example, MSCs are used to seed implants and directly differentiate *in situ* to provide structural integrity to the bone-implant interface^{27,28,29,30}. Although differentiation is important for some types of the tissue repair, it's the paracrine effects that appear increasingly important^{31,32}. In a paracrine tissue repair scenario, the MSCs would

secrete signaling molecules which activate or recruit endogenous tissue-specific progenitors. This is a promising scenario for tissue regeneration, as it is the one approach where the cells themselves aren't actually needed, therefore it's the area where existing drug development techniques can be leveraged to accelerate translation of research to application. Cases where paracrine signaling of MSCs to endogenous progenitors is an important part of the reparative action are: augmentation of HSC transplants after marrow ablation therapy^{33,34}, alleviation of kidney fibrosis^{35,36}, regeneration of injured hepatic tissue³⁷, and bone repair^{26,38}, where MSCs are a component of the autocrine loop that regulates bone remodeling and repair^{39,24}. Note that the paracrine action of MSCs needn't be a naturally-occurring paracrine effect; MSCs have been successfully engineered to secrete therapeutically-active molecules such as collagen and interferon. Successful approaches in this area have utilized the homing of MSCs to sites of tissue damage to effect much higher local concentrations of the active molecules than could be achieved through systemic administration.

Cell fusion is a rarer phenomenon, yet a significant contribution to the reparative effect of MSCs on cardiac and skeletal muscle. Because muscle is composed of multi-nucleated cells, cell fusion is not an uncommon occurrence in these tissues, and a unique therapeutic avenue in this context. When MSCs fuse with injured muscle tissue they can

alleviate the effects of ischemia by supplying fresh and undamaged mitochondria⁴².

A fourth approach to treatment would involve abstracting the effect of the cells to a therapeutic small molecule which reproduces the desired effect. This approach has been explored less extensively than the use of the cells themselves, in part because the exact actions of MSCs in a particular therapeutic setting aren't well characterized, and in part because, as discussed above, some effects depend on multiple interactions which must occur within the context of the specific tissue targeted. This work explores this fourth avenue in the bone repair context by using small molecules to disrupt the paracrine signaling loop between MSCs, myeloma cells, osteoblasts, and osteoclasts.

MSCs and Wnt Signaling

At the beginning of this work, Gregory *et al.*⁴³ had just discovered that the secreted glycoprotein, Dkk-1, an antagonist of the Wnt pathway, was a major regulator of MSC proliferation. Wnt signaling is traditionally considered a proliferative stimulus, based on studies conducted in osteoblastic and tumor cell lines^{44,45,46,47}, but the pathway was not well understood in MSCs. Wnts are a family of secreted glycoproteins that transduce extracellular signals via the frizzled family of receptors and the low-density lipoprotein-related protein (LRP) co-receptors. The Wnt signaling pathway (Figure II-1) acts intracellularly via β -catenin, initiating

a signal transduction cascade from genes which contain TCF response elements. In the absence of Wnt proteins, cytoplasmic β -catenin is phosphorylated by a multi-protein complex containing axin, the adenomatous polyposis coli protein, and glycogen synthase kinase 3 (GSK3 β) which targets β -catenin for degradation by the proteasome. Upon binding of Wnt to frizzled, GSK3 β is inactivated, and β -catenin levels rise. β -catenin levels are reduced by Dkk1, which binds to LRP and Kremen, triggering internalization of LRP and preventing association of LRP with Wnt. This allows GSK3 β to remain active in tagging β -catenin for degradation.

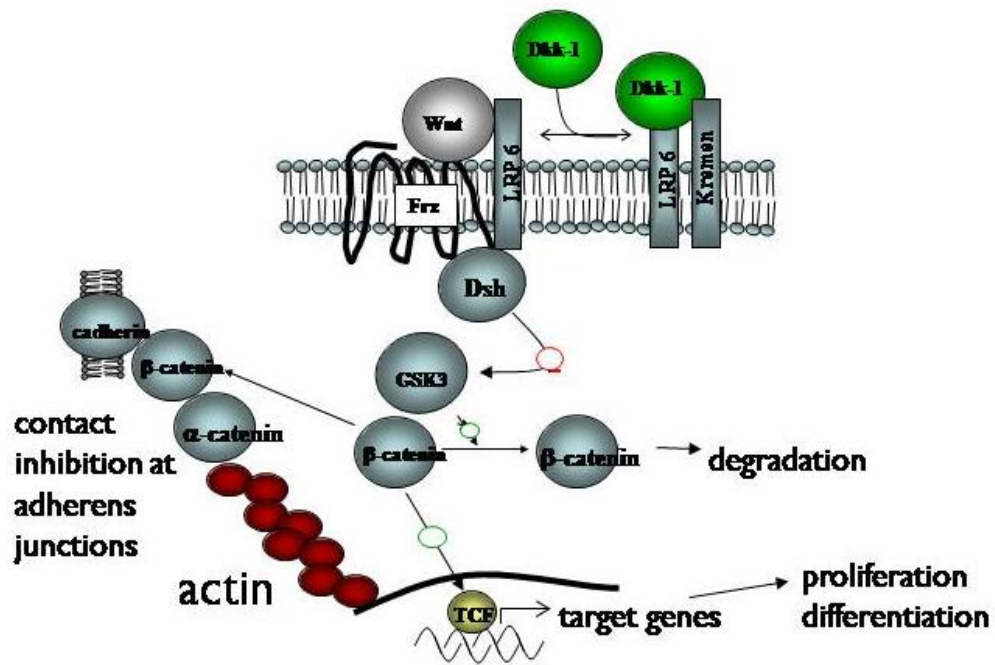


Figure II-1 - The Wnt Pathway

The role of Wnt in bone formation has been shown by two studies: patients with osteoporosis-pseudoglioma syndrome have an inactivating mutation in the Wnt co-receptor LRP5⁴⁸, whereas high bone mass syndrome is associated with a mutation which activates LRP5⁴⁹. Additionally, it has been shown that Dkk1 promotes cell cycle entry and MSC self-renewal⁴³. Because Dkk1 is an antagonist of canonical Wnt signaling⁵⁰, if one considers a stem cell to choose between continued proliferation or initiation of a differentiation program, the effects of

Dkk1 on MSCs are not consistent with the traditional view of positive Wnt signaling being a proliferative stimulus. In order for Dkk1 to be a useful agent for *in vitro* expansion of MSCs, it would have to inhibit differentiation, which implies that Wnt signaling promotes differentiation, not proliferation.

Further evidence supporting this activity was presented by Rawadi *et al.*⁴⁸ Their work presented the idea that Wnt signaling promoted osteogenesis through an autocrine mechanism. In response to osteogenic stimuli such as release of bone morphogenetic protein (BMP), some cells would begin to secrete Wnt3a, which initiated transcription of osteogenic genes and led to further Wnt3a secretion by neighboring cells. Based on these observations, we developed a model of MSC osteogenesis wherein MSCs initiate their osteogenic program upon exposure to Wnt, or, alternatively, relief from Dkk1 exposure. *In vitro* culture of MSCs under osteogenic conditions provided an easy means to examine the effects of modulating this pathway. My work connected the relationship between Dkk1 and osteolytic lesions to the action of Dkk1 on MSCs and was published in 2005²⁴.

MSCs and Multiple Myeloma

Multiple myeloma is a progressive hematologic disease and the second most prevalent blood cancer after non-Hodgkin's lymphoma. The disease is characterized by excessive numbers of abnormal plasma cells

in the bone marrow and overproduction of intact monoclonal immunoglobulin (IgG, IgA, IgD, or IgE) or Bence-Jones protein (free monoclonal κ and λ light chains)⁵¹. Hypercalcemia secondary to bone resorption, anemia due to tumor growth in bone marrow, renal damage due to elevated serum paraprotein, and increased susceptibility to bacterial infection due to impaired production of normal immunoglobulin are common clinical manifestations of MM. It is often also characterized by diffuse osteoporosis, usually in the pelvis, spine, ribs, and skull⁵². (Figure II-2)

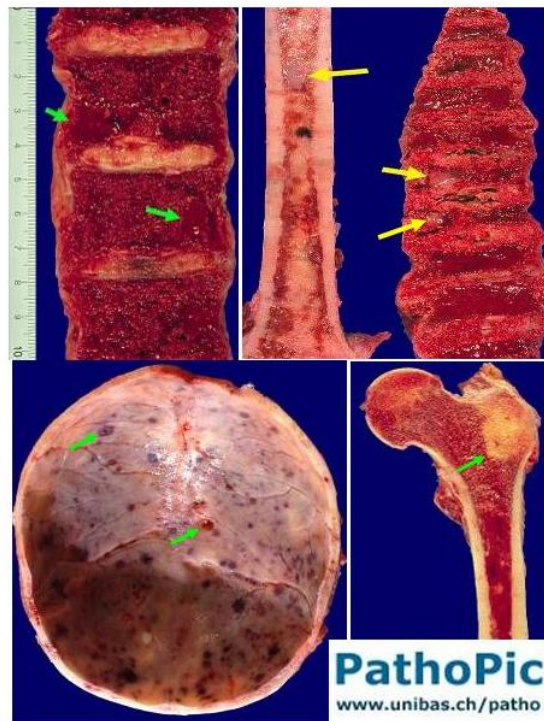


Figure II-2 - Osteolytic Lesions in Multiple Myeloma

MM cells specifically adhere to MSCs where they are exposed to higher levels of IL6 and receptor activator of nuclear factor κ B ligand (RankL), stimulating the proliferation of the tumor and the impairment of bone repair. Osteolytic lesions in MM are the major source of morbidity and occur where B-cell plasmacytomas stimulate bone resorption and angiogenesis⁵³. In patients with MM, the cancer cells are found in close association with sites of active bone resorption and the interactions among myeloma cells, osteoclasts, MSCs, and osteoblasts lead to osteolytic bone disease. MSCs differentiate into osteoblasts at the lesion

sites and attempt to repair the lesions, but cannot restore homeostasis, as the microenvironmental signals have become unbalanced. There's too much RankL stimulating osteoclasts and also too much Dkk1 inhibiting osteoblast differentiation. Because of this imbalance, adequate bone repair does not occur in myeloma patients.

In 2004, Tian *et al.*⁵⁴ found a correlation between increased serum Dkk1 levels and the presence of osteolytic bone lesions in MM patients. In normal human bone, osteoblasts are responsible for initiating bone formation, while osteoclasts promote bone resorption, in a process that operates continually throughout adult life⁵⁵. The relative actions of these two cell types promote bone turnover and effect bone repair. Osteoclasts and osteoblasts regulate each other's activity through proteins belonging to the TGF and TNF cytokine superfamilies, such as bone morphogenetic proteins (BMPs), osteoprotegerin (OPG), and RankL⁵⁶. Osteoclast maturation depends on RankL binding to Rank receptors on osteoclast precursors, whereas osteoblast maturation depends upon BMP and autocrine Wnt signaling. Under normal conditions RankL is mainly produced by osteoblasts and MSCs; However, RankL is also produced by lymphocytes in pathological conditions such as multiple myeloma or rheumatoid arthritis. OPG is a decoy ligand for RankL, produced by osteoblasts. The balance of these osteogenic and osteoclastic inputs determines the balance between bone formation and resorption. When

there is a failure of the coupling between osteoclasts and osteoblasts, normal bone turnover becomes disrupted, weakening or inappropriately depositing bone.

Myeloma Treatment

The current standard of care for multiple myeloma specifies autologous stem cell transplantation and aggressive chemotherapy including dexamethasone and thalidomide⁵⁷. For relapsed disease, the most recent additions to the standard of care include pegylated doxorubicin and bortezomib⁵⁸, and there are some Phase I and II trials using bortezomib, lenalidomide, dexamethasone, and cyclophosphamide which reported 100% response at the 2008 meeting of the American Society for Hematology.

As promising as these developments are, however, they only address the tumor cells, not the tumor-promoting microenvironment, and thus have little effect on the bone damage which is the major cause of disease-associated morbidity. Bisphosphonates are a form of supportive therapy that works by inhibiting bone resorption, and while this helps slow the progression of the disease, it has no effect on regrowth of lesions in the context of Dkk1-inhibited osteoblast activity⁵⁹. This work examines a therapeutic intervention targeted towards the microenvironment in which bone repair is inhibited and MM cell growth is promoted by targeting the interaction between MSCs and MM.

Model	Cell Administration	Radiation	Induction time (weeks)	tissue analyzed	% engraftment
5TGM1	IV	none	10	bone	60%
5THL	IV	none	8	bone	60%
ARH-77	IV	none	3-4	tumor	100%
CD1/RPMI8226	s.c.	none	2	tumor	100%
CAG-MM	IV	3 cGy	1-2	tumor	not given
BNX/RPMI8226	s.c.	None	4	tumor	not given
NODSCID/RPMI8226-S-GFP	iv	3 cGy	3-4	tumor, tissues, bone marrow via fluorescence	99%

Table II-2 - Animal Models of Multiple Myeloma^{59,60,61,62,63,64,65,66,67,68,69,70,71,72,73,74,75,76}

Animal models of multiple myeloma

The existing mouse models for MM are shown in Table II-2. At the time of this work, only one model was available for examining the effects of myeloma on bone, and this model required the implantation of human fetal bone and the use of primary human MM cells⁶³. The majority of the models focus on the proliferation of MM cells, and though Yaccoby et; al. have since refined their model to use rabbit bone instead of human⁷⁸, the usefulness of the model remains limited due to the technical skill needed to set up this model. The most recent development in modeling the disease process of MM uses tibial injections of luciferase-expressing MM cells and follows tumor growth via in vivo imaging and bone effects via micro CT⁶⁰. The course of development of lesions in this model closely

parallels the lesions found in the model discussed in this work. As previous work has shown that interactions between MSCs and MM cells support the proliferation of myeloma,^{79,80,81} the model discussed here provides an ideal context in which to study MSC-myeloma interactions.

II. Dkk1 in MSC differentiation

INTRODUCTION

In 2003, Gregory et al⁴³ found Dkk1, a soluble Wnt antagonist, to be a major regulator of MSC proliferation and Tian et al⁸². (2004) found a correlation between increased serum Dkk1 levels and the presence of osteolytic bone lesions in multiple myeloma (MM) patients. The myeloma studies implicated MSCs in the pathology of MM specifically, but in the context of the work we had been doing on MSCs and Dkk1, a more general role of MSCs in conditions where bone repair is defective became apparent. My hypothesis is that aberrant Wnt signaling in MSCs can lead to bone disorders as a result of defective repair.

Traditionally, Wnt signaling acts within diverse microenvironmental niches to maintain self-renewal of stem cells^{45,83}. The current understanding of the signaling process is that Wnt proteins secreted from neighboring cells bind to Frizzled and LRP proteins on the cell membrane⁴⁵. A relay of scaffolding proteins transduces the signal to the intracellular environment, inhibiting GSK3 β and slowing β -catenin degradation. This leads to β -catenin entering the nucleus and binding to TCF whereupon transcription of Wnt target genes takes place. Wnt signaling is regulated by expression of the receptors and ligands, which are themselves regulated by Wnt signaling, resulting in a feedback loop which maintains the right balance between proliferation and

differentiation. The Wnt proteins such as Wnt3 and Wnt1 transduce signals through this mechanism, called the canonical pathway. Wnt signaling also works through a non-canonical pathway in which the receptor tyrosine kinases ROR1 and 2 and Ryk bind Wnt via their extracellular Wnt binding domains. Wnt5a and Wnt11 are examples of Wnts which can work non-canonically and either suppress canonical Wnt signaling or have a β -catenin-independent effect⁴⁵.

Structurally, Wnt proteins are highly glycosylated proteins which have a secretion signal sequence and a series of conserved cysteines which are a site of palmitoylation. (Figure II-1) The palmitoylation is thought to affect the partitioning of the protein within the niche, ensuring that the potent effects of the protein are spatially restrained. Temporal restraint of Wnt signaling is also achieved due to the inherent instability of the proteins⁴⁶.

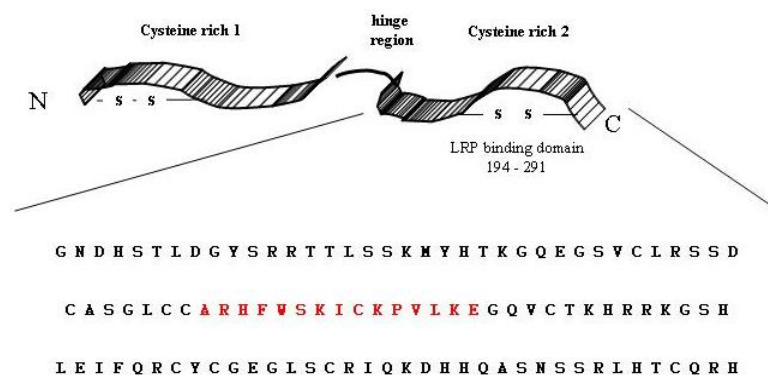


Figure II-1 - Dkk1 structural representation. Sequence indicates the position of bioactive peptides which block Dkk1 activity when

antibodies are directed to them. Figure from Gregory *et al.*, used by permission⁴³.

This work began with a study of the effect of Dkk1 on MSCs because Gregory *et al.*⁴³ had just discovered that the secreted glycoprotein, Dkk-1 (Figure II-1), had a significant role in MSC differentiation and cell-cycle renewal. Our initial studies focused on using Dkk1-derived compounds to manipulate the WNT pathway in MSCs. Because prior work in our lab had shown the expression of WNT pathway genes in MSCs, but the biological relevance of this pathway in MSCs remained not well understood, my initial work aimed to dissect the pathway as it operates in MSCs and examine how the WNT pathway functioned in the context of MSC differentiation.

My three specific aims were: (i) test which part of Dkk-1 binds to MSCs (ii) make peptide agonists/antagonists for control of MSCs and (iii) develop an assay for the effect of these agents on MSC differentiation.

MATERIALS AND METHODS

Dkk1 cell -binding assay

MSCs were cultured as previously described, and grown to 70% confluence. The expression plasmid pcDNA3.1 (Invitrogen, Carlsbad, CA, <http://www.invitrogen.com>) was used as the expression vector and RT-

PCR on RNA extracted from MSCs was used as the source of the genes to be cloned. The *in vitro* transcription and translation was performed using and *in vitro* transcription and translation kit (TnT, Roche, Indianapolis, <http://www.roche.com>), according to manufacturer instructions. Briefly, 10 ng DNA were added to 50 μ L reticulocyte lysate as supplied. One micromolar S^{35} methionine and tRNA charged with biotinylated amino acids were added as indicated. MSC cultures were washed with PBS, the radiolabeled Dkk1 was added in 5 mLs PBS, and the cultures were incubated for 30 minutes with gentle shaking at room temperature. The cultures were then washed again with PBS and the cells were lifted by scraping. The cells were added to 3 mLs scintillation fluid and read in a scintillation counter.

Radioligand binding assay

Superparamagnetic iron oxide beads conjugated to streptavidin were added to magnetic flow columns (QuadroMACS, Miltenyi Biotec Inc., Auburn CA) and equilibrated according to manufacturer recommendations. Fifty microliters of each transcription and translation reaction was used in column loading and ligand binding steps. The resulting fractions were analyzed by SDS-PAGE (NuPAGE, Invitrogen) and visualized by radiography using Kodak X-ray film.'

Spectrophotometry

All reagents were purchased from Sigma–Aldrich (St. Louis, MO). Alizarin Red S (ARS) (40 mM) was prepared in dH₂O and the pH was adjusted to 4.1 using 10% (v/v) ammonium hydroxide. Scanning spectrophotometry was achieved using a dual-beam instrument at 25 C (Beckman Coulter DU 640) and 1-cm-path-length acrylic cuvettes (Fisher Lifesciences). A 96-well plate reader (Benchmark Model, Bio-Rad Laboratories, Hercules, CA) was employed to measure absorbance during the assay. Duplicate plating demonstrated that error caused by pipetting and debris contributed to less than 10% variability. ARS solutions in cetylpyridinium chloride (CPC) (10% w/v) were prepared in 10 mM Na₂PO₄ (pH 7.0) and scanned as above.

Tissue culture

Human MSCs were prepared from bone marrow aspirates and cultured as previously described^{84,85}. Cells were recovered by incubation with 0.25% (w/v) trypsin and 1 mM EDTA (Invitrogen, Carlsbad, CA) for 5–7 min at 37 C, replated at 5000 cells per cm² in 10-cm² wells of six-well plates (Nunc, Fisher Lifesciences), and cultured until confluent.

Mineralization Protocol

Mineralization was induced on confluent monolayers by addition of α -MEM containing 20% (v/v) FCS, 100 $\mu\text{g} \cdot \text{mL}^{-1}$ streptomycin, 100 U mL^{-1}

penicillin, and 2 mM glutamine with osteogenic supplements, 1 mM sodium glycerophosphate, 50 mM Na ascorbate, and, in most cases, 10^{-1} M dexamethasone (all Sigma-Aldrich). Cultures were incubated at 37 °C with 5% (v/v) CO₂ with changes of medium every 4 days.

Detection and quantification of mineralization

Monolayers in 6-well plates (10 cm² per well) were washed with PBS and fixed in 10% (v/v) formaldehyde (Sigma-Aldrich) at room temperature for 15 min. The monolayers were then washed twice with excess dH₂O prior to addition of 1 mL of 40 mM ARS (pH 4.1) per well. The plates were incubated at room temperature for 20 min with gentle shaking. After aspiration of the unincorporated dye, the wells were washed four times with 4 mL dH₂O while shaking for 5 min. The plates were then left at an angle for 2 min to facilitate removal of excess water, re-aspirated, and then stored at -20 °C prior to dye extraction. Stained monolayers were visualized by phase microscopy using an inverted microscope (Nikon). For quantification of staining, 800 µL 10% (v/v) acetic acid was added to each well, and the plate was incubated at room temperature for 30 min with shaking. The monolayer, now loosely attached to the plate, was then scraped from the plate with a cell scraper (Fisher Lifesciences) and transferred with 10% (v/v) acetic acid to a 1.5-mL microcentrifuge tube with a wide-mouth pipette. After vortexing for 30 s, the slurry was overlaid with 500 µL mineral oil (Sigma-Aldrich), heated to

exactly 85 C for 10 min, and transferred to ice for 5 min. Care was taken at this point to avoid opening of the tubes until fully cooled. The slurry was then centrifuged at 20,000 x *g* for 15 min and 500 μ L of the supernatant was removed to a new 1.5-mL microcentrifuge tube. Then 200 μ L of 10% (v/v) ammonium hydroxide was added to neutralize the acid. In some cases, the pH was measured at this point to ensure that it was between 4.1 and 4.5. Aliquots (150 μ L) of the supernatant were read in triplicate at 405 nm in 96-well format using opaque-walled, transparent-bottomed plates (Fisher Lifesciences). Statistical analyses on three to six readings were carried out using Student's *t* test, and *p* values of less than 0.05 were considered significant. For CPC extractions, an adaptation of the protocol described in Stanford et al.²⁰ was followed. Monolayers on 6-well plates were washed five times in PBS and then fixed with ice-cold 70% ethanol for 1 h. The monolayers were then washed three times with dH₂O. ARS was extracted from the monolayer by incubation of the monolayers in 1 mL CPC buffer for 1 h. The dye was then removed and 200- μ L aliquots were transferred to a 96-well plate prior to reading at 550 nm.

Arsenazo III calcium assay

To prevent contamination, all solutions were prepared using ultrapure reagents (Sigma), HPLC-grade dH₂O, and sterile plasticware. Unfixed and unstained osteogenic monolayers of hMSCs were processed

by acid extraction and neutralization as described above. In a 96-well microtiter plate, 10 μ L of the extract was added to 100 μ M Arsenazo III in 90 μ L of dH₂O. After 10 min at room temperature, the absorbance of the samples was measured at 595 nm. Measurements were carried out in triplicate and for most of the samples, dilutions ranging from 10 to 0.3% (w/v) in neutralized extraction buffer were necessary to allow measurement within the linear range of the assay.

RESULTS

To continue with the work of Gregory *et al.* showing the temporally-restricted expression of Wnt proteins and the effect of Dkk1 on cell cycle of MSCs, I first wanted to establish that Dkk1 bound directly to MSCs through the LRP6 receptor. The most simple and direct approach involved using the MSCs as an affinity matrix to bind radiolabeled Dkk1 introduced into the medium. I first cloned the *DKK1* gene from MSCs into an expression plasmid, sequenced the constructs to confirm I had the correct gene and then prepared some mutant versions of the gene. One mutant had a cysteine to alanine mutation in the binding site (C→A), and I also prepared two truncated versions, one consisting of only the first cysteine-rich region (Cys1) and the other consisting of only the second cysteine -rich region (Cys2). Because Cys1 had been shown to have no effect in work done in *Xenopus*, we used it as our non-binding control product. After sequencing these to confirm their sequence was correct, I

used the constructs in an *in vitro* transcription and translation reaction to produce radiolabeled protein. Equal volumes of each translation reaction was added to MSCs, and after thorough washing, the residual radioactivity of the cells was measured. A schematic of the experiment is shown in Figure II-2a. To exclude the possibility that the binding was non-specific, mutant proteins devoid of binding activity were panned over MSCs. We found that labeled wild-type Dkk1 left approximately 4 times as much residual radioactivity as either the C->A mutant or the Cys1 truncation product. These results indicate that Dkk1 binds to MSCs in a manner dependent on structural features associated with LRP - Dkk1 interaction. The results are shown in Figure II-2b.

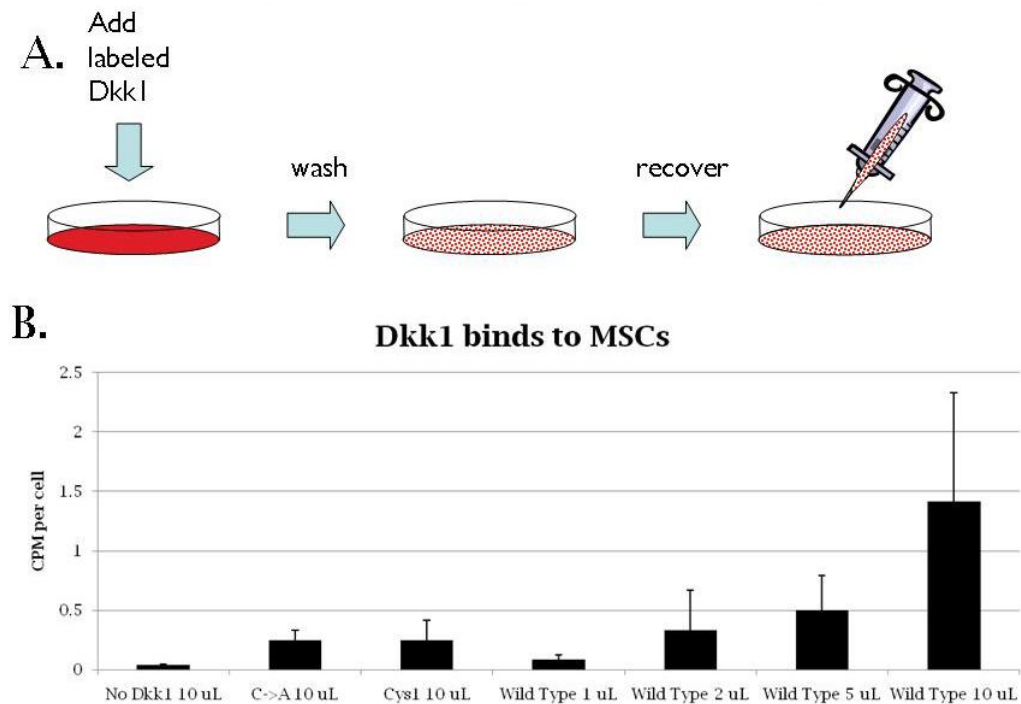


Figure II-2 - Dkk1 binding assay (A) Assay schematic (B) retained radioactivity is highest when wild-type full-length Dkk1 is used.

To more directly demonstrate LRP receptor interaction, I cloned the gene for LRP6 from MSCs and prepared an *in vitro* binding experiment. In the experiment shown in Figure II-3a, streptavidin-labeled paramagnetic iron beads were loaded on a column resting in a magnet. LRP6 was prepared by *in vitro* transcription and translation in the presence of S^{35} -methionine and tRNA coupled to biotinylated lysine and then applied to the column. After washing out unbound material, similarly prepared, unbiotinylated Dkk1 was prepared and run through the LRP6-functionalized columns. Further washing was done to remove

nonspecifically attached material and then the columns were removed from the magnet to elute bound antigen. The samples were then separated by SDS-PAGE and visualized by radiography on X-ray film. A band in the eluate fraction of the same molecular weight as the unfractionated IVT product indicated that Dkk1 was bound in the column. Flowing a 1:10 (vol:vol) mixture of radiolabeled full length Dkk1 and cold Cys2 mutant protein resulted in decreased Dkk1 in the eluate with a concomitant increase in flowthrough signal (Figure II-3b). The data

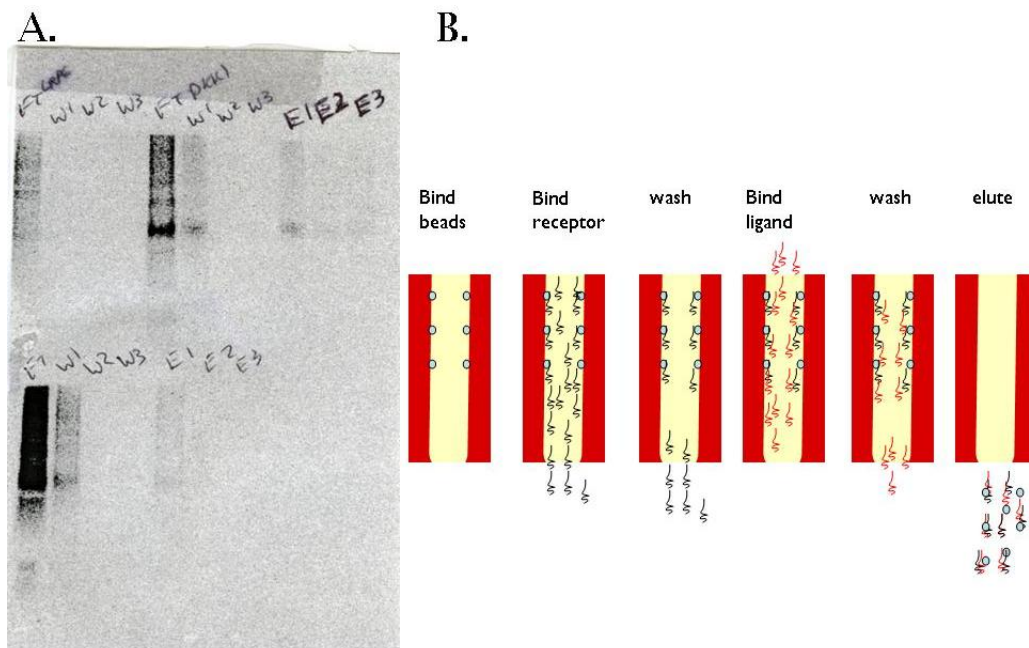


Figure II-3 - Radioligand binding assay. Panel A (top row): Dkk1/LRP5 binding assay with wild type Dkk1: lane 1, flow through fraction after LRP application; lane 2-4, washes; lane 5, flow through fraction after Dkk1 application; lanes 6-8 washes; lane 9-11, elution. Panel A (bottom row): Dkk1/LRP5 binding assay with mixed wild type Dkk1 and Cys2 mutant protein.

from the ligand binding experiments led to development of Dkk1 agonist and antagonist peptides. The more promising panel of peptides was used for Dkk1 blocking experiments described in Gregory et al (2005)⁸⁶.

Having shown that MSCs expressed the receptor for Dkk1, and that Dkk1 bound to the appropriate receptor, we were ready to examine the biological effect of Dkk1 on MSCs. Because previous work had been done in mice, we needed to show that Dkk1 had a direct effect on human MSCs. To this end, we needed to develop a model system in which the biological effects of Dkk1 exposure could be studied. Since the previous binding assays were time and labor intensive, we developed a fast and convenient assay that lent itself to testing a wide variety of compounds. Earlier, in Gregory et al. (2004), we developed a method for staining and quantifying mineralized deposits in MSC osteogenic culture. This culture system is what we used as my initial semi-quantitative model of osteogenesis. In the existing method, MSCs were cultured in osteogenic medium containing a source of phosphate, ascorbic acid, and dexamethasone in a rich medium such as α -MEM containing fetal calf serum (FCS)¹⁹. Mineralization was assessed by Alizarin red S (ARS) incorporation. This assay was only semi-quantitative, so we developed a sensitive quantitative assay for calcium (Figure II-4a). Using this assay, we confirmed that the calcium content of the mineralized monolayers was correlated to the extent of recoverable ARS stain (Figure II-4b). When

compared with acid extraction of ARS, the Arsenazo III assay produced equivalent data but, due to the low and narrow linear range of the Arsenazo III assay (0 to 80 μM), extensive dilution of the samples was required which resulted in a high level of variation (Figure II-4b). The samples were fixed with 10% buffered formalin in the ARS assay, but this did not appear to affect sensitivity or reproducibility since the acid extraction results were comparable to the Arsenazo III measurements that were carried out on unfixed hMSCs. At this point we had a quantitative assay, but not a fast one, as it required 21 days to complete.

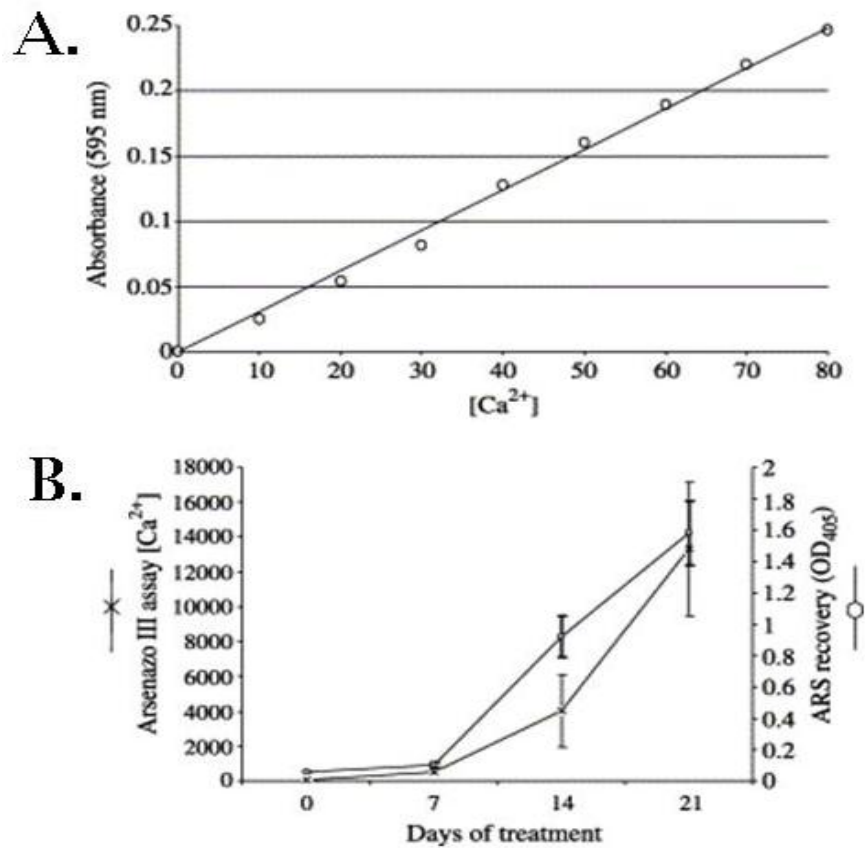


Figure II-4 - Comparison of ARS and arsenazo III calcium assays. (A) Linear range of arsenazo III assay, showing narrow micromolar range. (B) Comparison of arsenazo III with ARS in quantitation of calcium produced during MSC differentiation. Assay performed as previously described⁸⁷.

Alkaline phosphatase (ALP) is a product of early osteoprogenitors, used to release inorganic phosphate moieties from organic molecules so that they may be incorporated into hydroxylapatite, the major inorganic component of bone. We knew from earlier work that MSCs reached maximal ALP expression as soon as day

10 of osteogenic culture, so since this enzyme remains membrane-bound and is not secreted in large amounts, it seemed like a good candidate for a more rapid marker of osteogenesis. Examining osteogenesis via ALP is a relatively rapid and easy to method and had the further advantage of providing results relative to cell number, instead of total protein, which is important to prevent results from being skewed by test compounds which affect ECM secretion. The assay schematic is depicted in Figure II-5. Confluent layers of MSCs were washed to remove residual phosphatase activity from the medium and para-nitrophenol phosphate, a colorimetric indicator of phosphatase activity, was added in a Tris-saline buffer at alkaline pH. The change in absorbance at 405 nm over time is measured in a plate reader and then the cells are counted.

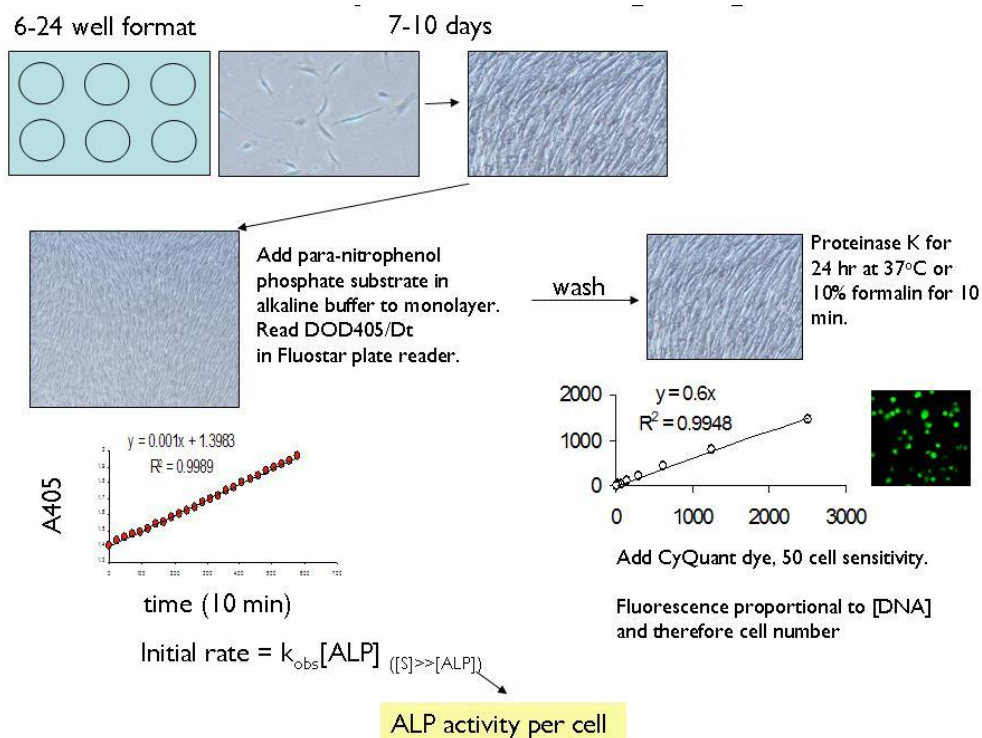


Figure II-5 - In-situ assay for alkaline phosphatase

To correct for variations in cell number among conditions, cells were counted using one of two methods. The nuclei were either stained *in situ* with the CyQuant NF DNA stain (Figure II-6), or the cells were lifted, lysed, and the nuclei were stained in the lysate using CyQuant GR. We counted the cells stained *in situ* using an automated image analysis routine and quantitated the cells in the lysate by correlating fluorescence measurements of the lysate with readings on lysates prepared from a known number of cells. We found that the CyQuant counts correlated well with manual counting of cells using a hemacytometer (Figure II-7).

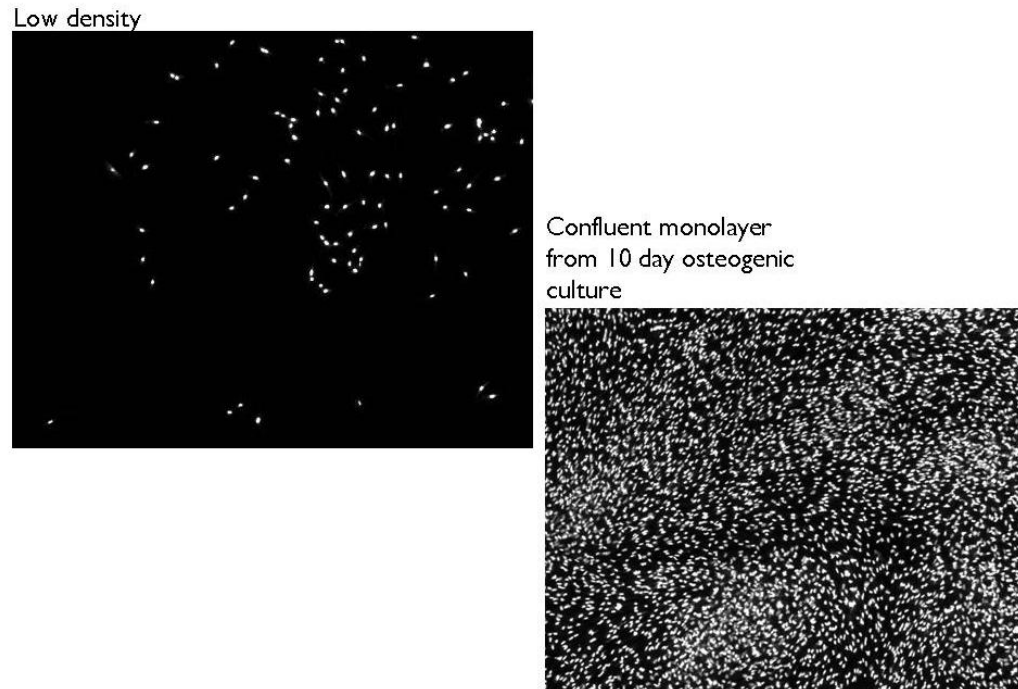


Figure II-6 - Fluorescent microscopy of in situ stained cell nuclei with CyQuant NF.

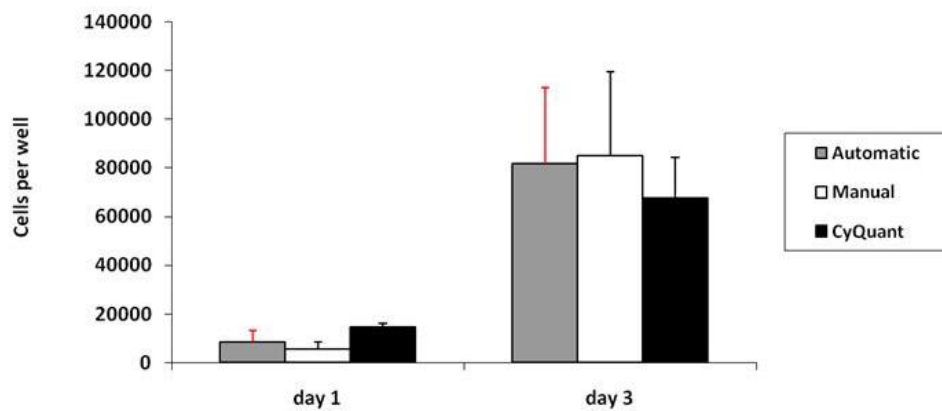


Figure II-7 - Comparison of in situ counting methods

We then compared this assay with ARS staining. MSCs were cultured for 10 and 24 days then ALP or mineral deposition was measured. ALP levels per cell at day 10 (Figure II-8a), were of similar relative magnitude to recoverable ARS stain at day 24. (Figure II-8b)

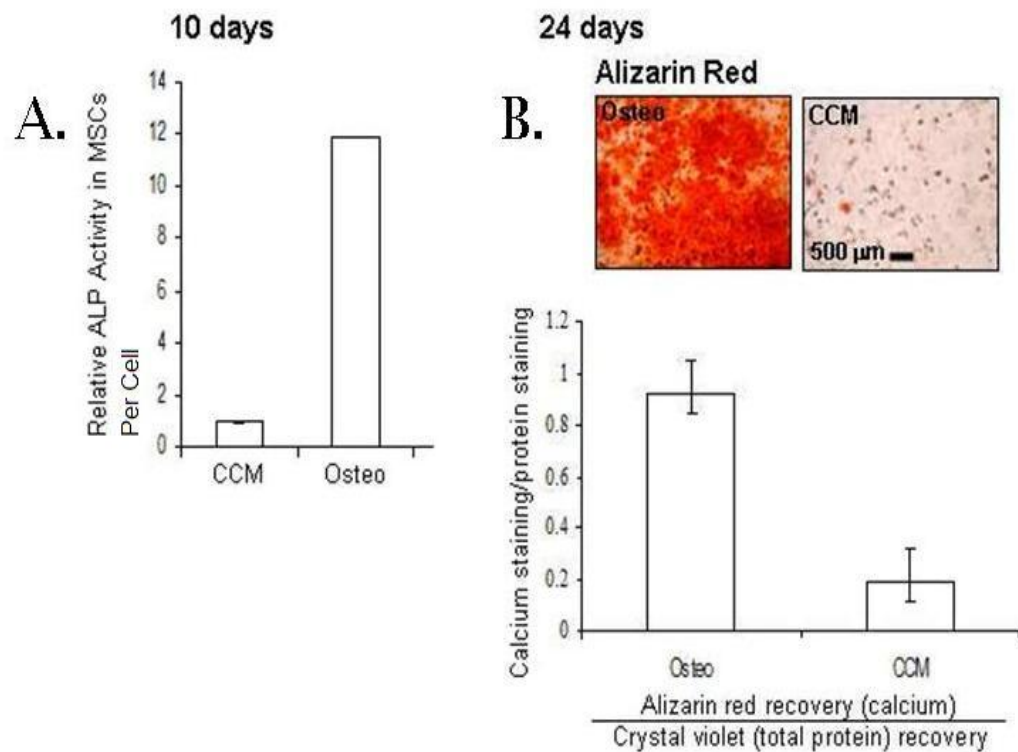


Figure II-8- Comparison of alkaline phosphatase assay with ARS. (A) Relative ALP activity in MSCs cultured in expansion medium and differentiation medium after 10 days. The units for relative activity are shown as the change in absorbance at 450 nm wavelength per minute per cell. (B) Calcium accumulation by MSCs cultured in expansion medium and differentiation medium after 21 days. Assay performed as previously described⁸⁷. The units are relative absorbance values.

CONCLUSION

The signals that regulate the transitions between the stem cell state, wherein any given cell is mostly quiescent but the population is capable of self-renewing for the life of the organism, and the progenitor

state, wherein the cells are capable of rapidly dividing yet retain multipotentiality, seemed like they must hold the keys to advancement of regenerative medicine, and Dkk1 looked particularly like one of these signals. My work on Wnt signaling in MSCs began as a continuation of prior work showing Dkk1 to play a role in MSC cell division.

Using a radio-ligand binding assay incorporating Dkk1 and LRP6, I first confirmed the *Xenopus* structural results in MSCs, and then we developed peptides for use in a receptor blocking strategy. My initial experiments indicated that MSCs express LRP6, so I used the cells as an affinity matrix to bind soluble full-length Dkk1. These experiments showed that MSCs specifically bound soluble Dkk1. To confirm that the interaction I measured was between Dkk1 and the LRP receptor, both as cloned from MSCs, I cloned the gene for LRP6 into an expression vector, transcribed, translated, and labeled the gene *in vitro*, then loaded the labeled translation product on a column, thereby forming an affinity column for doing Dkk1 binding assays. I localized the binding to the Cys2 region of Dkk1 by preparing deletion mutants of the full-length transcript and then using them to compete away the binding of the full-length translation product. This evidence that MSCs express both Dkk1 and LRP6 and the proteins interact in a cell-based and cell free assay system supports the idea that Dkk1 acts through the Wnt pathway. The results showing that *in vitro* osteogenesis was inhibited in the presence

of recombinant Dkk1, an effect which was relieved by GSK3 β inhibition, is consistent with this idea. Although these results did not appear to agree with the conventional wisdom that Wnt signaling promotes proliferation, these findings have since gained considerable experimental support. In fact, this pathway is now known to be important in many bone disorders, particularly cancer-induced osteolytic lesion formation^{24,70,82,88,89,90,91,92,93,94,95,96}. These results indicated the first aim had been achieved: to validate that the LRP-Dkk1 interaction exists in hMSCs and determine the active portions of the Dkk1 protein.

Based on this work, peptides were prepared from the Cys2 region of Dkk1. These peptides were found to increase the proliferation of MSCs *in vitro*⁸⁶ and selected for use in an *in vivo* study. It was eventually found, through western blotting of various mouse excreta, that the animals were clearing the peptides in less than an hour. These pharmacokinetic results were discouraging and precluded the utilization of small peptide agonists of Dkk1 for the *in vivo* mobilization of MSCs, so we then turned our focus towards small molecules which inhibit GSK3 β and I worked to develop model systems in which their effects could be studied. These results indicated partial success at the second aim: to generate peptide agonists/antagonists of the Wnt pathway.

When this work began, the standard assay for osteogenic differentiation involved culturing MSCs under conditions conducive to

development into bone progenitor cells and then staining the cultures for deposited mineralized matrix¹⁷. However, as these assays were being done, they took weeks to accomplish, were not particularly quantitative, and required large amounts of starting material. A more high throughput and sensitive assay was required to efficiently find osteogenic effectors. To make faster progress, a faster in vitro assay for osteogenesis that allowed for rapid screening of small molecule modulators of Wnt activity by measuring membrane-associated alkaline phosphatase (ALP) was designed. Using this assay, several small molecule modulators of the Wnt pathway were screened. We expected that activation of Wnt signaling would promote osteogenesis, however, initial experiments showed that Wnt activation under osteogenic conditions only modestly promoted osteogenesis. Later, we found that inhibition of Wnt with additional Dkk1 inhibited osteogenesis, and, in that context, Wnt activation restored normal osteogenesis. These findings at first seemed at odds with the results reported by DeBoer *et al*⁹⁷, on inhibition of osteogenesis by Wnt, but upon further examination are not actually inconsistent, considering the biphasic effect of Li⁺ ions on osteogenesis⁹⁸. Because these results indicate that the effects of Dkk1 are most easily distinguished in the context of disrupted bone homeostasis, a model system in which osteogenesis was impaired was developed so that we could examine removal of inhibition. The practical importance of the work for aim three was to establish MSC differentiation as a model system for the study of

bone disorders and to establish a rapid quantitative assay for use with the model. The *in vitro* osteogenesis model presents an experimentally accessible system which has been characterized extensively in terms of the gene expression profile and mineral deposition, two clinically relevant parameters of bone formation. In contrast to existing methods for the assay of osteogenesis of MSCs, this assay is both more rapid and quantitative. The results obtained using this assay correlated well with established assays for osteogenesis but extended the utility of the model by adapting it to a more high-throughput format.

III. MSCs and Multiple Myeloma

INTRODUCTION

As we were examining how MSC osteogenesis is regulated, Tian et al.⁸² demonstrated that Dkk1 is produced at high levels by MM cells from patients with osteolytic lesions. He concluded that MM-derived Dkk1 inhibited differentiation of bone marrow stromal cells into osteoblasts. Considered in the context of our results that Dkk1 inhibits differentiation of MSCs, the results raised the possibility that Dkk1 may be involved in osteolytic lesion formation in MM by tipping the osteoblasts to osteoclast ratio in favor of bone resorption. These observations formed the basis for my next model of osteogenesis. The aims of this section of the work were to develop and characterize an assay for osteogenesis in which the osteogenic effects of modulating Wnt could be studied, examine the interaction between MSCs and MM cells, and develop a therapeutic strategy for disrupting the MSC-MM interaction which could be adapted for *in vivo* use.

In normal human bone, osteoblasts are responsible for initiating bone formation, while osteoclasts promote bone resorption, in a process that operates continually throughout adult life⁵⁵. The relative actions of these two cell types promote bone turnover and effect bone repair. Osteoclasts and osteoblasts regulate each other's activity through proteins belonging to the TGF and TNF cytokine superfamilies, such as

bone morphogenetic proteins (BMPs), osteoprotegerin (OPG), and receptor activator of nuclear factor κ ligand (RankL)⁵⁶. Osteoclast maturation depends on RankL binding to Rank receptors on osteoclast precursors, whereas osteoblast maturation depends upon BMP and autocrine Wnt signaling⁹⁹. Under normal conditions RankL is mainly produced by osteoblasts and MSCs; However, RankL is also produced by lymphocytes in pathological conditions such as multiple myeloma or rheumatoid arthritis^{56,100}. OPG is a decoy ligand for RankL, produced by osteoblasts. The balance of these osteogenic and osteoclastic inputs determines the balance between bone formation and resorption. When there is a failure of the coupling between osteoclasts and osteoblasts, normal bone turnover becomes disrupted, weakening or inappropriately depositing bone^{80,89,90}. (

Figure III-1)

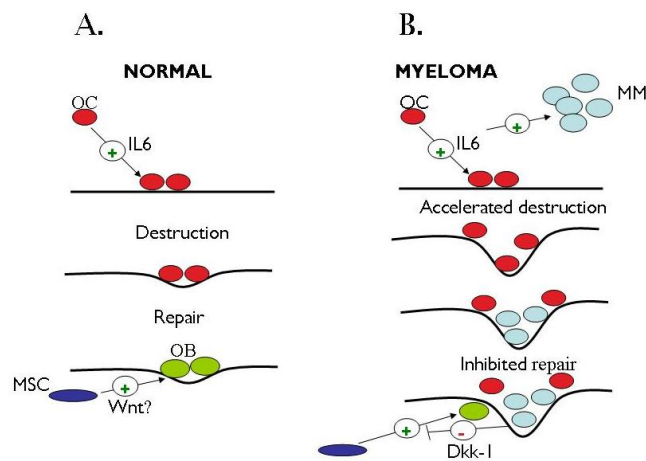


Figure III-1 - Disruption of coupled bone turnover in myeloma

In patients with multiple myeloma, myeloma cells are found in close association with sites of active bone resorption, and the interactions among myeloma cells, osteoclasts, MSCs, and osteoblasts lead to osteolytic bone disease. The presence of MSCs also promotes myeloma cell growth and survival in the bone marrow. Osteolytic lesions in MM are the major source of morbidity and occur where B-cell plasmacytomas stimulate bone resorption and angiogenesis¹⁰¹. MSCs differentiate into osteoblasts at the lesion sites and attempt to repair the lesions by restoring the balance between bone production and resorption. However, adequate bone repair does not occur in myeloma patients¹⁰², in part because of inhibition of repair by Dkk1. Previous work has shown that interactions between MSCs and MM cells support the proliferation of myeloma^{72,100,103,104,105,106,107}. In Gunn *et al.*,²⁴ we showed that an alteration of the bone marrow microenvironment by MM cells explains the formation of osteolytic bone lesions. The MM cells secrete Dkk1, which prevents the MSCs from differentiating into osteoblasts, and the undifferentiated MSCs produce interleukin-6 (IL-6), which stimulates the proliferation of Dkk1-secreting MM cells.

Other work conducted in the Gregory lab while my studies were ongoing examined several approaches to manipulating the Wnt pathway for the promotion of bone repair. LiCl was known to have effects on a wide spectrum of kinases¹⁰⁸, so while well-tolerated *in vivo*, might not

result in the most easily interpretable results in a cell-based assay^{98,109,110}. Dkk1-blocking peptides, in contrast, would be expected to be fairly specific in their mode of action, but are more complicated in their pharmacokinetics, so while applicable in a cell-based assay, were not suitable for use in an animal model¹¹¹. The small molecule GSK3 β inhibitor BIO^{83,112} was appropriately specific and well-tolerated by animals, so it became the agent of choice for manipulating Wnt in this model. We demonstrated that use of a Dkk1-blocking agent, such as 6-bromoindirubin-3'-monoxime (BIO), can release MSCs from the MM proliferation-promoting cycle induced by Dkk1, which may also enable MSCs to repair existing osteolytic lesions.

MATERIALS AND METHODS

Cell Culture

For the preparation and culture of MSCs, we obtained bone marrow aspirates from healthy donors under a protocol approved by the institutional review board. The Tulane Center for Preparation and Distribution of Adult Stem Cells (New Orleans) supplied frozen vials. To recover MSCs, we added thawed vials containing 1×10^6 cells to 25 ml of complete culture medium (CCM) comprised of α -minimum essential medium (Invitrogen, Carlsbad, CA, <http://www.invitrogen.com>), 2 mM L-glutamine (Invitrogen), and 20% fetal bovine serum (FBS; Atlanta Biologicals, Norcross, GA, <http://www.atlantabio.com>) per 145-cm² plate

(Corning Life Sciences, Pittsburgh, <http://www.corning.com/lifesciences>). Our cell culture core facility selected batches of FBS for rapid growth of cells. For some experiments, we added 100 units per mL penicillin G and 100 $\mu\text{g} \cdot \text{mL}^{-1}$ streptomycin to the CCM. After 1 day, we aspirated the medium, removing nonadherent and nonviable cells, then added fresh medium. Thereafter, we replaced the medium every 2 days. Four to 5 days after initial plating, we detached the cells by adding 0.25% (wt/vol) trypsin and 1 mM EDTA (Invitrogen) for 5 minutes at 37°C. We pelleted MSCs by centrifugation at 453*g* and then re-plated them at the indicated density. We expanded ANBL and XG1 MM cells (kindly provided by John Shaughnessy, University of Arkansas for Medical Sciences, Little Rock, AR) in myeloma medium consisting of RPMI 1640, 10% FBS, 10% MarrowMax supplement, 100 μM pyruvate, 100 units $\cdot \text{mL}^{-1}$ penicillin G, and 100 $\mu\text{g} \cdot \text{mL}^{-1}$ streptomycin (Invitrogen). In some cases, we added 1 ng $\cdot \text{mL}^{-1}$ IL-6 (Sigma, St. Louis, <http://www.sigmaaldrich.com>) to the expansion medium.

Production of Dkk1

We stably transfected COS cells (Fugene 6; Roche, Indianapolis, <http://www.roche.com>) with a construct encoding human Dkk1 in pcDNA3.1 (Invitrogen) and grew them in large-scale cell factories (Cell Factory; Nunc, Roskilde, Denmark, <http://www.nuncbrand.com>) in α -MEM containing 10% (v/v) FBS, 100 $\mu\text{g} \cdot \text{mL}^{-1}$ streptomycin, 100 units per mL

penicillin G, 2 mM glutamine, and 800 $\mu\text{g mL}^{-1}$ G418 (Sigma). At confluency, we transferred the cells to 1 L serum-free medium to allow them to finish metabolizing internalized serum, then transferred them to 1 L serum-free medium for 48 hours. We then dialyzed the Dkk1-containing medium into 10 mM ammonium carbonate (pH 8.0) (Sigma) using a customized large-scale dialysis apparatus and concentrated it by partial freeze-drying (ThermoSavant ModulyoD; Thermo Electron Corporation, Waltham, MA, <http://www.thermo.com>). We assayed the concentrated sample by Dkk1 enzyme-linked immunosorbent assay (ELISA) [1]. Purity averaged 80%, and yield averaged 4 mg per liter of medium. We produced protein preparations from untransfected COS cells in parallel with the Dkk1 extracts to serve as controls and found that control preparations contained no Dkk1 and had no effect in the mineralization assay (data not shown). We freeze-dried aliquots of Dkk1 at 10 μg per tube and prepared control medium using equivalent volumes.

Mineralization Assay

We plated cells at 5,000 cells per cm^2 in 10- cm^2 six-well plates and allowed them to adhere to the plastic. The next day, we replaced the medium. Two to three days later, the cultures attained approximately 70% confluence, and we started the assay. On day 1, we replaced the medium with mineralization medium consisting of CCM supplemented with 50 $\mu\text{g mL}^{-1}$ L-ascorbic acid and 5 mM β -glycerophosphate (Sigma). Some cultures

received Dkk1, LiCl (Sigma), or BIO (Calbiochem, San Diego, CA, <http://www.emdbiosciences.com>). We then replaced the medium on days 3, 5, 7, and 9. On day 10, we washed the monolayers first with 10 ml phosphate-buffered saline (PBS) and then with 5 ml wash buffer consisting of 100 mM Tris base (pH 10), 100 mM NaCl, and 1 mM MgCl₂ (Sigma). We quantified alkaline phosphatase activity by adding 1 ml paranitrophenol phosphate in diethanolamine buffer (One Step; Pierce, Rockford, IL, <http://www.piercenet.com>) directly onto the monolayer. We monitored light absorbance at 405 nm by spectrophotometry (FLUOstar; BMG Labtech, Durham, NC, <http://www.bmglabtech.com>) and determined reaction rates as the initial rate of change of absorbance of 405 nm light per minute. We normalized reaction rates to cell numbers, which we determined by using fluorescent dye intercalation (CyQuant; Molecular Probes, Eugene, OR, <http://probes.invitrogen.com>) to assay for DNA content. We related cell numbers to DNA content by measuring the fluorescence of a set of samples of known cell number ranging from 10,000 to 625 cells and compared fluorescence of experimental samples to the fluorescence per cell curve to determine the cell number of experimental samples. The mineralized monolayers secreted vast amounts of matrix and required overnight digestion at 37°C with 200 µg mL⁻¹ proteinase K (Invitrogen) in a digestion buffer composed of 100 mM NaCl, 100 mM Tris [pH 8], 10 µM CaCl₂, and 0.005% (v/v) Triton X-100 (Sigma) prior to fluorescence incorporation assay (CyQuant). Due to the

large variation in matrix secretion between donors and experiments, we normalized the assay to cell number rather than to total protein. To validate the measurement of ALP as an osteogenic marker, we exposed confluent cultures to CCM or osteogenic medium for a further 14 days. Using a slight modification of a previous protocol¹⁷, we then stained the cultures with ARS for calcified matrix and back-extracted the stain. Next, we stained the destained monolayers for total protein using Crystal Violet and back-extracted the dye. We calculated the ratio of optical densities of neutralized ARS to crystal violet to get a measure of the degree of mineralization in the cultures and expressed the data as the mean of three assays. The error bars represent the maximum variation possible after ratio calculation.

Preparation of conditioned medium and growth curves

We prepared MSC-conditioned medium (MSC-CM) by collecting CCM exposed for 2 days to confluent cultures of MSCs. We diluted the CCM to 10% FBS with serum-free CCM, then diafiltered at 4°C using a tangential-flow filtration system fitted with 150-cm² polyvinylidene difluoride 5-kDa filters (Millipore, Billerica, MA, <http://www.millipore.com>) against 10 changes of myeloma medium without FBS. We then filtered the medium through a 0.22-µm filter. For proliferation experiments, we plated MM cells at 150 cells per cm² in six-well plates with medium as indicated in Results. For each condition, we harvested cells every 24 hours and then

washed and froze the cells until the end of the experiment, at which time we determined cell numbers by DNA fluorescence incorporation (CyQuant). For IL-6-blocking experiments, we harvested the cells after 4 days. We used IL-6-blocking antibody (cat. no. I2143; Sigma) at $10 \mu\text{g} \cdot \text{mL}^{-1}$ for IL-6-blocking experiments.

Western Blotting

We recovered about 5×10^4 MM cells by centrifugation, counted them using a hemacytometer, washed them in PBS, and then suspended them in Laemmli sample buffer (Invitrogen) with complete protease inhibitor (Roche). We separated the samples on 4%-12% Bis-Tris polyacrylamide using the 4-morpholineethanesulfonic acid buffer system (Novex; Invitrogen). For detection of Dkk1, IL-6, and glyceraldehyde-3-phosphate dehydrogenase (GAPDH), we used R&D AF1096 (R&D Systems, Minneapolis, <http://www.rndsystems.com>), Sigma no. I2143, and Chemicon clone 6C5 (Chemicon, Temecula, CA, <http://www.chemicon.com>), respectively, all at 1:1,000 dilution. We used peroxidase-conjugated secondary antibodies at 1:2,500 dilution and detected the signal as described previously² (Sigma). We normalized load volumes of media to cell number.

Reverse transcription-polymerase chain reaction assay

We carried out conventional reverse transcription-polymerase chain reaction (RT-PCR) assays for IL-6³² and GAPDH² as previously described. We carried out real-time RT-PCR on the ABI Prism 7700 Sequence Detector using the following Assays-on-Demand primer sets: IL-6, Hs00174131_m1; DKK1, Hs00183740_m1. We normalized all expression levels to GAPDH using either Hs99999905_m1 or Endogenous Control no. 4310884E. All reactions used manufacturer-recommended universal cycling parameters. Briefly, we incubated samples for 30 minutes at 60°C to allow reverse transcription to take place, then ran 40 cycles at 94°C for 20 seconds and at 62°C for 1 minute. We defined the critical threshold as 10 standard deviations above the baseline fluorescence of cycles three to 15.

ELISA

We measured the level of IL-6 protein in cell culture supernates by ELISA using a kit (Quantikine; R&D Systems). Osteoprotegerin (OPG) levels were measured by ELISA using MAB8051 as the capture antibody and BAF805 as the detection antibody (R&D Systems) in a sandwich ELISA carried out in surface-treated 96-well plates (Immunomodule; Nunc). Streptavidin-conjugated horseradish peroxidase (R&D Systems and Pierce) was used to bind the biotinylated detection antibody and convert 2,2'-azino-di(3-ethylbenzthiazoline-6-sulfonate) substrate (1-Step ABTS;

Pierce). We derived a quantitative relationship between protein levels and the change in absorbance per minute at 405 nm using the FLUOstar plate reader (BMG Labtech). Recombinant OPG reference material was acquired from R&D Systems.

Microscopy

We labeled MM cells with CellTracker Green (Molecular Probes) and incubated them in an environmentally controlled chamber. We recorded images with a charge-coupled-device camera (ORCA ER; Hamamatsu, Bridgewater, NJ, <http://www.sales.hamamatsu.com>) and controlled microscopic functions with software (METAMORPH; Universal Imaging, Sunnyvale, CA, <http://www.moleculardevices.com>). For immunocytochemical labeling of β -catenin, we cultured MSCs for 4 days on chamber slides, then treated as indicated for 15 hours. We then removed the medium and washed the cells in PBS (Invitrogen) prior to fixation with 4% paraformaldehyde (USB, Cleveland, <http://www.usbweb.com>) for 12 minutes. The cells were then permeabilized and blocked with PBS containing 0.5% (v/v) Triton X-100 (Fisher Scientific, Pittsburgh, <http://www.fishersci.com>) and 0.5% (v/v) goat serum (Chemicon). β -Catenin was detected with a Cy3-conjugated β -catenin mouse monoclonal antibody (Clone 15B8; Sigma) for 90 minutes at a 1:200 dilution in PBS. We washed the slides three times with 1 mL PBS after each step and mounted the slides in Vectashield mounting medium

with 4'-6-diamidino-2-phenylindole (DAPI; Vector Laboratories, Burlingame, CA, <http://www.vectorlabs.com>). We captured images using a fluorescent microscope (Nikon Eclipse E800; Melville, NY, <http://www.nikon.com>) with Spot-RT imaging software (Diagnostic Instruments, Inc., Sterling Heights, MI, <http://www.diaginc.com>), using identical gain and exposure times. We prepared composite figures using Adobe Photoshop (Adobe Systems Incorporated, San Jose, CA, <http://www.adobe.com>) and then processed the composite image to remove background and improve contrast. The image from the red channel only is presented for clarity; however, the DAPI signal did overlay the nuclear β -catenin signal.

RESULTS

In initial experiments, we confirmed that MM cell lines express Dkk1. Two MM cell lines, XG1 and ANBL1, expressed high levels of both the message and the protein (Figure III-2). We then examined the effect of conditioned medium from undifferentiated MSCs (MSC-CM) on expression of Dkk1 by MM cells. We recovered the MSC-CM after a 2-day exposure to confluent MSCs and processed it as detailed in Materials and Methods. Interestingly, MM cells transcribed more Dkk1 in the presence of MSC-CM.

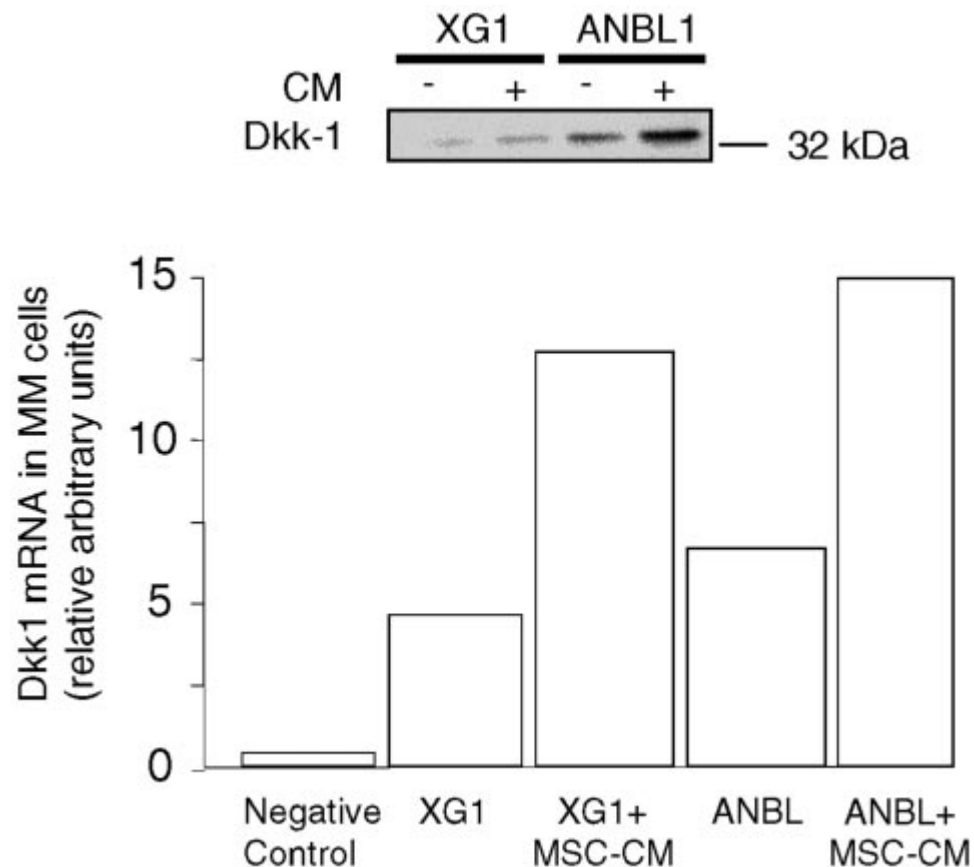


Figure III-2 - Expression of Dkk1 by MM cell lines XG1 and ANBL1. Western blotting of conditioned culture medium from the MM cell lines demonstrates the secretion of Dkk1 in the presence and absence of the <5-kDa fraction of MSC-CM (upper panel). Real-time RT-PCR assays (arbitrary units) for Dkk1 expression by the MM cell lines in the presence and absence of the <5-kDa fraction of MSC-CM (lower panel)

Using the *in vitro* osteogenesis assay described in the results chapter, we treated semi-confluent MSCs with osteogenic medium and either vehicle, Dkk1, inhibitors of GSK3- β , or Dkk1 together with inhibitors of GSK3- β . We found that high levels of Dkk1 prevented the

increase in ALP activity that occurred in control osteogenic cultures. As expected, BIO, a potent and selective inhibitor of GSK3- β that has been used to activate Wnt signaling in embryonic stem cells⁸³, was able to restore ALP activity to normal levels. However, LiCl, widely used to inhibit GSK3- β and activate Wnt signaling^{98,109,110}, did not restore ALP activity. In fact, levels were reduced (Figure III-3a). Of note is the relatively low specificity of lithium, which has numerous targets in addition to GSK3 β such as glycolytic enzymes, enzymes of the inositol processing pathway and a major component of the adenosine nucleotide processing pathway¹¹³. Immunocytochemical labeling of MSCs confirmed that BIO treatment resulted in β -catenin stabilization and that Dkk1 treatment resulted in degradation of β -catenin, at the doses used in our assay (Figure III-3b).

BIO blocks Dkk1's inhibition of osteogenesis

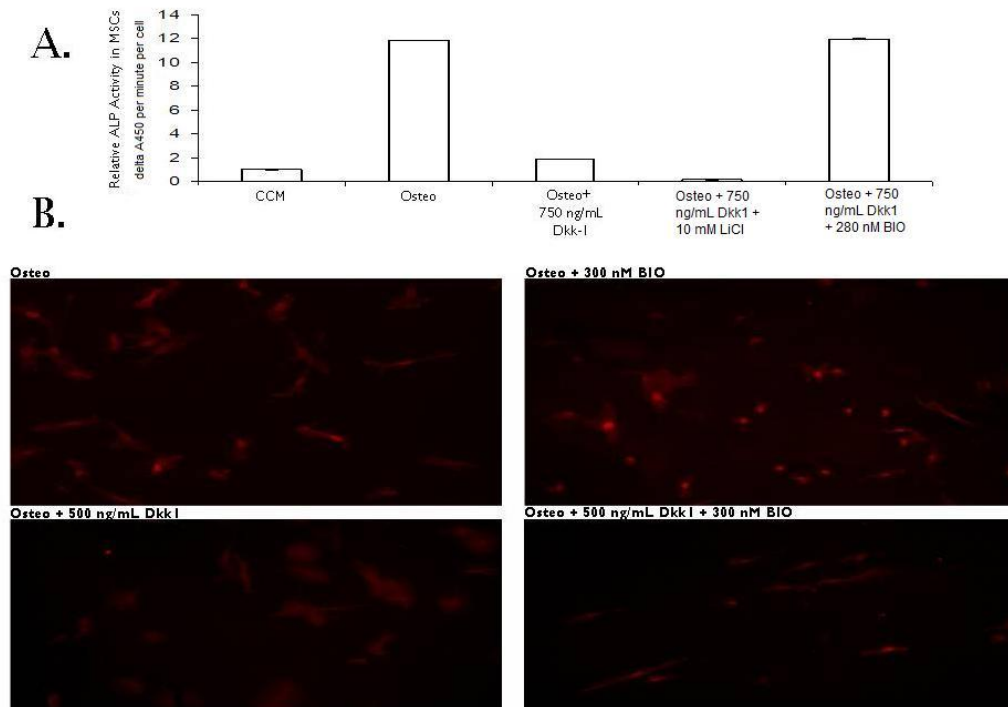


Figure III-3 - BIO blocks Dkk1's inhibition of osteogenesis. Panel A: ALP assays on confluent cultures of hMSCs demonstrate that 750 ng mL^{-1} Dkk1 inhibits ALP production. The action of Dkk1 is ablated upon addition of the GSK3 β inhibitor, BIO at 280 nM, but not Li⁺ ions at 10 mM (n=3). Panel B: Representative images of immunofluorescent staining demonstrates nuclear levels of β -catenin are reduced in response to Dkk1 activity, but can be restored by BIO.

The results suggested that Wnt signaling was necessary for the osteogenic differentiation process in hMSCs and this could be inhibited by high levels of Dkk1. We therefore performed some preliminary experiments to examine the observation in more detail. Because osteoporosis in the elderly often presents with increased fatty deposits in

the marrow, I hypothesized that a deficit in Wnt signaling may result in an imbalance between osteogenesis and adipogenesis in the disease. The hormone binding transcription factor, peroxisome proliferator-activated receptor (PPAR γ) is the master regulator of adipogenic differentiation. Because adipogenesis and osteogenesis in hMSCs is exclusive, we looked for a potential inhibitory relationship between Wnt signaling/osteogenesis and PPAR γ /adipogenesis through inhibition of PPAR γ . If such a relationship exists between adipogenic and osteogenic processes, inhibition of PPAR γ with nordihydroguaiaretic acid (NDGA) would be predicted to cause upregulation of osteogenesis. We did not find increased osteogenesis in NDGA treated cells (Figure III-4a), but interestingly, NDGA-treated cells also became unresponsive to BIO, suggesting a somewhat complex integration of the pathways.

The action of Dkk1 on canonical Wnt signaling is well characterized, and circumstantial evidence (Figure III-3B) suggests that Dkk1 acts on hMSCs through the classical mechanism. However, to examine alternative osteoinhibitory mechanisms for Dkk1, we examined NF κ B or JNK signaling, since Dkk1 has also been known to exert its effects through this axis. Inhibiting NF κ B with curcumin has a moderate effect at low doses of Dkk1, but JNK inhibition with anthra[1,9-*cd*]pyrazol-6(2*H*)-1,9-pyrazoloanthrone did not affect the action of Dkk1 in the osteogenic assay. Another non-specific GSK3 β inhibitor, 4-benzyl-2-

methyl-1,2,4-thiadiazolidine-3,5-dione, having inhibitory effects on protein kinase C activity similar to that of lithium, also reduced ALP levels. (Figure III-4b)

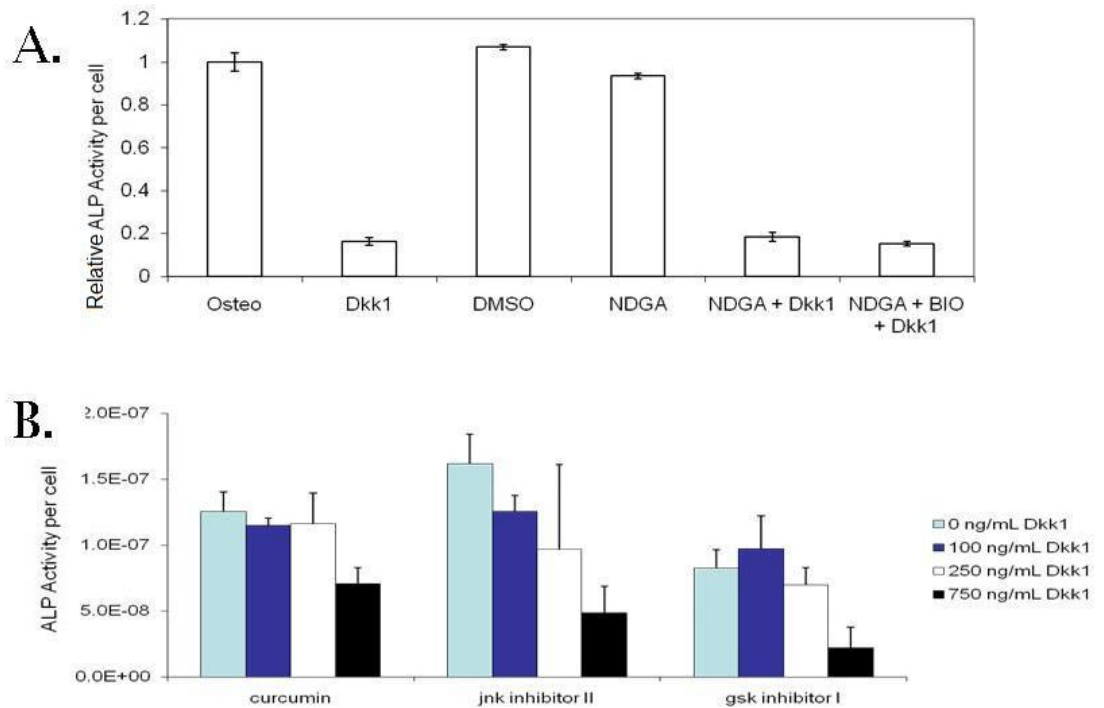


Figure III-4 - Panel A: ALP activity in response to Dkk1 and NDGA. Panel B: ALP activity in response to Dkk1 and a NF κ B inhibitor (curcumin), Jnk inhibitor, and 4-benzyl-2-methyl-1,2,4-thiadiazolidine-3,5-dione (gsk inhibitor I). All inhibitors were used at a concentration 10-fold greater than their IC₅₀.

We next examined the consequences of extended exposure of MM cells to MSC-CM to determine whether MSCs produce any factors that would stimulate the proliferation of MM cell lines in vitro. We grew

cultures of MM cells under four conditions: in RPMI with 10% FBS and 100 μ M pyruvate (MM medium), in MM medium with 1 ng mL⁻¹ IL-6, in MSC-CM diafiltered (> 5-kDa fraction) into MM medium, or in MSC-CM diafiltered into MM medium and diluted 1:5 with MM medium. We harvested cells every 24 hours and determined cell numbers by a DNA fluorescence incorporation assay. We found that the > 5-kDa protein component of MSC-CM had a strong stimulatory effect on the proliferation of MM cells (Figure III-5a).

Because IL-6 is known to be an important growth and survival factor for MM cells^{24,114,115,116,117}, we hypothesized that IL-6 would be the likely candidate for the growth-promoting component of MSC-CM. We cultured MM cells for 4 days in MSC-CM in the presence or absence of an IL-6-blocking antibody and found that the IL-6-blocking antibody inhibited the MSC-CM-enhanced proliferation of MM cells (Figure III-5b), whereas a control antibody had no effect on proliferation. To confirm the production of IL-6 by MSCs, we harvested MSCs, extracted RNA, and determined IL-6 expression levels by RT-PCR and Western blotting. We confirmed that undifferentiated MSCs expressed high levels of IL-6 message. (Figure III-5c)

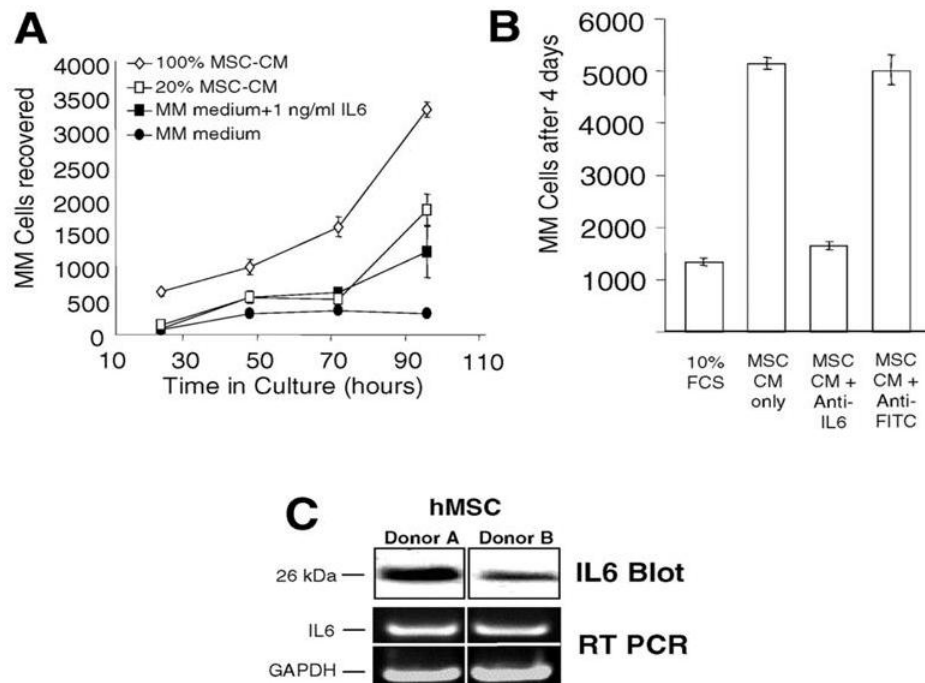


Figure III-5 - IL6 is expressed by MSCs and promotes myeloma cell proliferation. Panel A: Growth induction by MSC-CM and supplemental IL6. Panel B: Ablation of the growth inductive properties of MSC-CM by addition of IL6 blocking antibody. Panel C: Expression of IL6 in two MSC from two donors. Data from Gunn et al. (2006)²⁴.

Fully mature osteoblasts produce only small amounts of IL-6¹¹⁸. In agreement with this observation, we found that levels of IL-6 message were reduced in MSCs differentiated with osteogenic medium (Figure III-6a) but remained high if Dkk1 was added to the osteogenic medium. (Figure III-6a) Addition of BIO decreased IL-6 expression to below control levels, apparently by releasing MSCs from the MM proliferation-promoting

cycle induced by Dkk1. To examine this observation in more detail, we tested the effects of BIO on very early cultures of differentiating MSCs in which IL-6 is transiently upregulated prior to terminal differentiation and arrest of IL-6 production. Measurement of IL-6 protein in supernatants from cultures of differentiating MSCs confirms that they initially secrete high levels of IL-6, but secrete much less IL-6 if BIO is present in the medium, consistent with an earlier initiation of the osteogenic differentiation program. (Figure III-6b) Interestingly, BIO is a member of the aryl hydrocarbon family of molecules, which have been shown to suppress IL-6 expression via the aryl hydrocarbon receptor³⁹. The contribution of this effect to the suppression of IL-6 has not been determined in MSCs, but the space-filling models of BIO and a dioxin known to bind the receptor do have some apparent similarity. (Figure III-7).

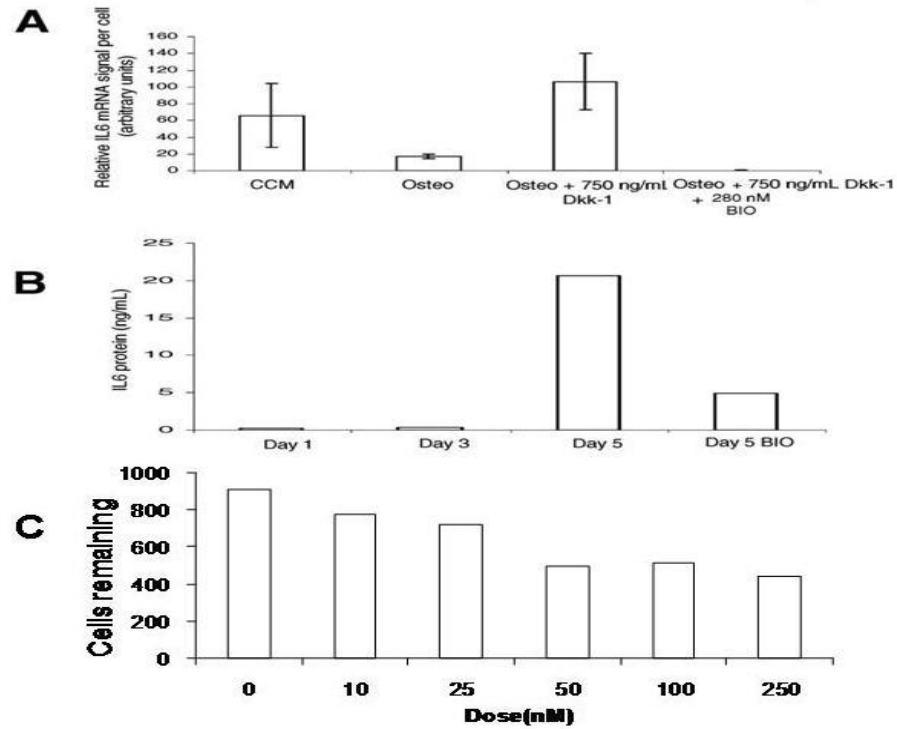


Figure III-6 - BIO treatment reduces the levels of IL6 produced by MSCs, but only has a moderate direct effect on myeloma cells. Panel A: relative IL6 expression in treated and untreated cells via real-time RT-PCR. Panel B: IL6 protein levels by ELISA in untreated MSC-CM compared with 5 day timepoint in BIO-treated medium via Western blot (normalized to cell number). Panel C: Dose-response effect of BIO on MM cells in culture. Values represent the number of cells MM cells remaining after 3 days. (n=8)

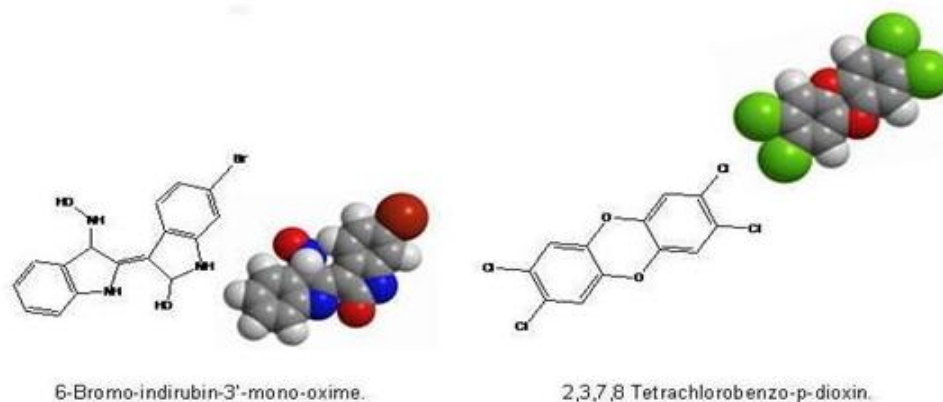


Figure III-7- Space-filling models of BIO and a dioxin known to bind the aryl hydrocarbon receptor.

CONCLUSION

Tian *et al.*⁸² first reported the high level of expression of the Wnt inhibitor Dkk1 in MM cells and suggested that it may affect osteogenesis. We confirmed the secretion of Dkk1 in two MM cell lines and found that the presence of MSC-CM enhanced the production of Dkk1. Using an *in vitro* osteogenesis assay, we showed that treating MSCs with Dkk1 inhibited the osteogenic differentiation of the cells. BIO, a potent and selective inhibitor of GSK3- β , blocked the effects of Dkk1. Surprisingly, LiCl did not block the action of Dkk1 but resulted in a further inhibition of differentiation. In preliminary experiments, we also found that administration of 20 mM LiCl in drinking water did not stimulate osteogenesis in a transgenic mouse model of osteogenesis imperfecta,

whereas BIO did have a pro-osteogenic effect (Emigdio Reyes and Carl Gregory, Tulane University, New Orleans, unpublished data). This observation is not surprising since lithium has documented side effects not related to inhibition of GSK3 β whereas BIO is far more specific.

We found that MSC-CM promoted the proliferation of two MM cell lines *in vitro* and that this stimulation of growth was principally due to IL-6 production by MSCs. Previous reports described a positive feedback loop between bone marrow stromal cells, which are similar to MSCs and MM cells leading to enhanced stromal expression of IL-6^{79,81}, and subsequent work has strengthened the role of the MSC-MM interaction in MM pathology. A study of MSCs derived from MM patients found 146 differentially expressed genes between normal and MM patient MSCs, 46% of which are genes involved in tumor-microenvironment crosstalk¹⁰⁵. Which of the differentially expressed set of genes were induced by MM cell exposure and which were differences existing pre-cancer is not completely known, but the work reported here and elsewhere shows upregulation of IL6, Dkk1, OPN, and sIL6r^{53,90,119}. Other studies have found a decrease in VCAM and fibronectin expression by MM cell exposed MSCs^{90,105,119}. The *in vitro* osteogenesis assay makes it easy to study the effect of modulating Wnt on not only osteogenesis, but also on the expression of these regulatory molecules.

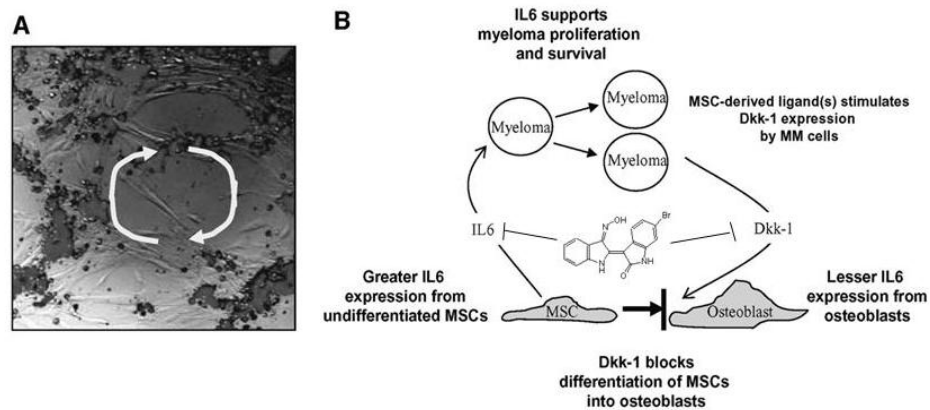


Figure III-8 - Model for the IL-6- and Dkk1-dependent cyclic interaction between MM cells and bone marrow stromal cells. (A): Cell tracker green-labeled XG1 myeloma cells adhere to an unlabeled MSC monolayer (pseudocolored fluorescent/phase composite, x10). (B): Hypothetical model of IL-6- and Dkk1-dependent interactions between MM cells and MSCs in the osteolytic lesions of MM. Data from Gunn et al. (2006)²⁴.

The work reported here shows that when MM cell lines are co-cultured with a monolayer of MSCs, the MM cells adhere to the MSCs and proliferate, becoming a component of the monolayer (Fig. II-5A). Taken in context with the other studies showing the MSC-MM interaction, it would appear that MM cells in the presence of MSCs are able to take full advantage of the high local concentrations of the soluble factors secreted by MSCs and the MSCs are, in turn, exposed to the maximal dose of Dkk1 from the MM cells, resulting in a cyclic interaction that may explain the aggressive and irreversible destruction of the bone in MM (Fig. II-5B)^{81,115}. Furthermore, maintenance of MSCs in an immature state by exposure to

high levels of Dkk1 may predispose the cells adopt a pro-osteoclastogenic phenotype, accompanied by expression of high levels of RankL, the master regulator of osteoclast differentiation¹²⁰. These effects synergistically decrease the osteoblast-to-osteoclast ratio near the site of osteolytic lesions, but current treatment strategies for MM only pursue inhibition of osteoclast activation and lowering available IL-6 levels. These strategies have no effect on repair of existing osteolytic lesions^{121,92,94}. Use of a Dkk1-blocking agent, such as BIO, holds promise both for enhancing current therapies that only slow disease progression and for enabling future therapies that may permit repair of existing osteolytic lesions.

IV. Multiple Myeloma as a model bone disorder in the mouse.

INTRODUCTION

These *in vitro* findings suggested that the defective bone repair occurring in MM might be addressed by a strategy targeting Wnt. But at the time, the existing animal models were inadequate as they focused exclusively on the tumor and not the bone effects. The one model in which bone effects were studied when I began my work required primary MM cells, a specialized strain of mice and the implantation of human fetal bone, significantly complicating the work⁶³. Additionally, the dependency of this model on bone explants obscured the effects of the tumor microenvironment on MSC-MM cell interaction. In order to examine the effects of Dkk1 blocking agents on repair of myeloma-induced bone lesions, I developed an animal model which produced radiologically-observable bone lesions within 4 weeks of injection.

At the time, two main approaches were used to model MM. The most commonly used approach called for subcutaneous administration of the cancer cells to immunodeficient mice^{66,67,122}. This model works well for the study of agents which work directly on the cancer cells and allows anti-mitotic effects to be easily assessed by simply measuring the diameter of the tumor. However, the model does not recapitulate any of the systemic effects of myeloma, especially the bone involvement, which were the primary focus of my study. Since I was interested in multiple

myeloma as a model system for Dkk1's effects on bone, and wasn't interested in the cancer *per se*, this model didn't seem useful. Recently, some newer models have been developed to focus on the bone involvement aspect of the disease. There were models which did recapitulate some of the bone marrow engraftment, but one required implantation of human fetal bone tissue into immunocompromised mice (the scid-hu model)^{63,123}, making the work significantly more complicated, and another required a special strain of mice and depended on spontaneous generation of tumors^{124,125}. Recently, a model has been developed which allows study of bone lesions via intravenous inoculation of cells in a special strain of mice to which the cells have been adapted¹²⁵. However, this model requires a longer induction time, making it less suitable for efficient examination of bone anabolic agents based on Wnt. Also, the scid-hu model has been adapted to use rabbit bone,⁵⁹ and while this makes procuring the tissue much easier, the model is still technically challenging to implement.

This model essentially used myeloma cells as a Dkk1 delivery vehicle. In order to maximize the chance of getting bone marrow infiltration by myeloma, while minimizing the loss of animals due to experimental injury, I injected cells directly into the marrow cavity of the tibia. This method allowed the myeloma cells to engraft and form tumors

while not circulating in high numbers in the bloodstream where they may form less interesting yet more fatal tumors.

The aims of the study were to establish a disease model in which rapid destruction of bone would occur, characterize the model in terms of biochemical markers, and determine the effects of GSK3- β inhibition via BIO on the induced bone resorption. In this model, the progression of the tumor could be seen and measured using techniques developed for subcutaneous tumors and the effect of the drug could be determined by examination of biochemical markers of bone turnover and histomorphometric analysis of the bone.

MATERIALS AND METHODS

Animal Handling

Following a protocol approved by the Tulane University Institutional Animal Care and Use Committee, C57BL6/Prkdc *scid* mice received 200 cGy and were allowed to recover for 1 day. The following day, they were anaesthetized with isoflurane and placed on their backs. The left leg was flexed to 90° and the patellar tendon was located. In the initial studies, 1×10^5 RPMI 8226 cells (ATCC) were administered via tail vein. Later, 1×10^5 INA6 myeloma cells were administered by inserting a 21 gauge needle underneath the patellar tendon and using the needle tip

to create a small opening into the marrow cavity of the tibial head, then injecting the cells into this opening.

Submandibular collection was performed without anaesthesia by holding the mouse securely in one hand, using the thumb to prevent the mouse from moving his head. The submandibular vein was found by tracing the jaw back to the end of the jawbone and moving slightly upwards. The vein was pierced using a lancet designed for this purpose (Goldenrod lancet, Medipoint, Mineola, NY). Three hundred microliters of blood were collected in a tube containing 30 μL of a 10000 $\text{U}\cdot\text{mL}^{-1}$ sodium heparin solution in PBS, then a clean compress was applied to the area for several seconds or until the bleeding stops, at which point the animal was allowed to return to the cage.

Animals were monitored every other day, and tumor size was measured via caliper. Tumors were classified as small, medium, or large according to the following rules: measuring across the largest diameter, tumors less than 0.5 cm were classified as small; tumors between 0.5 and 1.0 cm were classified as medium sized; and tumors measuring greater than 1.0 cm in diameter were classified as large. Upon attainment of a large tumor, difficulty moving, apparent pain or cachexia, animals were euthanized according the animal welfare protocol.

Histology

Mice were sacrificed according to the IACUC approved procedure and leg bones were dissected and placed immediately in 10% buffered formalin, then stored at 4°C for 24 hours to 3 days. Decalcification was done using 0.5 M EDTA in PBS until X-ray showed loss of bone opacity. Processing, embedding, and sectioning were performed at the Tulane histology core facility.

Decalcified, formalin-fixed, paraffin-embedded bone sections were processed for immunostaining as follows. Sections were deparaffinized with xylene and rehydrated by incubating sequentially in 100% EtOH, 95% EtOH, 70% EtOH, and dH₂O. They were then stained for tartrate-resistant alkaline phosphatase (TRAP) by adding the ELF97 dye to 200 μM in the classical TRAP buffer, which is 0.05 M acetate, sodium tartrate at 0.03 M, and 0.1% Triton X-100. The solution should be warmed to 37°C and the ELF97 should be added just before use. Osteoclasts were counterstained for cathepsin K (Invitrogen) after blocking the sections with 3% goat serum. After immunostaining, the sections were incubated in 50 μg·mL⁻¹ RNase A for 20 minutes, then in 0.5 μM PI for 5 minutes.

Pathology

A relative scoring system was used such that a '1' represents a small area of neoplasia and '3' represents a much larger area. When early

lymphoproliferation (ELP), was apparent, suggesting that had these animals not been sacrificed at this time lymphoid neoplasia would have developed more extensively, ELP was scored as '1'.

When hemorrhage or thrombosis or infarction were found, they were interpreted as applying to the neoplastic tissue (since there was essentially no hemorrhage or necrosis elsewhere), and considered equivalent to "tumor necrosis", since in fast growing tumors, disruption of blood supply may lead to circumscribed areas of necrosis, which was clearly apparent in the neoplasia tissue (as opposed to actual thrombi in vessels or infarcted blood vessels, which were not apparent).

"Fracture" is a diagnosis best made grossly or by radiology. Cutting planes and even artifacts are sources of ambiguity concerning whether or not a fracture was present. Fractures were scored if probable, but not certain, based upon the degree of bone disruption related to tumor infiltration and also to bone remodeling activity.

Histomorphometry

Static histomorphometric measurements selected were bone fraction, bone perimeter, bone area, trabecular thickness (including growth plates), nucleator marrow (MSV) and trabecular star volume (TSV) for trabecular bone, which were measured within a standard region of interest (Figure IV-1), excluding the cortices and incorporating the femoral and tibial endplates^{126,127}. The bone fraction (frac*100) is defined

as the percentage of bone area in the region of interest. A higher $\text{frac} \times 100$ or bone area (B. Area) indicates bone growth or reduced bone resorption. Cortical and trabecular thicknesses indicate thicker and stronger bone shafts and reduced resorption activity, respectively. The star volume is defined as the mean volume of all the parts of an object which can be seen unobscured in all directions from a particular point with the mean value taken over all points inside the object. If there is removal or perforation of trabecular bone, this is reflected in an increase in the marrow star volume. Similarly, a decrease in trabecular star volume reflects a removal or decrease in the amount of trabecular bone. The star volumes were gathered using a volumetric ray transformation after passing rays in random directions from selected starting points as described by Vesterby *et al.*^{128,129}(Figure IV-2). This volumetric calculation was performed at 5 locations per bone. Cortical thicknesses were measured and averaged across 5 random locations along the chondylar surfaces of the knee joint. Each method was defined and incorporated into a semi-automated analysis custom subroutine (ImagePro Plus, Media Cybernetics, Silver Spring, MD). Color images (obtained with ScanScope Plus) of formalin-fixed, paraffin-embedded, decalcified, sagittal cut knee H&E sections were segmented, converted to black and white, and filtered to reduce noise. The binary outputs (black and white) underwent semi-automated processing to gather all histomorphometrical measures. All histomorphometry work was done at Premier Laboratories (Boulder CO).

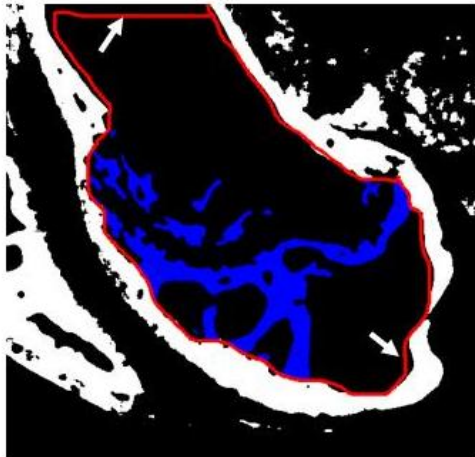


Figure IV-1 - Histomorphometry measurement area. The indicated line delineates the region of interest for collecting trabecular bone information, including bone area, bone perimeter, fraction of bone, and trabecular bone thickness.

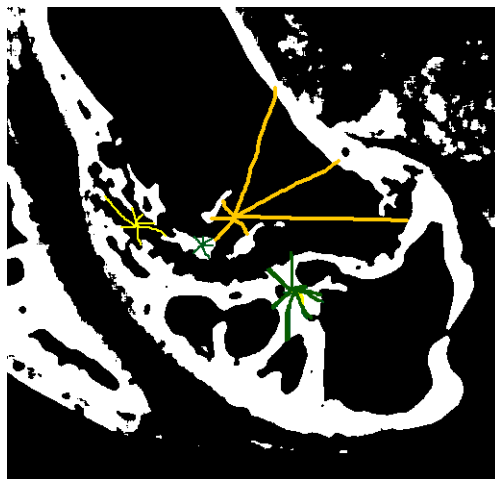


Figure IV-2 - Marrow Star Volume (yellow) and Trabecular Star Volume (green) examples. MSV is the larger “star” and TSV is the smaller one.

MSV is the larger “star” and TSV is the smaller one in Figure IV-2. Nucleator star volume was measured in 5 marrow and 5 trabecular spaces. MSV and TSV are reported for the entire slide image by femur and tibia.

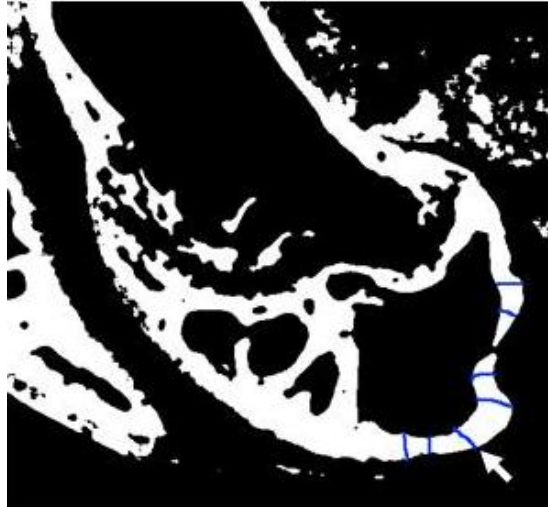


Figure IV-3 - Cortical thickness measurement

Cortical thicknesses were measured in 5 locations on every chondylar cortex; Figure IV-3 shows 7 cortical thickness markers which appear like bands across the cortex. Cortical thicknesses were measured by hand using a semi-automated routine.

Drug administration

Fifty microliters of 280 nM BIO in sterile DMSO was injected directly into the tumor proximal to the bone, or between the muscle and bone for those animals without tumors. The drug was administered every 2 days. Control animals received only 50 μ L sterile DMSO.

ELISAs

The CTx ELISA was obtained from Nordic Bioscience Diagnostics a/s (Herlev, Denmark) and is an assay for C-terminal collagen I degradation products. The PYD ELISA was obtained from Quidel Corporation and is an assay for pyridinoline crosslinks, which results from the action of osteoclasts on bone. (San Diego CA). The TRAP5b ELISA was obtained from Quidel and is an assay for tartrate-resistant acid phosphatase isoform 5b (TRAP), a soluble product secreted by osteoclasts. The beta-catenin ELISA was obtained from R&D Systems and used to assay for inhibited activity in the Wnt signaling pathway. The ELISA for human lambda antibody was obtained from Bethyl Laboratories. Where appropriate, values were normalized to cell number using hemacytometry.

STATISTICS

Student's t was calculated for all comparisons where there was sufficient data, and significance at the 0.05 level is indicated as *.

Threshold significance at the 0.1 level is indicated as **. For a small number of comparisons, there were not enough members of the data set, so error bars are not present and p-values are not calculated.

RESULTS

To establish an osteolytic lesion model such that it would present a measurable and potentially treatable bone phenotype, we had to develop a new route of administration, a new way to monitor disease progress, and a new means of measuring outcomes. Initial efforts to establish tumors were frustrating. During the development of this model, variables associated with cell line, tumor monitoring method, and engraftment protocols were examined.

We first administered RPMI8226 MM cells intravenously to 10 irradiated immunocompromised (C57BL6/*Prkdc-scid*) mice, but unfortunately, 100% of the animals died within 1 week. Whether this was a reflection of the increased radiation sensitivity of the immunodeficient mouse strain, a result of infection or embolism brought about during the procedure, or some other cause was never determined, but for the next attempt a more targeted approach was used.

For the next stage of model development, 20 C57BL6/*Prkdc-scid* mice were used and the cell line RPMI8226 was employed. Animal survival improved, but the efficiency of tumor development remained low. In order to maximize engraftment of cells into the bone marrow, in

the next experiment MM cells were injected directly into the marrow cavity of the tibia of non-irradiated animals. This method allowed the myeloma cells to engraft and form tumors while not circulating around the bloodstream where they might likely form less interesting yet more fatal tumors. The progression of the tumor could be monitored as with the subcutaneous model and bone effects could also be easily followed by Xray of the injected leg. The contralateral leg also provided a convenient control for assessment of clinical parameters of bone metabolism, such as bone mineral density and trabecular volume, as well as effects due to the tumor bulk. Human lambda antibody fragments, secreted by RPMI8226 cells, were examined for use as a marker of tumor burden. In culture, there was a good correlation between soluble lambda levels and cell number ($r=0.91$) (Figure IV-4).

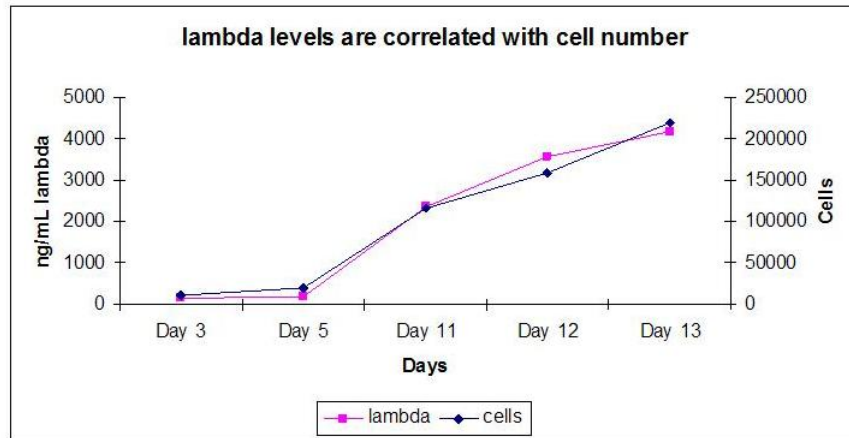


Figure IV-4 - In vitro study of human lambda antibody secretion by RPMI8226 myeloma cells.

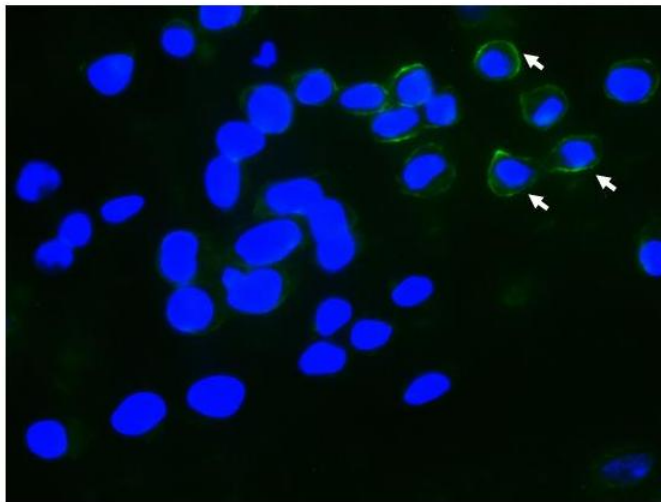


Figure IV-5 - CD138 immunostain of bone marrow from injected mouse.

In this case, half of the animals (10) were found to have tumors in the injected leg. Seven of the tumor-bearing animals were found to have elevated levels of human lambda antibody fragments in their serum, and one had large numbers of CD138⁺ cells in the bone marrow (Figure IV-5). I found no significant elevation of serum calcium, telopeptides, or Dkk1 in the animals in this preliminary study (Figure IV-6).

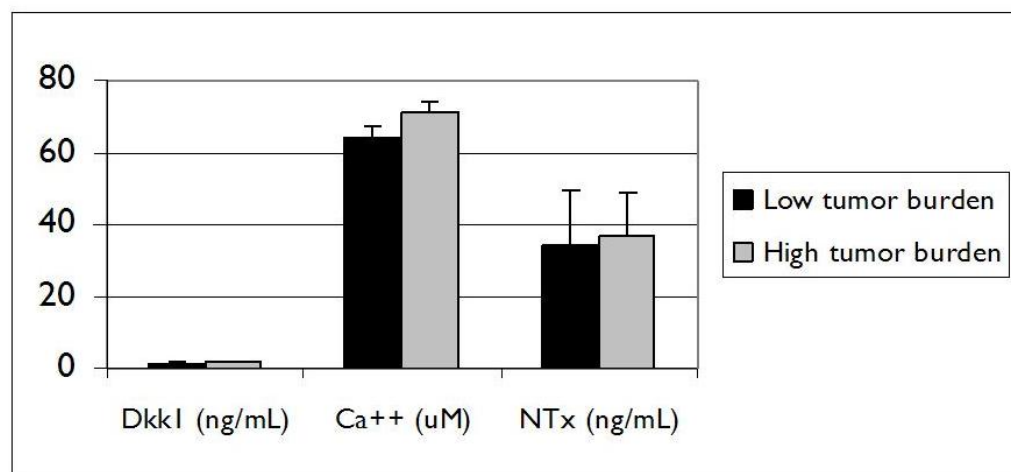


Figure IV-6 - Initial study of markers of bone resorption in myeloma mouse model.

To look more closely at the effect of the MM cells and the drugs on the osteoclast and osteoblast numbers in the bone, a cytochemical stain for TRAP was used. Comparison of experimental conditions was challenging, in part due to the concomitant increase in macrophages, which are also TRAP⁺, in tumor-bearing animals. To address this issue,

bone sections were stained with a fluorescent substrate for TRAP¹³⁰. Bone is very autofluorescent, so most dyes that excite in the visible range also excite substances present in bone as well, making it hard to find the specific signal generated by the dye-conjugated antibody. Additionally, formalin-fixed tissue presents a higher level of autofluorescence than that found in frozen tissue¹³¹. However, bone isn't autofluorescent in the UV range where DAPI excites, so a secondary antibody conjugated to Alexa350 was used, resulting in clear immunostains with no autofluorescent background. Because the harsh processing required for immunostaining paraffin sections distorts cellular morphology, macrophages were distinguished from osteoclasts by cathepsin K staining. Using this technique, we were able to unambiguously identify osteoclasts and osteoblasts in sections (Figure IV-7); however, the lengthy processing steps involved made this method cumbersome for use as a screening tool, and the thin sections required for low-background immunostains are not appropriate for stereological estimates of cell numbers. Figure IV-8 shows a high-magnification confocal image of TRAP⁺ osteoclasts.

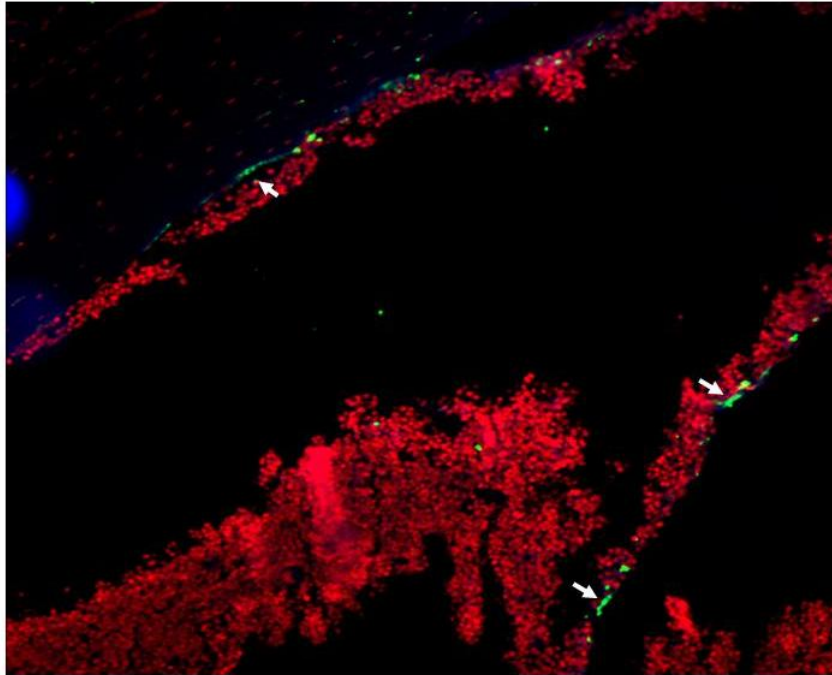


Figure IV-7 - Fluorescent stain for TRAP. Arrows indicate osteoclasts on bone surface.

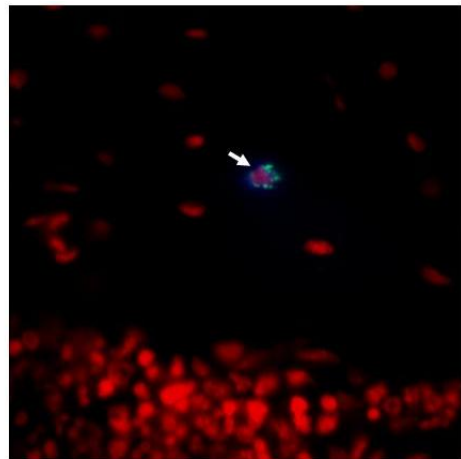
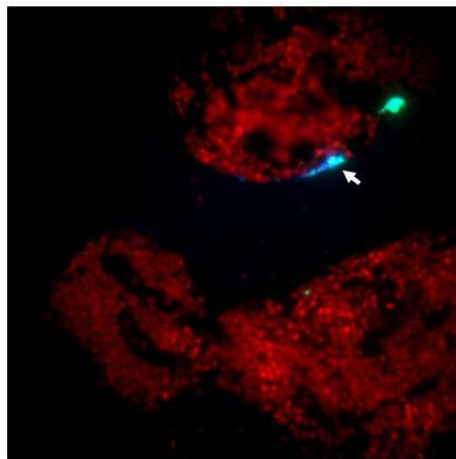


Figure IV-8 - Fluorescent TRAP stain at high magnification. (400x) Punctate staining of TRAP-containing vesicles is indicated by arrows.

While this approach was an improvement on the previous attempt, the engraftment (50%) remained low, and the tests used to follow progression of the tumor and the effects of the drug were not highly informative. To improve on this result, the experimental protocol was modified to increase the size of the experiment to ensure sufficient yield of tumor-bearing animals and a different and more aggressive cell line was used. Forty C57BL6/*Prkdc-scid* mice were used, and the INA6 cell line was administered. The experimental strategy was also modified to focus on the most informative of blood marker assays. This time, the speed of tumor development varied widely, with some animals developing noticeable tumors after as little as one week and others showing little sign of tumor presence until as late as 4 weeks, but tumor induction efficiency was 97%. Once the tumor became evident, it increased in size rapidly. No animals were lost in the week post-injection, indicating that the protocol minimized the acute effects of the cell administration and irradiation.

Before and after irradiation, hematological smears were prepared and stained for the presence of white blood cells. Before radiation,

significant levels of white blood cells were detected in most of the animals (Table IV-1). However, the white cell counts decreased to near zero afterwards. At endpoint, the white cell counts of the animals remained near zero, indicating that the immune system remained suppressed and also suggesting that not many of the injected cells entered the bloodstream.

For examination of the effects of BIO on MM-induced bone resorption, the animals were divided into treated and untreated groups. Because I wanted to ensure a representative amount of tumor-bearing animals in the treated and untreated groups, drug administration did not begin until after the first set of animals had developed tumors. A schematic of the experimental setup is shown in Figure IV-9. Mice were sacrificed at days 3, 17, and 30. Twelve mice were sent out after 3 days for detailed histomorphometric analysis, while 4 reached the endpoint criteria by 17 days and were sacrificed then. Twelve more mice had reached the endpoint criteria by Day 30 at which point the remaining 3 non-tumor bearing mice and 3 control mice were sacrificed. The Day 17 and Day 30 animals were used for X-rays and biochemical studies.

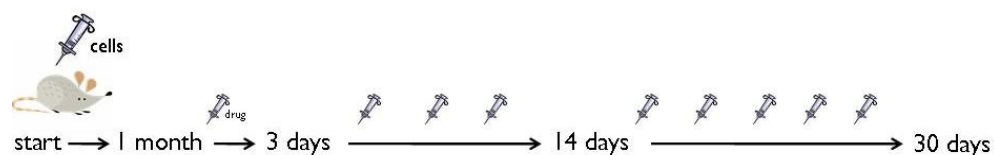


Figure IV-9 - Experimental scheme for treatment of mice.

	Neut	Lymph	Mono	Eo	Baso
DMSO Average	16	2	6	0	0
BIO Average	14	2	4	0	0
Tumor Average	15	2	7	0	0
No Tumor Ave	14	3	6	0	0

Table IV-1 - Initial white cell counts of immunodeficient animals. (n=11 for DMSO, n=12 for BIO, n=15 for tumor, and n=8 for no tumor)

X-rays were taken at various stages during the development of the model. While lesions were not apparent in whole body X-rays taken at earlier stages (Figure IV-11), osteolytic lesions and localized bone resorption was detected in post-mortem X-ray of dissected bones and Day 17 (Figure IV-12) and Day 30 (Figure IV-13) of the experiment. In addition to the cortical resorption, focal lesions characteristic of multiple

myeloma were also apparent in the injected leg. The severity of the bone resorption was scored in blinded fashion by a veterinarian according to the degree of osteopenia, periosteal reaction, and bony regeneration. BIO treated animals had predominantly mild and moderate bone resorption at all times examined, while animals receiving only vehicle had exclusively moderate to severe resorption (Table IV-2). There was no relationship between tumor size and radiological appearance of bone resorption (Figure IV-10).

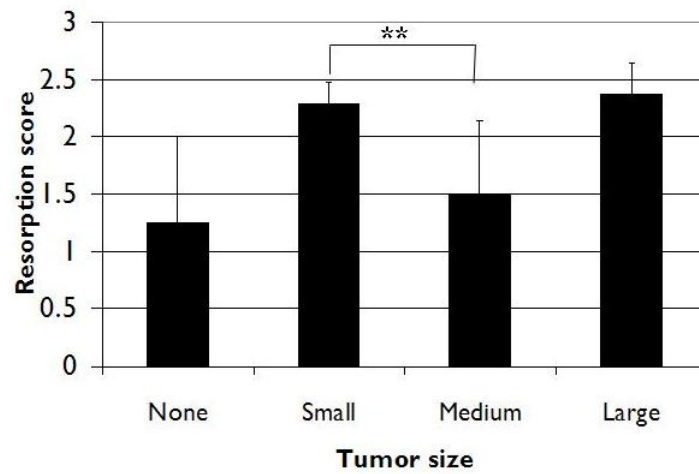


Figure IV-10 - Relationship between tumor size at autopsy and radiologically apparent bone resorption (n=7 for small, n=4 for medium, n=5 for large). ** = $p < 0.1$



Figure IV-11 - Whole body X-ray of tumor-bearing animal. A large tumor is apparent surrounding the knee on the left.

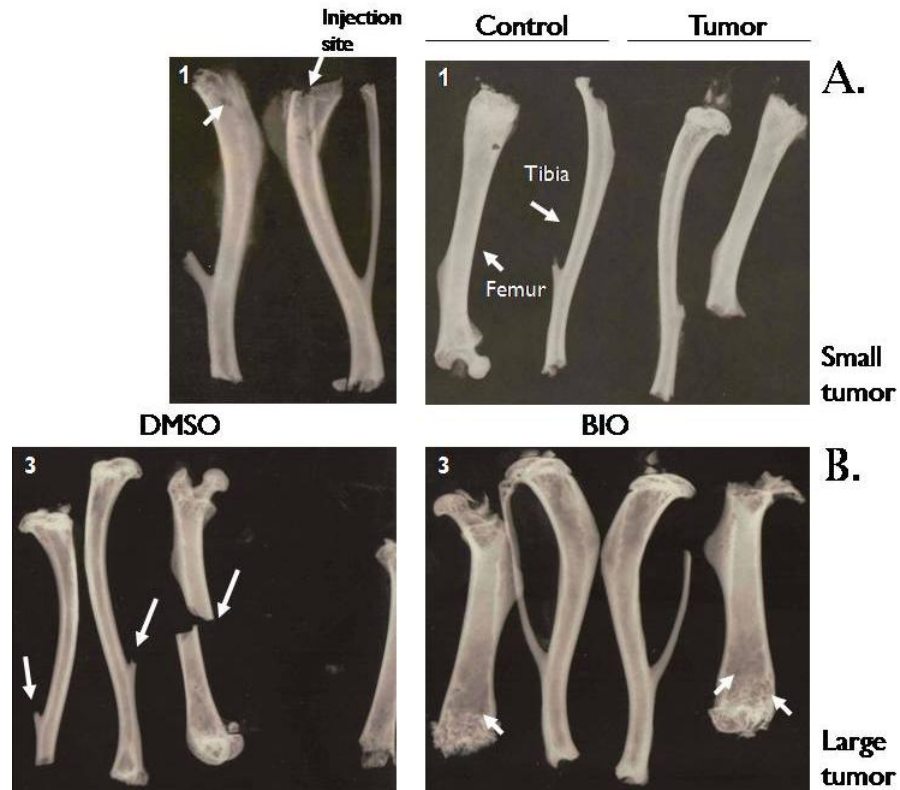


Figure IV-12 - Post-mortem Xray of dissected bones 17 days after start of drug treatment. (A) Bones from animals with small tumors. The left panel is from untreated animals, the right is from treated animals. Arrows indicate the presence of lesions or fractures, except for the ones indicating the tibia and femur in the right panel. (B) Bones from animals with large tumors. Note the fractured bone and absence of finer structures in the untreated animals.

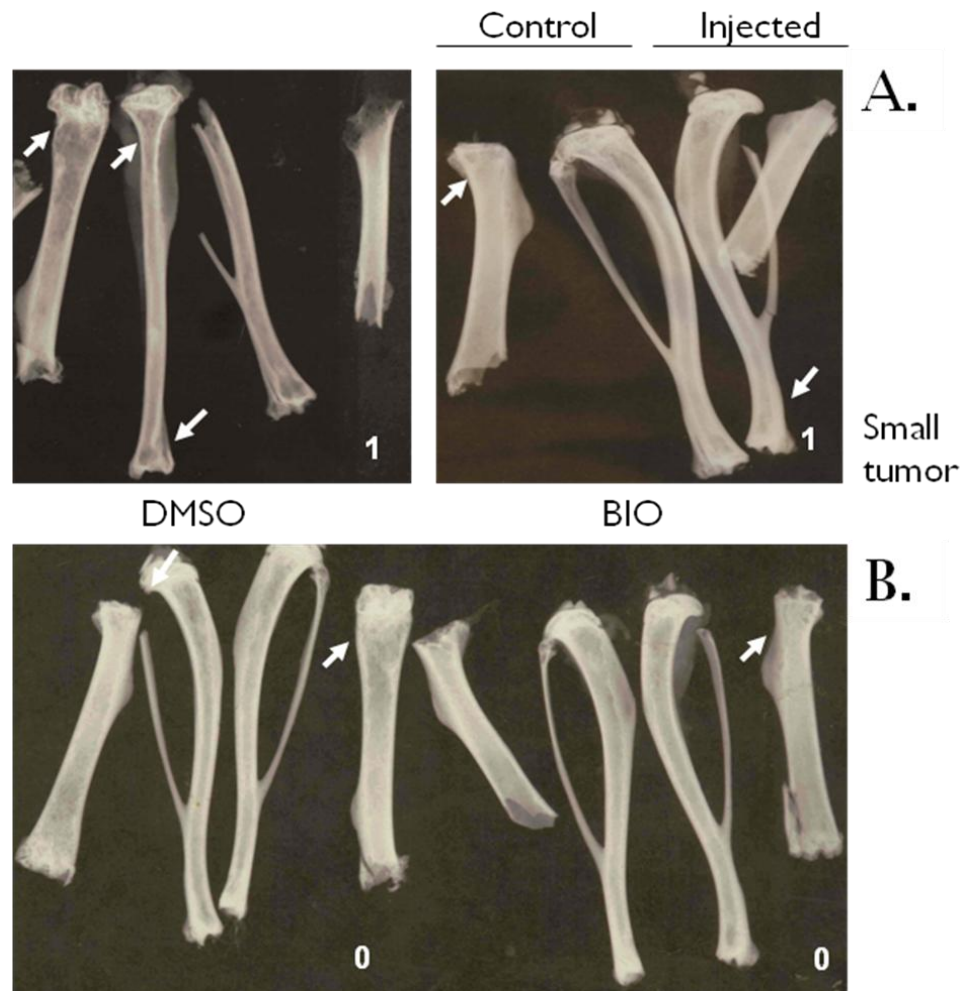


Figure IV-13 - Post-mortem X-ray of dissected bones 30 days after start of treatment. (A) Bones from animals with small tumors. Note the translucent appearance and crushed ends of the bones (due to their excessive fragility) of the untreated animals. (B) Bones from non-tumor bearing animals. The bones are opaque and able to be dissected fully intact.

	Mild	Moderate	Severe	% survival 30 days
DMSO	1	5	5	25%
BIO	3	7	1	40%

Table IV-2 - Analysis of bone resorption in post-mortem X-rays. Scoring of severity was performed by a veterinarian who remained blinded to the treatment conditions.

To confirm that the drug was reaching the tumor, I assayed the level of β -catenin in cells from a biopsy taken from two untreated animals and two treated animals. Approximately 70% more β -catenin was detected in tumor samples from treated animals than in untreated tumors, indicating that the drug was effective in the given dose and route of administration in inhibiting GSK3 β in the cells in the tumor area (Figure IV-14). However, there was a statistically insignificant relative risk between the two groups (RR = .81, SE = .35, p = .62) (Figure IV-15).

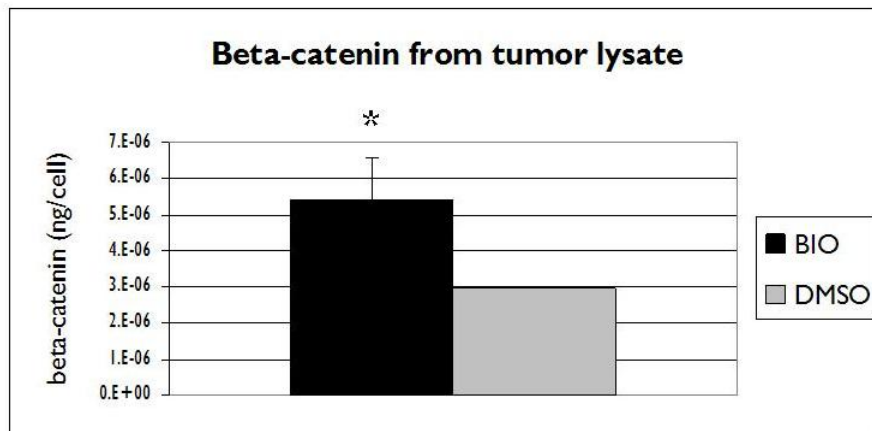


Figure IV-14 - ELISA for beta-catenin in tumor cell lysate (n=3), * = $p < 0.01$.

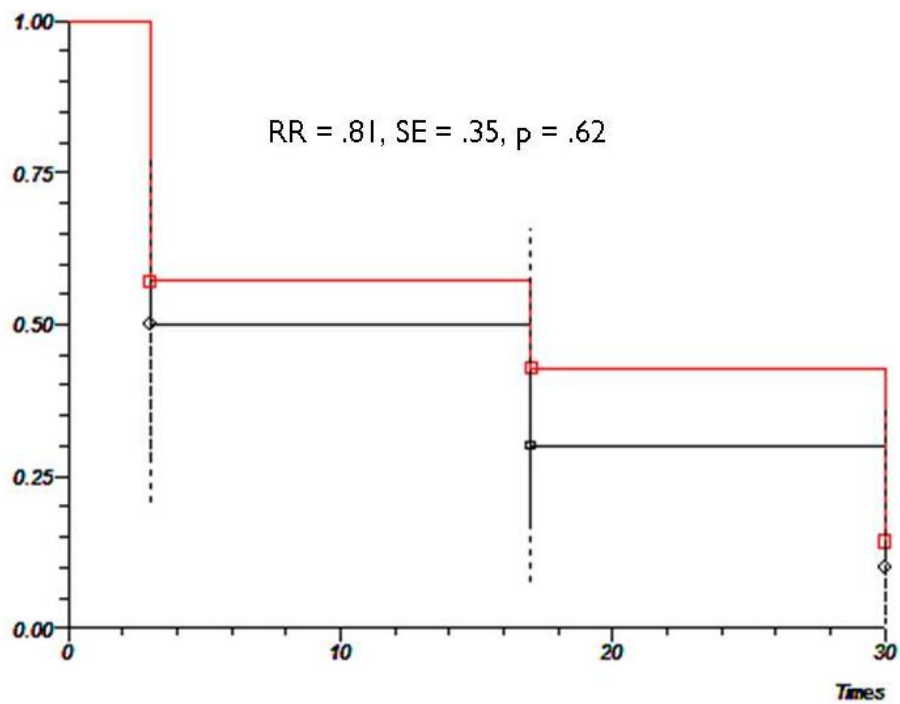


Figure IV-15 - Survival curves of treated and untreated animals.

Gross inspection of the bones upon autopsy (Figure IV-16) revealed the absence of red marrow in the injected legs, which also were noticeably fragile and prone to breaking or crushing. All animals receiving myeloma cells had a loss of red marrow in the injected leg in both the treated and untreated groups. The significance of this finding is unclear, but it is suggestive of colonization of the marrow cavity by myeloma cells. Isolation and culture of the marrow from one animal yielded MSC-like cells and smaller, non-adherent cells which adhered to the MSCs, but contamination of the cultures from myeloma cells adhering to the outside of the bone could not be ruled out, and because my focus was on this system as a model bone disorder, and I was not interested in the myeloma *per se*, no further work was done in this area.

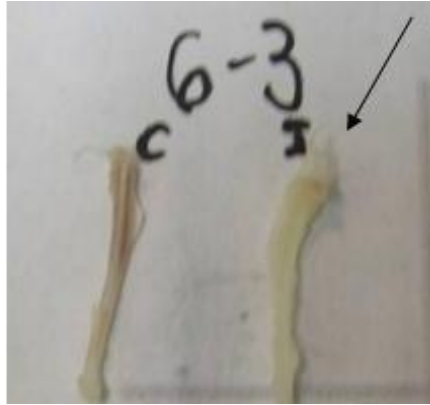


Figure IV-16 - Gross inspection of bone. A representative set of bones is shown from the day 30 timepoint. Note the absence of red marrow in the injected leg.

Microscopic examination of tumor-bone cross-sections revealed extensive bone degradation and colonization of the tibial marrow cavity with myeloma cells, as well as extensive cortical degradation (Figure IV-17). A most obvious lesion in these samples was the massive infiltration of the bone and surrounding soft tissue with uniform sheets of neoplastic cells consistent with lymphoid origin. All sections from tumor-injected legs demonstrated massive infiltration by neoplastic cells, both within the bones and replacing the surrounding tissues, including skeletal muscle (Figure IV-18). There were no meaningful differences in the degree of neoplasia in treated and untreated groups. Interestingly, uninjected legs showed evidence of a neoplasia similar to that seen in injected legs, simply not as advanced (Figure IV-19). There was only one

slide that contained a section of an actual fracture zone, with localized cortical bone being replaced with hemorrhage, fibroplasia and minimal inflammation. Generally, there was very little evidence of bone necrosis, inflammation, or fibroplasia in these sections. With respect to bone resorption, there was evidence of extensive osteoclast activity, usually in the sub-epiphyseal zone of the tibia and femur. Increased osteoblast activity was seen in the cortical bone adjacent to the bone resorption areas, but also in a periosteal pattern on the shafts of the long bones. Newly deposited 'woven' or lamellar bone was interpreted as being evidence of osteoblast activity. The epiphyseal plates were often irregular and distorted. There was an increase in tumor necrosis and a decrease in tumor cell presence evident in sections from treated animals (Figure IV-20).

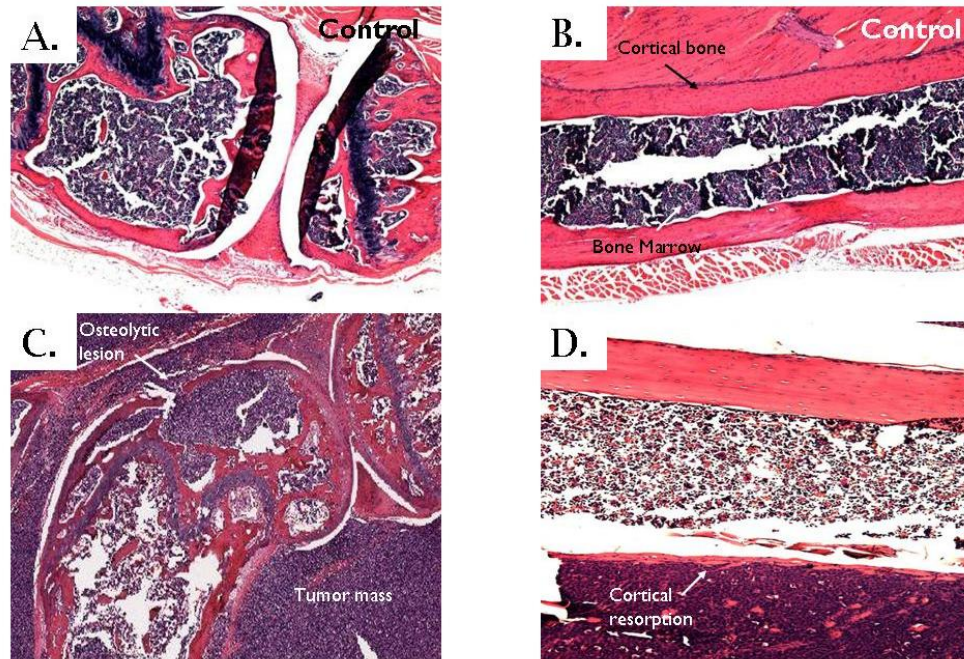


Figure IV-17 - Microscopic examination of bone. (A) Normal growth plate and marrow. (B) Normal cortical bone. (C) Osteolytic lesions (D) Cortical resorption

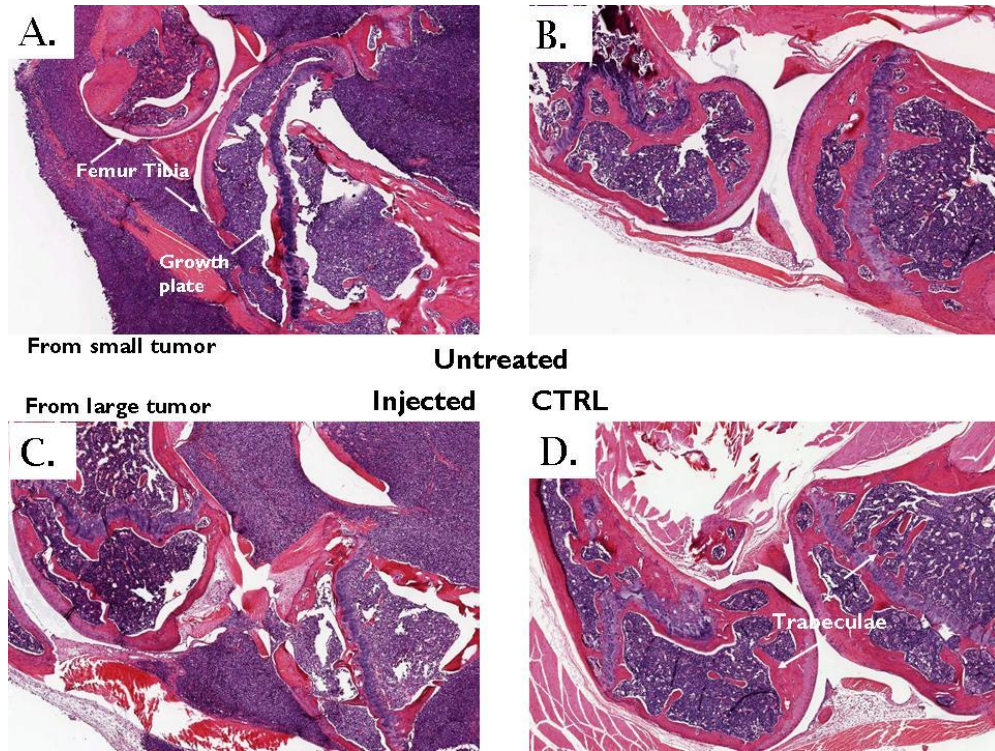


Figure IV-18 - Myelomatous bone. (A) crooked growth plate and marrow infiltration in bone from animal with a small tumor. (B) Control for (A) (C) Invasion of marrow and synovium by tumor cells in from animal with large tumor. (D) Control for (C)

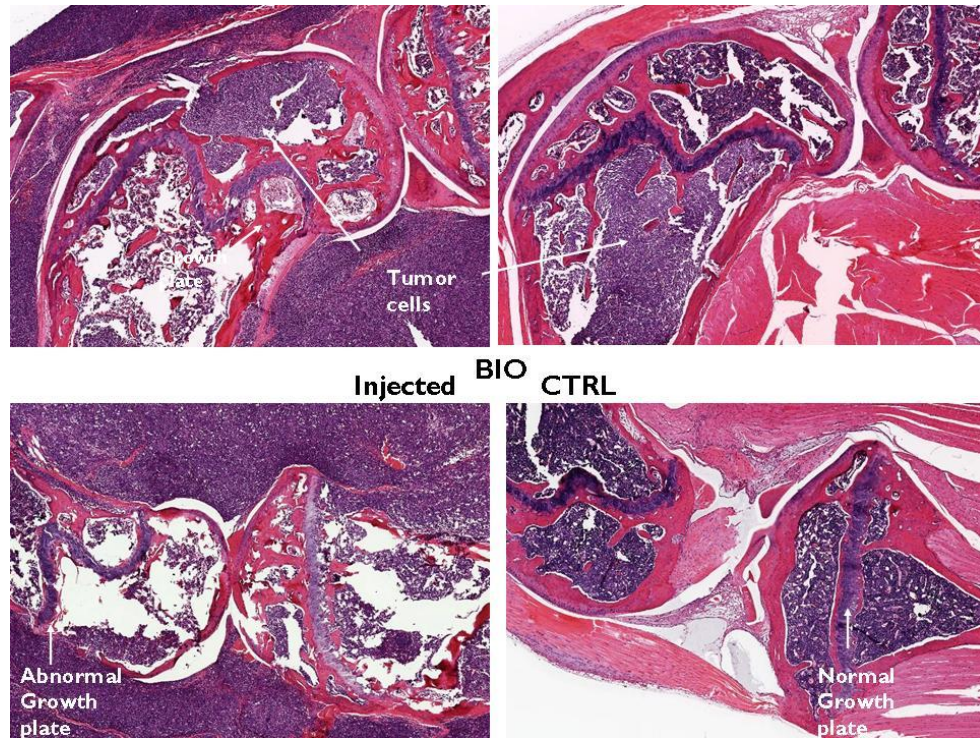


Figure IV-19 - Myelomatous bones from treated animal. (A) osteolytic lesion in bone from animal with small tumor. (B) Control for (A) with evidence of tumor engraftment. (C) Abnormal growth plate and severe resorption in bone from animal with large tumor. (D) Control for (C) showing normal growth plate.

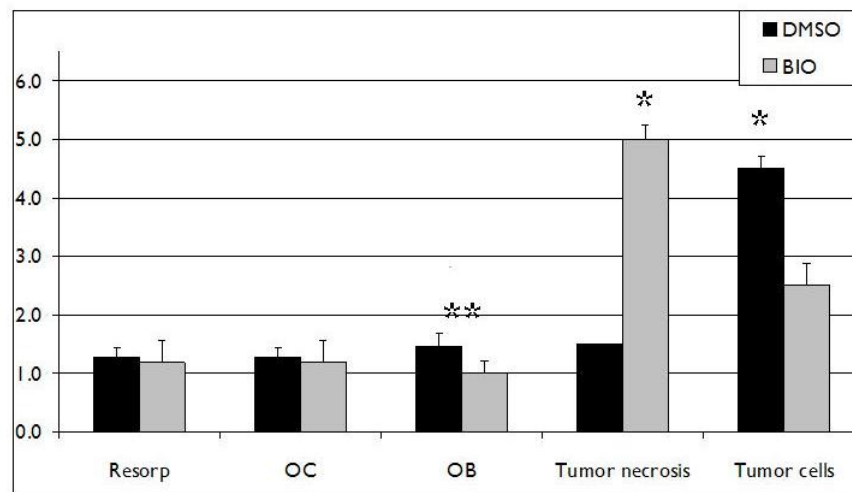


Figure IV-20 - Mouse bone pathology. The scale indicates relative severity on a 1-5 scale. (n=6) * = $p < 0.05$ ** = $p < 0.1$

Histomorphometric analysis was then performed to take a closer look at more sensitive parameters of bone remodeling. The histomorphometric measurements selected were bone fraction, bone perimeter, bone area, trabecular thickness (including growth plates), marrow star volume and trabecular star volume, and measurements were performed on both the femur and the tibia from tumor-injected and uninjected legs. The femurs on the injected side show significantly less bone resorption relative to untreated animals in the measurements of total bone area, trabecular thickness, and bone perimeter. Interestingly, the contralateral legs from treated animals had significantly thicker

trabeculae and an increase in MSV, indicating remodeling in the contralateral leg as well (Figure IV-21).

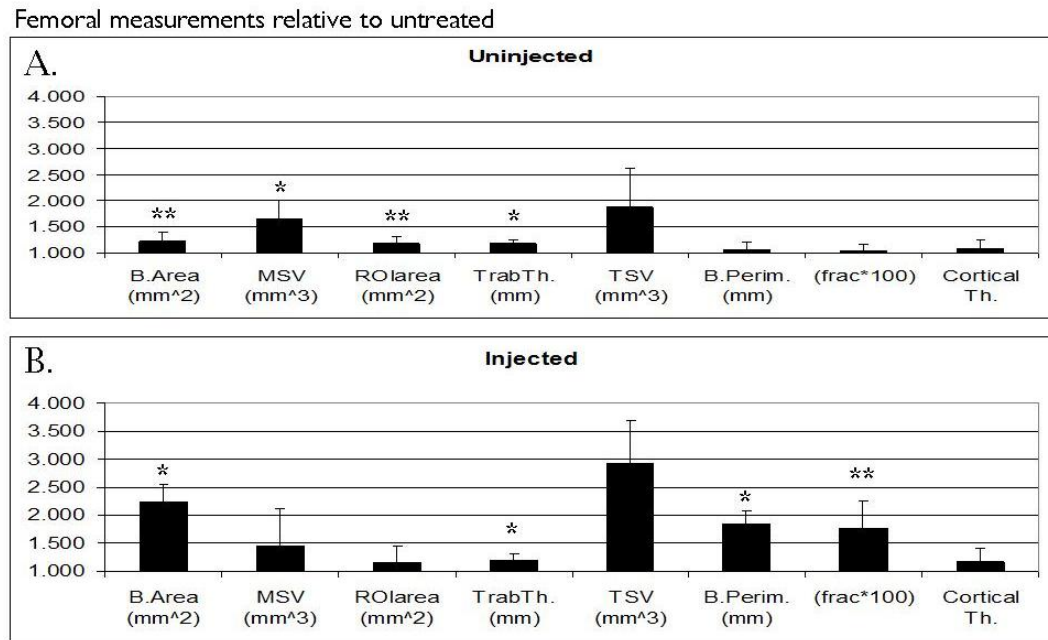


Figure IV-21 - Histomorphometric measurements of treated and untreated mouse femurs. (A) Relative differences between treated and untreated animals in the uninjected leg. (B) Relative differences between treated and untreated animals in the injected leg (n=6) * = $p < 0.05$ ** = $p < 0.1$

Unexpectedly, the tibias from treated animals appeared to have significantly less bone area, bone perimeter, and percent bone relative to untreated animals, although this trend did not hold on the contralateral side, however, the overall size of the region of interest was less as well (Figure IV-22).

Tibial measurements relative to untreated

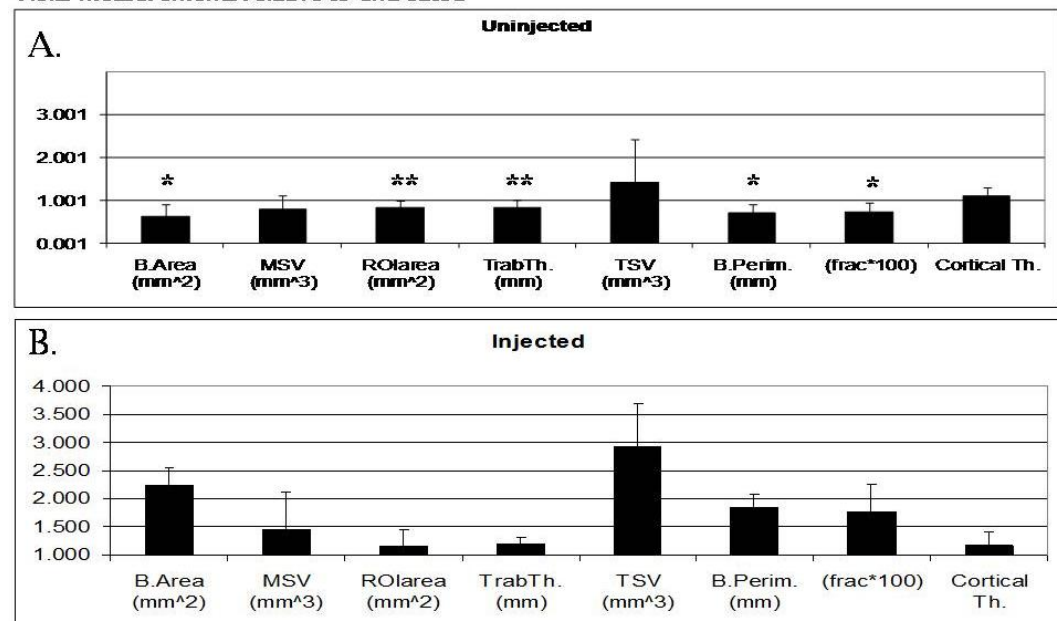


Figure IV-22- Histomorphometric measurements of treated and untreated mouse tibias. (A) Relative differences between treated and untreated animals in the uninjected leg. (B) Relative differences between treated and untreated animals in the injected leg (n=6). * = $p < 0.05$ ** = $p < 0.10$

Because the histomorphometrical measurements span 5 logs, from tens of mm for cortical thickness to thousandths of a mm for MSV, relative measurements are presented in these graphs only for the sake of clarity; Figures IV-23 - 26 show these measurements in more detail and with the correct units.

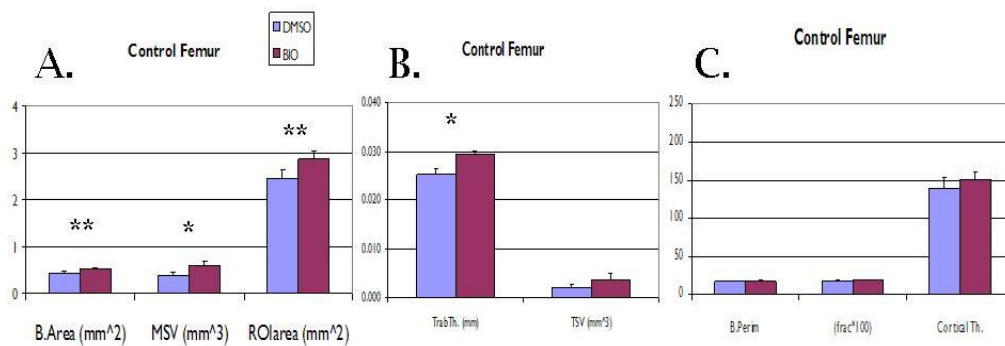


Figure IV-23 - Histomorphometry of femurs from uninjected bones (n=6) * = $p > 0.05$, ** = $p > 0.1$

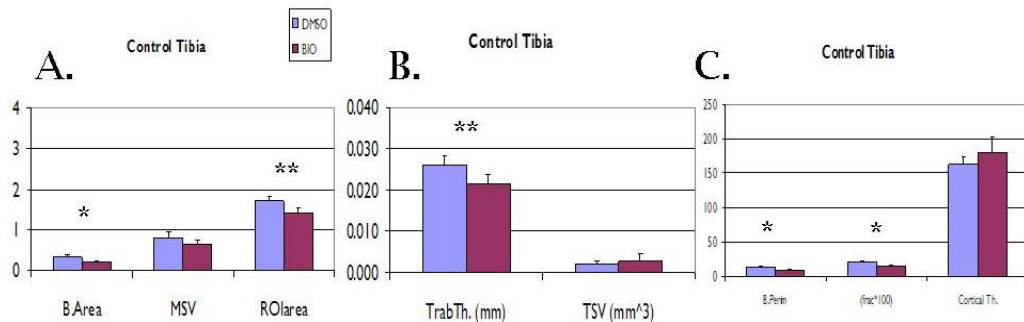


Figure IV-24 Histomorphometry of tibias from uninjected bones (n=6). * = $p > 0.05$, ** = $p > 0.1$

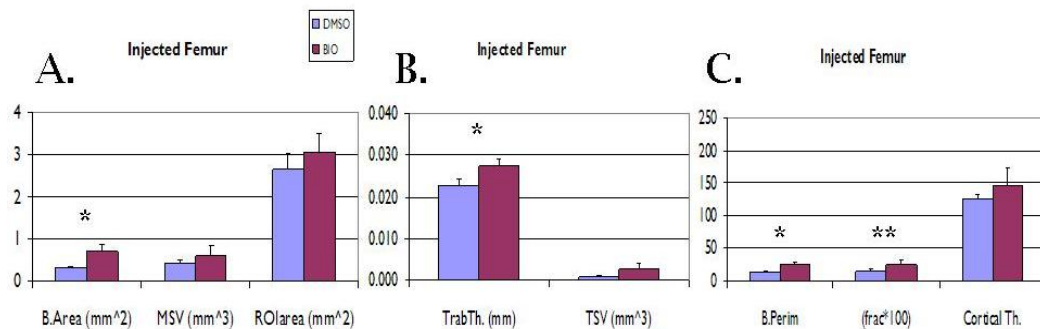


Figure IV-25 - Histomorphometry of femurs from injected bones (n=6). * = $p > 0.05$, ** = $p > 0.1$

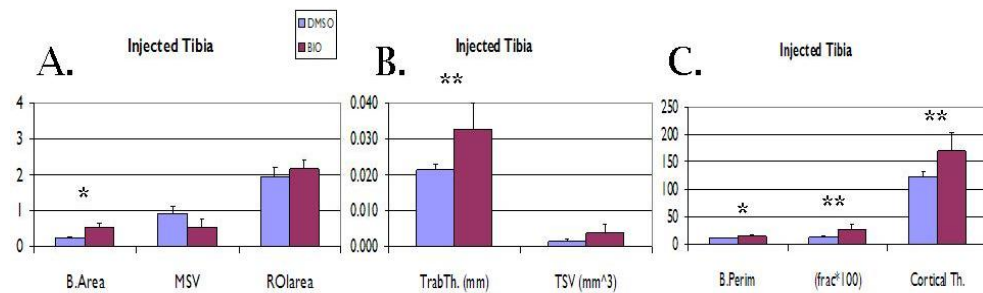


Figure IV-26 - Histomorphometry of tibias from injected bones (n=6). * = $p > 0.05$, ** = $p > 0.1$

A similar trend was observed in biochemical markers of bone resorption. Assaying Dkk1 in serum is challenging, both due to the inherent instability of the protein and due to interference from the many soluble ligands for Dkk1. We found detectable levels of human Dkk1 in only 28% of samples (Figure IV-27). Unless Dkk1 levels are very high, it does not serve as a useful marker in this model. However, all tumor-bearing animals were found to have significantly higher levels of hsIL6r via serum ELISA (Figure IV-28). However, there was no apparent relationship between sIL6r levels and tumor size, nor was there radiologically apparent bone resorption (Figure IV-29).

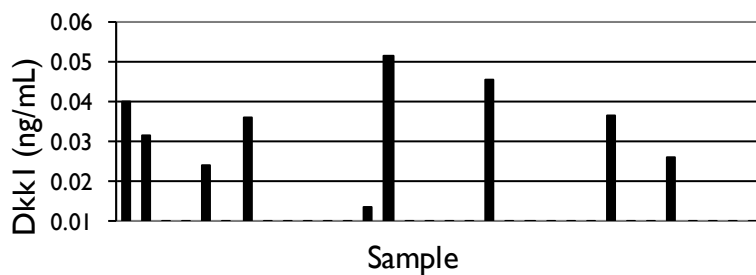


Figure IV-27 - Assay for Dkk1 in mouse serum. Of 32 samples, only 9 had detectable levels of human Dkk1.

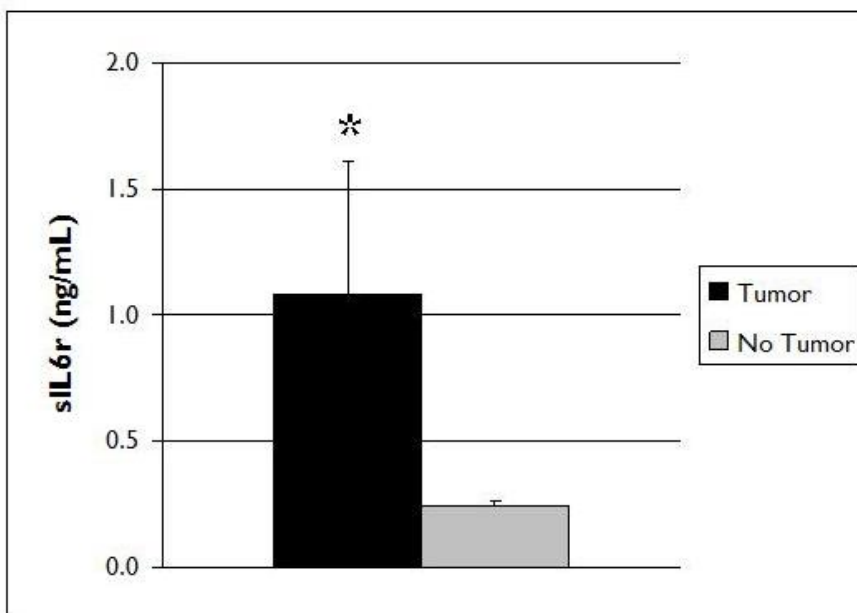


Figure IV-28 - sIL6r levels indicate tumor presence (n=10 tumor, n=8 no tumor). * = $p < 0.01$

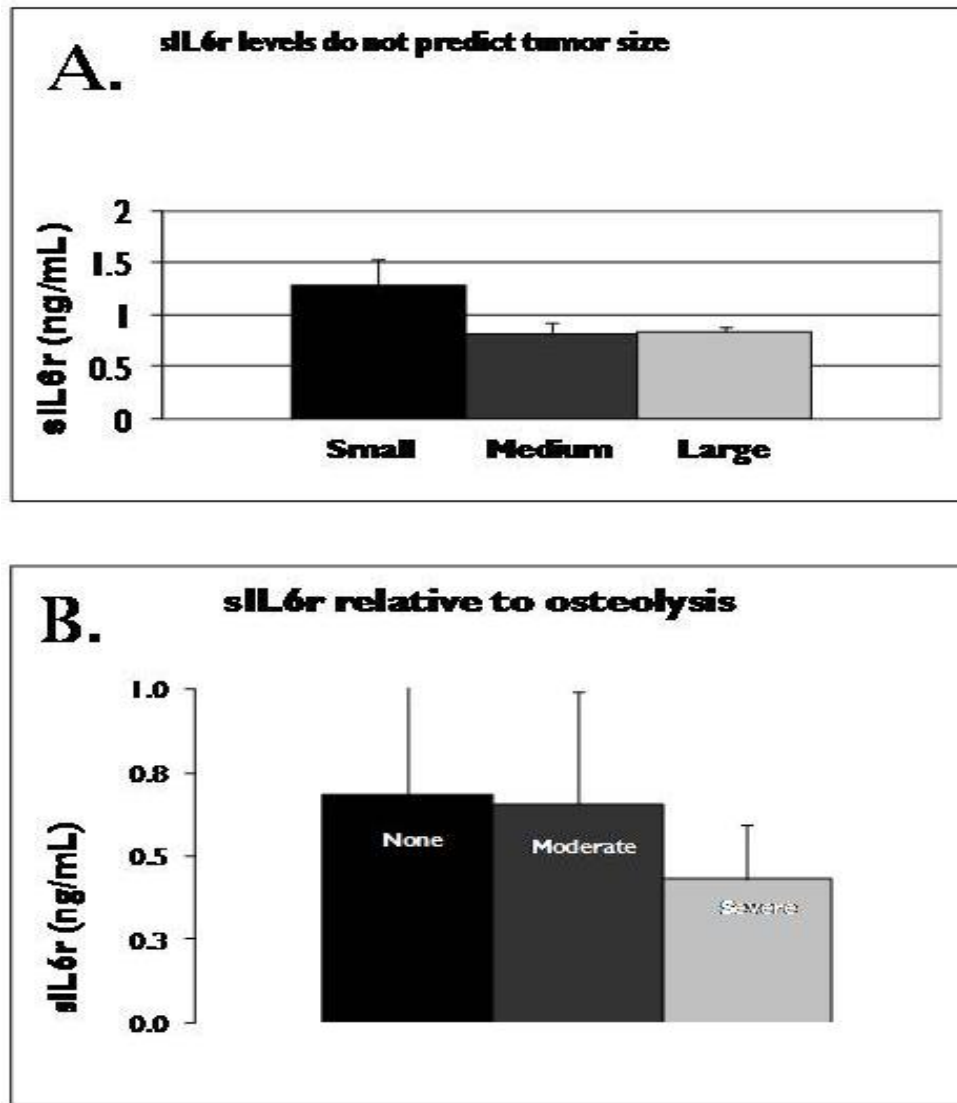


Figure IV-29 - Assay for soluble IL6 receptor. (A) sIL6r levels in animals with different tumor sizes. The y-axis is in units of ng/mL (n=7 small, n=3 medium, n=2 large). (B) sIL6r levels from animals with different degrees of radiologically apparent bone resorption (n=2 none, n=4 moderate, n=3 severe).

To find a more predictive set of biochemical markers, two different measurements of collagen degradation were examined, pyridoline (PYD),

derived from hydroxylysine crosslinks in type I collagen fibers, and c-terminal telopeptides, derived from the C-terminal ends of collagen I fibers. The assay for PYD showed statistically insignificant difference between treatment conditions. Higher levels of PYD were not found in animals with more severe radiologically apparent bone resorption (Figure IV-30). However, the assay for CTx showed both a significant increase in bone resorption with longer exposure to MM cells in untreated animals and animals with larger tumors had higher levels of CTx. Higher levels of CTx were not found in animals with more severe radiologically apparent bone resorption (Figure IV-31). Finally, serum TRAP5b was significantly increased in untreated animals having longer tumor exposure, indicating fewer osteoclasts were active in the treated group, but there was no apparent relationship to tumor size (Figure IV-32).

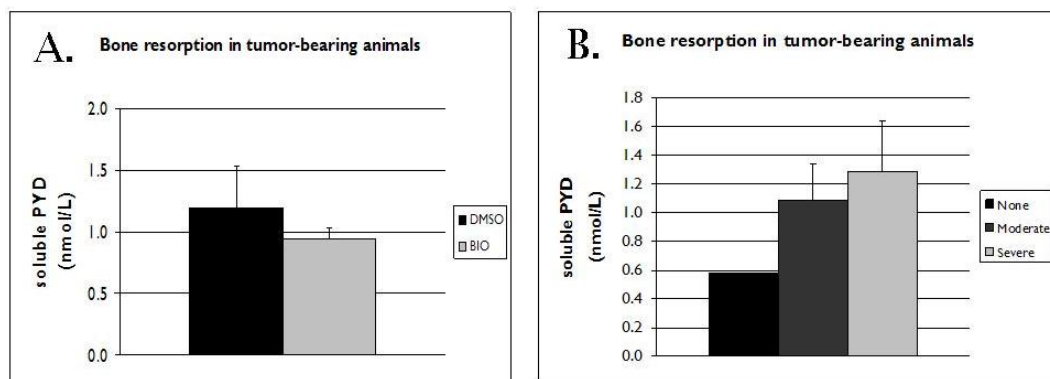


Figure IV-30 - Assay for serum PYD. (A) PYD levels among treated and untreated groups (n=7 DMSO, n=5 BIO). (B) PYD levels from animals with different degrees of radiologically apparent bone resorption (n=1 none, n=6 moderate, n=2 severe).

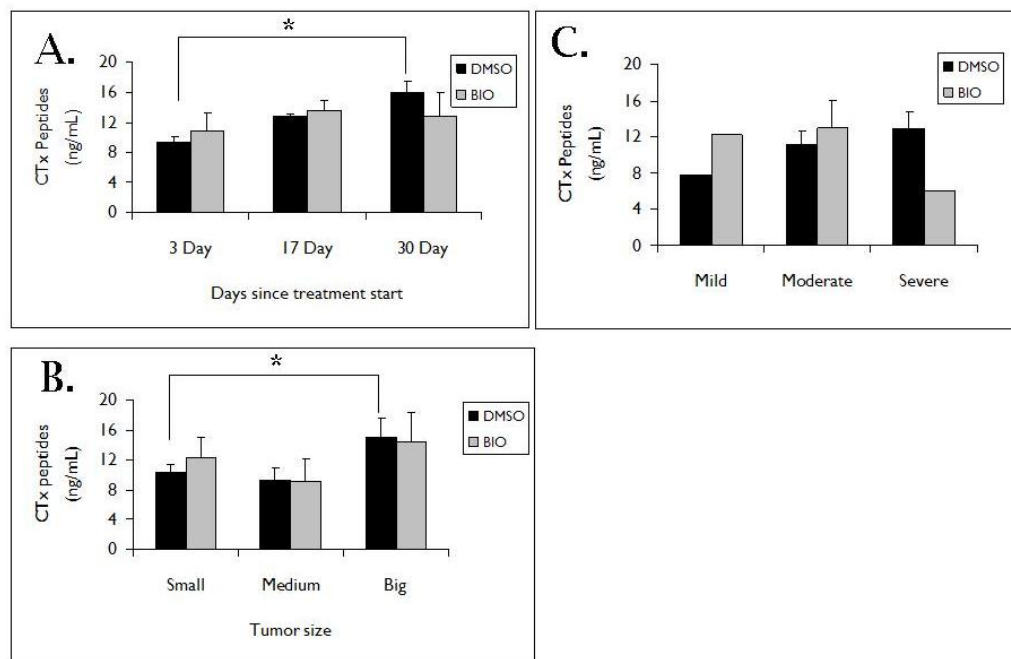


Figure IV-31 - Assay for CTx. (A) CTx peptide levels in animals with varying lengths of tumor exposure (n=13 3 Day, n=4 17 Day, n=5 30 Day). (B) CTx peptides from animals with different tumor sizes (n=10 small, n=4 medium, n=5 large). (C) CTx peptides from animals with different degrees of radiologically apparent bone resorption (n=10 mild, n=9 moderate, n=5 severe).

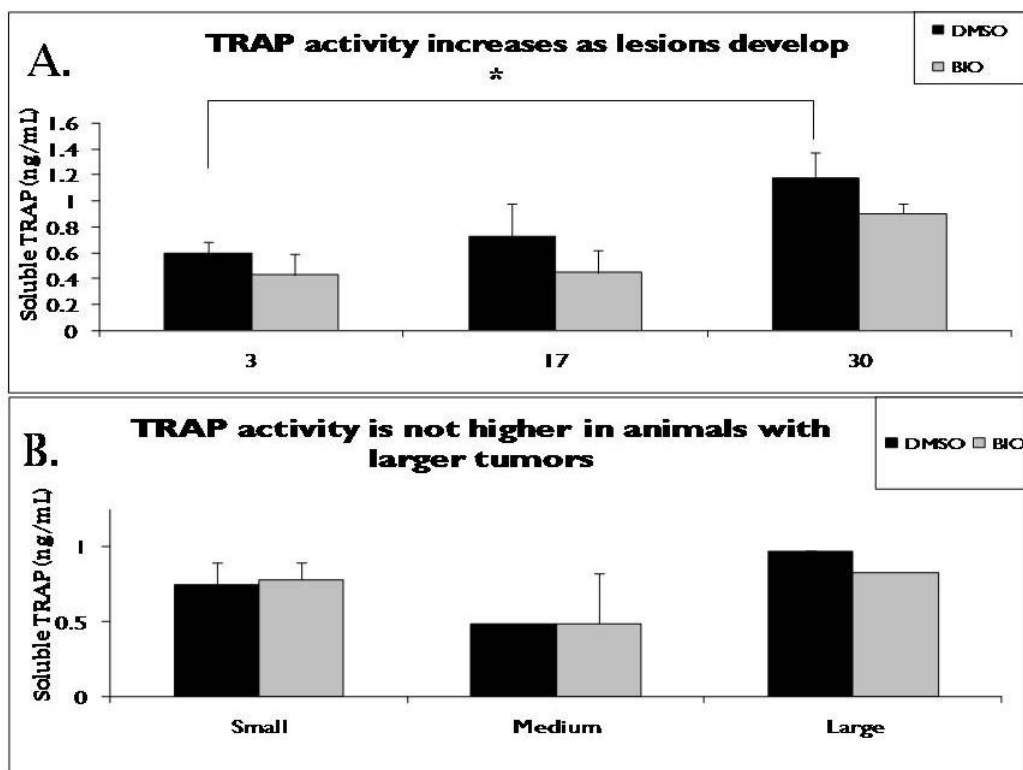


Figure IV-32 - Assay for TRAP5b. (A) TRAP activity of serum from animals with varying lengths of tumor exposure (n=10 3 Day, n=4 17 Day, n=5 30 Day). (B) TRAP activity from animals with different size tumors (n=10 small, n=4 medium, n=5 large).

CONCLUSION

In this last phase of my work, I developed a model bone disorder in mice. This model is novel for the speed with which easily detectable lesions develop. Previous models required GFP fluorescence to identify lesion sites at 30 days⁶⁰, but this model allows tumors to be detected by gross examination. Additionally, the myeloma cells in this model invaded the bone marrow, which expands the utility of the model to examination of drugs for resorption and strategies for inhibiting invasion, as well as drugs targeting the tumor cells directly. Unlike existing models of myeloma, no special strain or fetal human tissue is required to show characteristic signs of multiple myeloma bone involvement. This model allows the effects of drugs on bone to be measured using both serum markers of bone resorption and histomorphometry.

Further refinements to the model, allowing a longer incubation time and greater dissemination of the lesions, may yield a clearer picture via soluble markers, but the speed with which pronounced localized bone defects are achieved in this model remains attractive for the screening of compounds which affect bone metabolism. Although there was some disagreement among the biochemical markers studied, the results are overall consistent in showing detectable bone resorption and a reduction of resorption in the BIO treatment group. PYD turned out to be a better marker for following the progress of bone resorption, perhaps due to

diurnal variation, a known confound in CTx assays¹³². The reduction in β -catenin in tumor cell lysate indicates that the drug was reaching the tumor and, at the dose given, did inhibit GSK3 β . Furthermore, the specificity of the action of BIO suggests that if the drug is having an effect, that effect is likely mediated via GSK3 β . A clearer picture via soluble markers could be obtained by using larger numbers of animals so that measurements could be stratified according to tumor size and degree of angiogenesis, but the results are generally consistent and overall indicative of an effect by BIO on bone resorption mediated by MSC-MM cells interaction.

At the later stages, bone resorption is detectable by gross inspection of dissected bone as well as post-mortem X-ray of dissected leg bones. Whole animal X-rays were taken, but the clearest images were obtained from dissected bones, which also gave an indication of BMD. The only obvious visible signs of bone resorption are proximal to the tumor. Although we did not investigate in detail, it is possible that there was a low level of bone resorption disseminated throughout the skeleton. Slightly reduced histomorphometric parameters in the contralateral leg support this theory. Detectable bone resorption is achieved in this model quite quickly, but investigations focused on a more faithful reproduction of the disease state may want to administer fewer cells to achieve a

longer incubation time and a less severe disease manifestation, allowing more subtle and more disseminated effects to occur.

The histomorphometry measurements were consistent with the biochemical results, with the most prominent effect shown in cortical thickness. In these localized measurements, a clearer picture of the localized effects emerges. The overall amount of bone as a percentage of total area did not appear to be different in the sections from treated and untreated animals, but this measurement does not capture the density of bone and may also be a measurement artifact caused by the local physical deformation in the area of the tumor. The high degree of variability seen in the measurement of MSV may also be a reflection of this. While no significant difference was seen in the measurement of trabecular thickness, TSV measurements did show differences between the treated and untreated groups, and due to the smaller scale over which TSV is calculated, it would be expected to show less variability due to gross deformation.

In the novel *in vivo* model of bone resorption I developed, I was able to demonstrate clear differences in the severity of bone lesions experienced by BIO-treated and untreated mice. Additionally, the effects of this strategy targeting the Wnt pathway are consistent with other studies targeting Wnt using diverse methodologies. For example, the most recent study used LiCl administration in a mouse model of MM and

found similar effects on the number of osteoclasts per bone area and bone mineral density. Other studies used Dkk1 blocking antibodies to restore OPG expression in MM serum or conditioned medium-inhibited osteoblasts, and the follow-up study used both Wnt3a-expressing MM cells and direct exposure of myelomatous bones to recombinant Wnt3a to achieve a reduction in tumor burden and BMD. Some disagreement on the collateral effects of Wnt on MM cell proliferation exists in the literature, but all the studies are consistent regarding the bone effects. Finally, a study of human patients with MGUS undergoing various chemotherapy regimens showed a significant decrease in Dkk1 levels (p-values ranging from 0.001 to 0.039), only in the ones responding to treatment.⁸²

The advantages of this model are in the speed of tumor induction, ease of animal handling procedures, straightforward monitoring of disease progression by blood marker assay and X-ray, and clear and obvious differences in some bone resorption parameters measured histomorphometrically. Because the actions of osteoclasts and osteoblasts, like that of MSCs and myeloma cells, are coupled, the effect of treatment cannot be unambiguously attributed to a direct effect on the MSCs, MM cells, osteoblasts, or osteoclasts. This model also does not perfectly recapitulate many features of MM in human patients, however, and not all of the clinical features are present. To make the model more closely resemble the clinical progress of multiple myeloma, I would use a

lower dose of cells to allow a longer incubation time, and perhaps use multiple injection sites to better simulate the disseminated skeletal effects. To further develop the model for rapid screening of drugs, I would use a larger number of animals and begin the treatment with the drug before the administration of the cells.

V. FINAL DISCUSSION AND FUTURE PERSPECTIVES

The aim of these studies was to determine whether the effect of MM-derived Dkk1 promotes osteolytic lesions by inhibiting bone repair by MSCs. To this end, I explored the effect of Wnt in osteogenic cultures of MSCs, determined the effect of MM cells on MSC osteogenesis, and set up an animal model to test a potential treatment for MM which interrupts the effect of MM cells on bone repair. By developing a sensitive and high-throughput osteogenesis assay, I confirmed that Dkk1 inhibits MSC osteogenesis. Using the results from these studies, I screened some small molecules to find one which could interrupt the synergy between MSCs and MM cells. I then developed a mouse model for MM which recapitulates the bone effects using human MM cells. The model shows clinical features of MM in a rapid and predictable manner and I showed that attenuation of the Dkk1 signal with the drug BIO reduced the effect of MM cells on markers of bone resorption and repair. This work furthers the understanding of the role of MSCs in bone repair, provides new tools for examining the effect of compounds which affect bone repair, and demonstrates for the first time enhanced bone repair *in vivo* by promotion of Wnt signaling using a Dkk1 antagonist.

Despite these promising pre-clinical observations, there remain some important unanswered questions. Because the study focused almost exclusively on bone, the effects of the human myeloma cells on

the experimental animals needs to be further characterized. Different routes of administration and dosage would produce different disease manifestations, and while the direct tibial administration of the cells resulted in rapid and severe lesions useful for drug screening, it remains possible that periodic intravenous administration would eventually lead to a slowly developing disease, which would be more interesting from the viewpoint of cancer biology. For example, MM is known to affect kidney function, but only in the later stages of the disease, so a longer incubation time would be necessary to carry out these studies. Additionally, the degree to which these human MM cells affect kidney function needs to be known as it is a confound in pharmacokinetic studies. The possibility for liver metastasis should also be more thoroughly examined for similar reasons. It is likely that a slower development of the tumor would lead to more bone marrow engraftment of the tumor and may yield more sensitive measurements of bone resorption without the gross distortions caused by the direct high-dose administration.

The drug BIO is also in need of further characterization. Although the affinity of BIO for GSK3 β is much lower than its affinity for other kinases, the degree to which the drug bioaccumulates in a target tissue and the different levels of Wnt activity in those tissues may lead to effects on non-target organs. The direct administration route used in

these studies ensured that variability due to metabolic confounds did not play a role and limited systemic exposure. The effectiveness of BIO administered orally and intravenously would need to be characterized if the drug were to be interesting as a therapeutic candidate in humans. To this end, the pharmacokinetics of the drug would need to be established and effects of the drug on the non-target organs would need to be identified.

The animal model is not the only avenue for further exploration. There remain unanswered questions about how Dkk1 acts on MSCs to inhibit differentiation and indeed how MSCs differentiate in the first place. As a secreted protein, Dkk1 seems to function as a damage sensor, allowing MSC proliferation to occur subsequent to injury, generating the amount of progenitor cells needed to repair the damaged tissue. Because secretion of growth factors is a known important mechanism by which MSCs effect tissue repair, this and other pieces of circumstantial evidence such as the co-occurrence of Dkk1 and connective tissue growth factor among the most highly upregulated genes in MM and the relationship between p53 and Dkk1 suggest a larger role for Dkk1 beyond its well-studied functions during development.

Assays for differentiation could also be improved. Existing techniques only have the sensitivity to detect differentiation after it has occurred to a culture, a process which takes weeks to months, depending

on the type of differentiation desired. Unsolved problems in this area primarily arise from the lack of quantitative ability and poor temporal resolution of the analytical techniques. An interesting avenue of examination in this area concerns the kinetic parameters of differentiation. Does it occur as a phase change whereby upon activation of a transcriptional circuit the whole cell switches state from multipotential to differentiated very rapidly, or is it a gradual process wherein there is no clear event that marks differentiated and non-differentiated? Advances in real-time single molecule detection techniques promise to deliver the resolution needed to answer these questions.

REFERENCES

1. Friedenstein, A.J., Chailakhjan, R.K. & Lalykina, K.S. The development of fibroblast colonies in monolayer cultures of guinea-pig bone marrow and spleen cells. *Cell and tissue kinetics* **3**, 393-403(1970).
2. Owen, M. & Friedenstein, A.J. Stromal stem cells: marrow-derived osteogenic precursors. *Ciba Foundation symposium* **136**, 42-60(1988).
3. Friedenstein, A.J., Chailakhyan, R.K. & Gerasimov, U.V. Bone marrow osteogenic stem cells: in vitro cultivation and transplantation in diffusion chambers. *Cell and tissue kinetics* **20**, 263-72(1987).
4. Friedenstein, A.J., Chailakhyan, R.K. & Gerasimov, U.V. Bone marrow osteogenic stem cells: in vitro cultivation and transplantation in diffusion chambers. *Cell and tissue kinetics* **20**, 263-72(1987).
5. Gronthos, S. et al. The STRO-1+ fraction of adult human bone marrow contains the osteogenic precursors. *Blood* **84**, 4164-4173(1994).
6. Gronthos, S. et al. Molecular and cellular characterisation of highly purified stromal stem cells derived from human bone marrow. *Journal of Cell Science* **116**, 1827-1835(2003).

7. Bianco, P., Robey, P.G. & Simmons, P.J. Mesenchymal stem cells: revisiting history, concepts, and assays. *Cell stem cell* **2**, 313-9(2008).
8. Potian, J.A. et al. Veto-like activity of mesenchymal stem cells: functional discrimination between cellular responses to alloantigens and recall antigens. *Journal of immunology (Baltimore, Md. : 1950)* **171**, 3426-34(2003).
9. Rasmusson, I. et al. Mesenchymal stem cells inhibit lymphocyte proliferation by mitogens and alloantigens by different mechanisms. *Experimental cell research* **305**, 33-41(2005).
10. Blanc, K.L. et al. Treatment of severe acute graft-versus-host disease with third party haploidentical mesenchymal stem cells. *The Lancet* **363**, 1439-1441(2004).
11. Ringdén, O. et al. Mesenchymal stem cells for treatment of therapy-resistant graft-versus-host disease. *Transplantation* **81**, 7(2006).
12. Maitra, B. et al. Human mesenchymal stem cells support unrelated donor hematopoietic stem cells and suppress T-cell activation. *Bone marrow transplantation* **33**, 597-604(2004).
13. Ball, L.M. et al. Cotransplantation of ex vivo expanded mesenchymal stem cells accelerates lymphocyte recovery and may reduce the risk of graft failure in haploidentical hematopoietic stem-cell transplantation. *Blood* **110**, 2764-2767(2007).

14. Ball, L. et al. Third party mesenchymal stromal cell infusions fail to induce tissue repair despite successful control of severe grade iv acute graft-Versus-Host disease in a child with juvenile myelo-Monocytic leukemia. *Leukemia* **22**, 1256-1257(2007).
15. Zappia, E. et al. Mesenchymal stem cells ameliorate experimental autoimmune encephalomyelitis inducing T-cell anergy. *Blood* **106**, 1755-61(2005).
16. Bartholomew, A. et al. Mesenchymal stem cells suppress lymphocyte proliferation in vitro and prolong skin graft survival in vivo. *Experimental hematology* **30**, 42-8(2002).
17. Chen, X., Armstrong, M.A. & Li, G. Mesenchymal stem cells in immunoregulation. *Immunology and cell biology* **84**, 413-21(2006).
18. Uccelli, A., Moretta, L. & Pistoia, V. Immunoregulatory function of mesenchymal stem cells. *European journal of immunology* **36**, 2566-73(2006).
19. Le Blanc, K. et al. HLA expression and immunologic properties of differentiated and undifferentiated mesenchymal stem cells. *Experimental hematology* **31**, 890-6(2003).
20. Le Blanc, K. Immunomodulatory effects of fetal and adult mesenchymal stem cells. *Cytotherapy* **5**, 485-9(2003).

21. Angoulvant, D. et al. Human mesenchymal stem cells suppress induction of cytotoxic response to alloantigens. *Biorheology* **41**, 469-76(2004).
22. Tse, W.T. et al. Suppression of allogeneic T-cell proliferation by human marrow stromal cells: implications in transplantation. *Transplantation* **75**, 389-97(2003).
23. Zappia, E. et al. Mesenchymal stem cells ameliorate experimental autoimmune encephalomyelitis inducing T-cell anergy. *Blood* **106**, 1755-61(2005).
24. Gunn, W.G. et al. A crosstalk between myeloma cells and marrow stromal cells stimulates production of DKK1 and interleukin-6: a potential role in the development of lytic bone disease and tumor progression in multiple myeloma. *Stem cells (Dayton, Ohio)* **24**, 986-91(2006).
25. PEREIRA, R.F. et al. Cultured adherent cells from marrow can serve as long-lasting precursor cells for bone, cartilage, and lung in irradiated mice. *Proc. Natl. Acad. Sci. USA* **92**, 4857-4861(1995).
26. Otto, W.R. & Rao, J. Tomorrow's skeleton staff: mesenchymal stem cells and the repair of bone and cartilage. *Cell Proliferation* **37**, 97 - 110(2004).

27. Cooper, L.F. et al. Incipient analysis of mesenchymal stem-cell-derived osteogenesis. *Journal of dental research* **80**, 314-20(2001).
28. Frosch, K. et al. Stem cell-coated titanium implants for the partial joint resurfacing of the knee. *Biomaterials* **27**, 2542-9(2006).
29. Kalia, P. et al. Do autologous mesenchymal stem cells augment bone growth and contact to massive bone tumor implants? *Tissue engineering* **12**, 1617-26(2006).
30. Tasso, R. et al. Recruitment of a Host's Osteoprogenitor Cells Using Exogenous Mesenchymal Stem Cells Seeded on Porous Ceramic. *Tissue engineering. Part A* **15**, (2009).
31. Caplan, A.I. & Dennis, J.E. Mesenchymal stem cells as trophic mediators. *Journal of cellular biochemistry* **98**, 1076-84(2006).
32. Prockop, D.J. "Stemness" Does Not Explain the Repair of Many Tissues by Mesenchymal Stem/Multipotent Stromal Cells (MSCs). *Clinical Pharmacology and Therapeutics* **82**, 6-8(2007).
33. Fang, B. et al. Cotransplantation of haploidentical mesenchymal stem cells to enhance engraftment of hematopoietic stem cells and to reduce the risk of graft failure in two children with severe aplastic anemia. *Pediatric transplantation* **13**, 499-502(2009).
34. Meuleman, N. et al. Infusion of Mesenchymal Stromal Cells can aid Hematopoietic Recovery following Allogeneic Hematopoietic Stem

- Cell Myeloablative Transplant: A Pilot Study. *Stem cells and development* **13**, 499-502(2009).
35. Ninichuk, V. et al. Multipotent mesenchymal stem cells reduce interstitial fibrosis but do not delay progression of chronic kidney disease in collagen4A3-deficient mice. *Kidney international* **70**, 121-9(2006).
36. Tögel, F. et al. Autologous and allogeneic marrow stromal cells are safe and effective for the treatment of acute kidney injury. *Stem cells and development* **18**, 475-85(2009).
37. Yan, Y. et al. Mesenchymal stem cells from human umbilical cords ameliorate mouse hepatic injury in vivo. *Liver international : official journal of the International Association for the Study of the Liver* **29**, 356-65(2009).
38. Bianco, P. et al. Bone Marrow Stromal Stem Cells: Nature, Biology, and Potential Applications. *Stem Cells* **19**, 180-192(2001).
39. Etheridge, S.L. et al. Expression Profiling and Functional Analysis of Wnt Signaling Mechanisms in Mesenchymal Stem Cells. *Stem Cells* **22**, 849-860(2004).
40. Etheridge, S.L. et al. Expression Profiling and Functional Analysis of Wnt Signaling Mechanisms in Mesenchymal Stem Cells. *Stem Cells* **22**, 849-860(2004).

41. Gunn, W.G. et al. A crosstalk between myeloma cells and marrow stromal cells stimulates production of DKK1 and interleukin-6: a potential role in the development of lytic bone disease and tumor progression in multiple myeloma. *Stem cells (Dayton, Ohio)* **24**, 986-91(2006).
42. Spees, J.L. et al. Differentiation, cell fusion, and nuclear fusion during ex vivo repair of epithelium by human adult stem cells from bone marrow stroma. *Proceedings of the National Academy of Sciences of the United States of America*. **100**, 2397-2402(2003).
43. Gregory, C.A. et al. The Wnt signaling inhibitor dickkopf-1 is required for reentry into the cell cycle of human adult stem cells from bone marrow. *The Journal of biological chemistry* **278**, 28067-78(2003).
44. Chien, A. & Moon, R. WNTS and WNT receptors as therapeutic tools and targets in human disease processes. *Frontiers in bioscience : a journal and virtual library* **12**, 448-457(2007).
45. Nusse, R. Wnt signaling and stem cell control. *Cell research* **18**, 523-7(2008).
46. Gordon, M.D. & Nusse, R. Wnt signaling: multiple pathways, multiple receptors, and multiple transcription factors. *The Journal of biological chemistry* **281**, 22429-33(2006).

47. Kim, J. et al. Bone regeneration is regulated by wnt signaling. [J Bone Miner Res. 2007] - PubMed Result. *Journal of bone and mineral research : the official journal of the American Society for Bone and Mineral Research* **22**, 1913-1923(2007).
48. Baron, R. & Rawadi, G. Targeting the Wnt/beta-Catenin Pathway to Regulate Bone Formation in the Adult Skeleton. *Endocrinology* **148**, 2635-2643(2007).
49. Boyden, L.M. et al. High bone density due to a mutation in LDL-receptor-related protein 5. *The New England journal of medicine* **346**, 1513-21(2002).
50. Semenov, M. et al. Head inducer Dickkopf-1 is a ligand for Wnt coreceptor LRP6. *Current Biology* **11**, 951-961(2001).
51. Esteve, F.R. & Roodman, G.D. Pathophysiology of myeloma bone disease. *Best practice & research. Clinical haematology* **20**, 613-24(2007).
52. Giuliani, N., Rizzoli, V. & Roodman, G. Multiple myeloma bone disease: Pathophysiology of osteoblast inhibition. *Blood* **108**, 3992-3996(2006).
53. Roodman, G.D. Pathogenesis of myeloma bone disease. *Leukemia : official journal of the Leukemia Society of America, Leukemia Research Fund, U.K* **23**, 435-41(2009).

54. Tian, E. et al. The role of the Wnt-signaling antagonist DKK1 in the development of osteolytic lesions in multiple myeloma. *The New England Journal of Medicine* **349**, 2483-2494(2003).
55. Bielby, R., Jones, E. & McGonagle, D. The role of mesenchymal stem cells in maintenance and repair of bone. *Injury* **38 Suppl 1**, S26-32(2007).
56. Romas, E., Gillespie, M.T. & Martin, T.J. Involvement of receptor activator of NFkappaB ligand and tumor necrosis factor-alpha in bone destruction in rheumatoid arthritis. *Bone* **30**, 340-6(2002).
57. Harousseau, J. & Moreau, P. Autologous hematopoietic stem-cell transplantation for multiple myeloma. *The New England journal of medicine* **360**, 2645-54(2009).
58. Curran, M.P. & McKeage, K. Bortezomib: a review of its use in patients with multiple myeloma. *Drugs* **69**, 859-88(2009).
59. Pennisi, A. et al. The proteasome inhibitor, bortezomib suppresses primary myeloma and stimulates bone formation in myelomatous and nonmyelomatous bones in vivo. *American Journal of Hematology* **84**, 6-14(2009).
60. Mitsiades, C. et al. Fluorescence Imaging of Multiple Myeloma Cells in a Clinically Relevant SCID/NOD in Vivo Model: Biologic and

- Clinical Implications -- Mitsiades et al. 63 (20): 6689 -- *Cancer Research*. *Cancer Research* **63**, 6689-6696(2003).
61. Urashima, M. et al. The Development of a Model for the Homing of Multiple Myeloma Cells to Human Bone Marrow -- Urashima et al. 90 (2): 754 -- *Blood*. *Blood* **90**, 754-765(1997).
 62. Zhang, X.G. et al. Reproducible obtaining of human myeloma cell lines as a model for tumor stem cell study in human multiple myeloma. *Blood* **83**, 3654-3663(1994).
 63. Epstein, J. & Yaccoby, S. The SCID-hu myeloma model. *Methods in molecular medicine* **113**, 183-90(2005).
 64. Miyakawa, Y. et al. Establishment of a new model of human multiple myeloma using nod/scid/ γ cnull (nog) mice. *Biochemical and Biophysical Research Communications* **313**, 258-262(2004).
 65. Miyakawa, Y. et al. Establishment of a new model of human multiple myeloma using NOD/SCID/gammac(null) (NOG) mice. *Biochemical and biophysical research communications*. **313**, 258-262(2004).
 66. Frost, P. et al. In vivo antitumor effects of the mTOR inhibitor CCI-779 against human multiple myeloma cells in a xenograft model. *Blood* **104**, 4181-7(2004).
 67. Wu, K. et al. Investigation of antitumor effects of synthetic epothilone analogs in human myeloma models in vitro and in vivo.

Proceedings of the National Academy of Sciences of the United States of America **102**, 10640-5(2005).

68. XG, Z. et al. Reproducible obtaining of human myeloma cell lines as a model for tumor stem cell study in human multiple myeloma. *Blood* **83**, 3654-3663(1994).
69. Labrinidis, A. et al. Apo2L/TRAIL inhibits tumor growth and bone destruction in a murine model of multiple myeloma. *Clinical cancer research : an official journal of the American Association for Cancer Research* **15**, 1998-2009(2009).
70. Qiang, Y., Shaughnessy, J.D. & Yaccoby, S. Wnt3a signaling within bone inhibits multiple myeloma bone disease and tumor growth. *Blood* **112**, 374-82(2008).
71. Pellat-Deceunynk, C. et al. Human myeloma cell lines as a tool for studying the biology of multiple myeloma: a reappraisal 18 years after [letter]. *Blood* **86**, 4001-4002(1995).
72. Edwards, C.M. et al. Increasing Wnt signaling in the bone marrow microenvironment inhibits the development of myeloma bone disease and reduces tumor burden in bone in vivo. *Blood* **111**, 2833-42(2008).

73. Ito, M. et al. NOD/SCID/gamma cnull mouse: an excellent recipient mouse model for engraftment of human cells. *Blood* **100**, 3175-3182(2002).
74. Feo-Zuppari, F.J. et al. Long-term engraftment of fresh human myeloma cells in SCID mice -- Feo-Zuppari et al. 80 (11): 2843 -- *Blood*. *Blood* **80**, 2843-2850(1992).
75. Pilarski, L. et al. Myeloma progenitors in the blood of patients with aggressive or minimal disease: engraftment and self-renewal of primary human myeloma in the bone marrow of NOD SCID mice -- Pilarski et al. 95 (3): 1056 -- *Blood*. *Blood* **95**, 1056-1065(2000).
76. Arguello, F., Baggs, R.B. & Frantz, C.N. A murine model of experimental metastasis to bone and bone marrow -- Arguello et al. 48 (23): 6876 -- *Cancer Research*. *Cancer Research* **48**, 6876-6881(1988).
77. Feo-Zuppari, F.J. et al. Long-term engraftment of fresh human myeloma cells in SCID mice -- Feo-Zuppari et al. 80 (11): 2843 -- *Blood*. *Blood* **80**, 2843-2850(1992).
78. Yaccoby, S. et al. Atacicept (TACI-Ig) inhibits growth of TACIhigh primary myeloma cells in SCID-hu mice and in coculture with osteoclasts. *Leukemia* **22**, 406-413(2007).

79. Uchiyama, H. et al. Adhesion of human myeloma-derived cell lines to bone marrow stromal cells stimulates interleukin-6 secretion. *Blood* **82**, 3712-20(1993).
80. Qiang, Y. et al. Myeloma-Derived dickkopf-1 disrupts wnt-Regulated osteoprotegerin and rankl production by osteoblasts: a potential mechanism underlying osteolytic bone lesions in multiple myeloma. *Blood* **112**, 196-207(2008).
81. Dankbar, B. et al. Vascular endothelial growth factor and interleukin-6 in paracrine tumor-stromal cell interactions in multiple myeloma. *Blood* **95**, 2630-6(2000).
82. Tian, E. et al. The role of the Wnt-signaling antagonist DKK1 in the development of osteolytic lesions in multiple myeloma. *The New England journal of medicine* **349**, 2483-94(2003).
83. Sato, N. et al. Maintenance of pluripotency in human and mouse embryonic stem cells through activation of Wnt signaling by a pharmacological GSK-3-specific inhibitor. *Nature medicine* **10**, 55-63(2004).
84. Prockop, D.J., Sekiya, I. & Colter, D.C. Isolation and characterization of rapidly self-renewing stem cells from cultures of human marrow stromal cells. *Cytotherapy*. **3**, 393-396(2001).

85. Colter, D.C. et al. Rapid expansion of recycling stem cells in cultures of plastic-adherent cells from human bone marrow. *Proc. Natl. Acad. Sci. USA* **97**, 3213-3218(2000).
86. Gregory, C.a. et al. Dkk-1-derived synthetic peptides and lithium chloride for the control and recovery of adult stem cells from bone marrow. *The Journal of biological chemistry* **280**, 2309-23(2005).
87. Gregory, C.A. et al. An Alizarin red-based assay of mineralization by adherent cells in culture: comparison with cetylpyridinium chloride extraction. *Analytical biochemistry* **329**, 77-84(2004).
88. Kaiser, M. et al. Serum concentrations of DKK-1 correlate with the extent of bone disease in patients with multiple myeloma. *European journal of haematology* **80**, 490-4(2008).
89. Qiang, Y. et al. Dkk1-induced inhibition of Wnt signaling in osteoblast differentiation is an underlying mechanism of bone loss in multiple myeloma. *Bone* **42**, 669-80(2008).
90. Giuliani, N. & Rizzoli, V. Myeloma cells and bone marrow osteoblast interactions: role in the development of osteolytic lesions in multiple myeloma. *Leukemia & lymphoma* **48**, 2323-9(2007).
91. Haaber, J. et al. Myeloma cell expression of 10 candidate genes for osteolytic bone disease. Only overexpression of DKK1 correlates with clinical bone involvement at diagnosis. *Br J Haematol* (2007).

92. Harousseau, J., Shaughnessy, J.J. & Richardson, P. Multiple myeloma. *Hematology (Am Soc Hematol Educ Program)* 237-256(2004).
93. Terpos, E. et al. Bortezomib reduces serum dickkopf-1 and receptor activator of nuclear factor-kappaB ligand concentrations and normalises indices of bone remodelling in patients with relapsed multiple myeloma. *British Journal of Haematology* **135**, 688-692(2006).
94. Yaccoby, S. et al. Antibody-based inhibition of DKK1 suppresses tumor-induced bone resorption and multiple myeloma growth in vivo. *Blood* **109**, 2106-2111(2007).
95. Edwards, C.M., Zhuang, J. & Mundy, G.R. The pathogenesis of the bone disease of multiple myeloma. *Bone* **42**, 1007-1013(2008).
96. Gregory, C. Advances in myeloma therapy: breaking the cycle. *Blood* **109**, 1798-1798(2007).
97. de Boer, J. et al. Wnt signaling inhibits osteogenic differentiation of human mesenchymal stem cells. *Bone* **34**, 818-26(2004).
98. Jope, R.S. Lithium and GSK-3: one inhibitor, two inhibitory actions, multiple outcomes. *Trends in pharmacological sciences* **24**, 441-3(2003).
99. Atkins, G.J. et al. RANKL expression is related to the differentiation state of human osteoblasts. *J Bone Miner Res* **18**, 1088-1098(2003).

100. Giuliani, N. et al. Myeloma cells induce imbalance in the osteoprotegerin/osteoprotegerin ligand system in the human bone marrow environment. *Blood* **98**, 3527-3533(2001).
101. Barillé-Nion, S. & Bataille, R. New insights in myeloma-induced osteolysis. *Leukemia & lymphoma* **44**, 1463-7(2003).
102. Giuliani, N., Rizzoli, V. & Roodman, G.D. Multiple myeloma bone disease: Pathophysiology of osteoblast inhibition. *Blood* **108**, 3992-6(2006).
103. Giuliani, N. et al. Production of Wnt Inhibitors by Myeloma Cells: Potential Effects on Canonical Wnt Pathway in the Bone Microenvironment. *Cancer Research* **67**, 7665-7674(2007).
104. Yaccoby, S. et al. Myeloma interacts with the bone marrow microenvironment to induce osteoclastogenesis and is dependent on osteoclast activity. *British journal of haematology* **116**, 278-90(2002).
105. Corre, J. et al. Bone marrow mesenchymal stem cells are abnormal in multiple myeloma. *Leukemia* **21**, 1079-1088(2007).
106. Zhu, Y. et al. Human mesenchymal stem cells inhibit cancer cell proliferation by secreting DKK-1. *Leukemia : official journal of the Leukemia Society of America, Leukemia Research Fund, U.K* **23**, 925-33(2009).

107. Shiozawa, Y. et al. The bone marrow niche: habitat to hematopoietic and mesenchymal stem cells, and unwitting host to molecular parasites. *Leukemia* **22**, 941-950(2008).
108. Bain, J. et al. The specificities of protein kinase inhibitors: an update. *Biochem J* **371**, 199-204(2003).
109. Hedgepeth, C. et al. Activation of the Wnt Signaling Pathway: A Molecular Mechanism for Lithium Action. *Developmental Biology* **185**, 82-91(1997).
110. Phiel, C.J. & Klein, P.S. Molecular targets of lithium action. *Annual Review of Pharmacology and Toxicology* **41**, 789-813(2001).
111. Gregory, C.A. et al. Dkk-1-derived synthetic peptides and lithium chloride for the control and recovery of adult stem cells from bone marrow. *The Journal of biological chemistry* **280**, 2309-23(2005).
112. Sato, N. & Brivanlou, A.H. Manipulation of self-renewal in human embryonic stem cells through a novel pharmacological GSK-3 inhibitor. *Methods in molecular biology (Clifton, N.J.)* **331**, 115-28(2006).
113. Quiroz, J.A., Gould, T.D. & Manji, H.K. Molecular effects of lithium. *Molecular interventions* **4**, 259-72(2004).
114. van Zaanen, H.C. et al. Endogenous interleukin 6 production in multiple myeloma patients treated with chimeric monoclonal anti-

- IL6 antibodies indicates the existence of a positive feed-back loop. *J Clin Invest* **98**, 1441-1448(1996).
115. Teoh, G. & Anderson, K.C. Interaction of tumor and host cells with adhesion and extracellular matrix molecules in the development of multiple myeloma. *Hematol Oncol Clin North Am* **11**, 27-42(1997).
116. Kawano, M. et al. Autocrine generation and requirement of BSF-2/IL-6 for human multiple myelomas. *Nature* **332**, 83-85(1988).
117. Bataille, R. et al. Serum levels of interleukin 6, a potent myeloma cell growth factor, as a reflect of disease severity in plasma cell dyscrasias. *J Clin Invest* **84**, 2008-2011(1989).
118. Dodds, R.A. et al. Expression of mRNA for IL1 beta, IL6 and TGF beta 1 in developing human bone and cartilage. *The journal of histochemistry and cytochemistry : official journal of the Histochemistry Society* **42**, 733-44(1994).
119. Wallace, S.R. et al. Abnormalities of Bone Marrow Mesenchymal Cells in Multiple Myeloma Patients. *Cancer* **91**, 1219-1230(2001).
120. Atkins, G.J. et al. RANKL expression is related to the differentiation state of human osteoblasts. *Journal of bone and mineral research : the official journal of the American Society for Bone and Mineral Research* **18**, 1088-98(2003).

121. van Zaanen, H.C. et al. Chimaeric anti-interleukin 6 monoclonal antibodies in the treatment of advanced multiple myeloma: a phase I dose-escalating study. *Br J Haematol* **102**, 783-790(1998).
122. Cuendet, M. et al. Multiple Myeloma Regression Mediated by Bruceantin. *Clinical Cancer Research* **10**, 1170 -1179(2004).
123. Tassone, P. et al. A SCID-hu in vivo model of human Waldenström macroglobulinemia. *Blood* **106**, 1341-5(2005).
124. Radl, J. et al. Tenfold increased incidence of spontaneous multiple myeloma in long-term immunosuppressed aging C57BL/KaLwRij mice. *Clinical immunology and immunopathology* **79**, 155-62(1996).
125. Vanderkerken, K. et al. Multiple myeloma biology: lessons from the 5TMM models. *Immunological reviews* **194**, 196-206(2003).
126. Parfitt, A.M. et al. Bone histomorphometry: standardization of nomenclature, symbols, and units. Report of the ASBMR Histomorphometry Nomenclature Committee. *Journal of bone and mineral research : the official journal of the American Society for Bone and Mineral Research* **2**, 595-610(1987).
127. Parfitt, A.M. Bone histomorphometry: proposed system for standardization of nomenclature, symbols, and units. *Calcified tissue international* **42**, 284-6(1988).

128. Vesterby, A. et al. Unbiased stereologic estimation of surface density in bone using vertical sections. *Bone* **8**, 13-7(1987).
129. Vesterby, A., Gundersen, H.J. & Melsen, F. Star volume of marrow space and trabeculae of the first lumbar vertebra: sampling efficiency and biological variation. *Bone* **10**, 7-13(1989).
130. Filgueira, L. Fluorescence-based Staining for Tartrate-resistant Acidic Phosphatase (TRAP) in Osteoclasts Combined with Other Fluorescent Dyes and Protocols. *Histochemistry* **52**, 411-414(2004).
131. Viegas, M.S. et al. An improved and cost-effective methodology for the reduction of autofluorescence in direct immunofluorescence studies on formalin-fixed paraffin-embedded tissues. *European journal of histochemistry : EJH* **51**, 59-66
132. Huber, F. et al. Markers of bone resorption--measurement in serum, plasma or urine? *Clinical laboratory* **49**, 203-7(2003).

BIOGRAPHY

William Gunn did his undergraduate work at the University of Southern Mississippi. He joined the Molecular and Cellular Biology program at Tulane University in 2002. He now lives with his wife and dog in San Diego, CA.